UNIVERSIDADE ESTADUAL PAULISTA - UNESP
FACULDADE DE ENGENHARIA DE ILHA SOLTEIRA
DEPARTAMENTO DE ENGENHARIA ELÉTRICA
PROGRAMA DE PÓS-GRADUAÇÃO EM ENGENHARIA ELÉTRICA

PROGRAMA DE ESTÁGIO DE PÓS-DOUTORADO

Relatório de Pós-Doutorado

Período: 01-02-2023 a 31-01-2024

Aprendizado de Máquina Visando à Resolução de Problemas no Ambiente da Matemática Aplicada

Candidato : **Carlos Roberto dos Santos Júnior**
Orientadora : **Mara Lúcia Martins Lopes**

Ilha Solteira - SP, Setembro-2025.

1. INTRODUÇÃO

Este relatório apresenta as atividades desenvolvidas no âmbito do estágio de pós-doutorado realizado junto ao Departamento de Engenharia Elétrica (FEIS/UNESP), no período de 01 de fevereiro de 2023 a 31 de janeiro de 2024. O projeto teve por foco investigar e implementar soluções de Aprendizado de Máquina (AM), com ênfase em redes neurais da família ART (*Adaptive Resonance Theory*) e sua integração com aprendizado profundo (*Deep Learning*), para enfrentar problemas típicos de séries temporais e outros cenários da matemática aplicada. A motivação central é explorar a estabilidade–plasticidade das redes ART e avaliar ganhos quando combinadas a arquiteturas profundas, buscando modelos robustos, incrementais e eficientes para aplicações reais

2. OBJETIVOS

- Desenvolver e estudar arquiteturas ART-Deep (ART com camadas profundas) para previsão/diagnóstico em séries temporais e problemas correlatos.
- Comparar o desempenho com abordagens clássicas (por exemplo., Box-Jenkins) e redes MLP (*Multilayer Perceptron*) treinadas pelo algoritmo *BackPropagation*.
- Avaliar a plasticidade (aprendizado contínuo) e a estabilidade das arquiteturas propostas em cenários com grande diversidade de dados.
- Produzir material científico (artigos, comunicações) e consolidar colaborações interdisciplinares.

3. METODOLOGIA / PLANO DE TRABALHO

O plano seguiu as etapas previstas no projeto de pesquisa:

1. Revisão e atualização bibliográfica (periódicos CAPES, IEEE, livros-chave).
2. Desenvolvimento, implementação, simulação e testes das variantes ART-Deep (camadas ART em sequência; possibilidade de módulo de transformação/código ativo; uso de ARTMAP na saída quando supervisionado).

3. Aplicações em séries temporais (previsão multidimensional) e estudos-piloto em domínios correlatos (engenharias, processos industriais).
4. Análise de resultados e redação do relatório e manuscritos.

4. ATIVIDADES DE PESQUISA DESENVOLVIDAS

- Levantamento bibliográfico sobre ART, Deep Learning e previsão de séries temporais; consolidação de referências para uso didático/científico.
- Modelagem ART-Deep: definição de topologias (número de camadas ART; critérios de vigilância; estratégia de treinamento incremental; opção ARTMAP na saída).
- Implementação computacional: protótipos em Python, com rotinas de pré-processamento (normalização, janelas deslizantes) e pipelines de avaliação.
- Experimentos com séries temporais (curto prazo) comparando com metodologias consolidadas como MLP.
- Discussão técnica: análise de estabilidade, plasticidade e profundidade (nº de camadas) vs. tempo de treinamento.
- Produção científica: preparação de manuscritos.

5. RESULTADOS E DISCUSSÃO

- Viabilidade ART-Deep: comprovação de treinamento incremental estável com ganhos de tempo de convergência em cenários com grande diversidade de padrões (vs. *BackPropagation* puro), mantendo boa acurácia.
- Generalização: resultados indicam potencial de transferência para domínios além de energia (por exemplo, processos de qualidade e agronegócio), conforme previsto no projeto.
- Limitações: necessidade de afinação de hiperparâmetros de vigilância em ART.

6. ATIVIDADES COMPLEMENTARES

Além do escopo estrito do projeto, foram realizadas ações de apoio acadêmico e científico:

Suporte a alunos de doutorado:

- Acesso ao supercomputador *Lovelace* (UNICAMP): estudo, documentação e treinamento de usuários (contas, módulos, filas, boas práticas).
    - Aluna: Andréia Brasil Alves Ferreira
- Apoio à escrita de projetos de pesquisa (estrutura, objetivos, métodos, cronograma e viabilidade computacional).
    - Alunos: Joaquim Ribeiro Júnior e Camilla Nayara dos Santos Mota

Participação acadêmica:

- Bancas: atuação como membro em TCC, mestrado e doutorado.
- Minicursos e oficinas nos eventos: (tópicos: fundamentos de IA/AM, estatística aplicada, pipelines experimentais).
    - Semana da Matemática 2023- FEIS
    - Encontro Regional de Matemática Aplicada e Computacional (ERMAC-regional 11)- FEIS
- Colaborações: testes, simulações e experimentos em parceria com pós-graduandos (validações cruzadas, replicabilidade etc.).

7. CONSIDERAÇÕES FINAIS

O estágio de pós-doutorado permitiu avançar a integração de ART com *Deep Learning* em problemas de séries temporais, com resultados promissores em robustez e eficiência. As atividades complementares potencializaram a formação de recursos humanos, infraestrutura computacional e produção colaborativa, alinhadas ao escopo e às metas previstas no projeto.

8. COMENTÁRIOS DO SUPERVISOR

O pós-doutorando desenvolveu suas atividades junto ao Departamento de Engenharia Elétrica da FEIS/UNESP no período de 01/02/2023 a 31/01/2024. O projeto desenvolvido é intitulado "Aprendizado de Máquina Visando à Resolução de Problemas no Ambiente da Matemática Aplicada" e teve como principal objetivo investigar as soluções de aprendizado de máquina, em especial as redes neurais da família ART integradas a modelos de Deep Learning.

Durante o estágio, observou-se o desenvolvimento das etapas do plano de trabalho, incluindo: revisão bibliográfica atualizada, implementação computacional de variantes ART-Deep. Os resultados alcançados evidenciaram avanços relevantes, como a demonstração da viabilidade do aprendizado incremental onde foram analisados os ganhos em tempo em termos de convergência e a acurácia dos modelos. Também se verificou potencial de generalização da abordagem para diferentes domínios, ainda que com a necessidade de maior refinamento nos parâmetros de vigilância.

Além da pesquisa central, o pós-doutorando desempenhou papel ativo em atividades acadêmicas e científicas, incluindo apoio a alunos de pós-graduação no uso de infraestrutura computacional, orientação na elaboração de projetos, participação em bancas e contribuição em minicursos e oficinas. Tais iniciativas ampliaram o impacto formativo e colaborativo do estágio.

De modo geral, a avaliação é positiva. O pós-doutorando demonstrou competência técnica, autonomia na condução das simulações desenvolvidas e engajamento institucional, cumprindo os objetivos previstos e gerando resultados científicos promissores. O trabalho desenvolvido contribuiu tanto para o avanço do estado da arte quanto para a formação de recursos humanos e fortalecimento das colaborações interdisciplinares.

Diante do exposto, manifesto estar de acordo com o relatório apresentado e aprovo o relatório de atividades do estágio de pós-doutorado, que cumpriram de forma satisfatória o plano de trabalho estabelecido.

9. PRINCIPAIS REFERÊNCIAS

Abreu, T.; Amorim, A.J.; Santos-Junior, C.R.; Lotufo, A. D.P. and Minussi, C.R. “Multinodal load forecasting for distribution systems using a Fuzzy-ARTMAP neural network”, Applied Soft Computing, Vol. 71, pp. 307-316, 2018. Doi: 10.1016/j.asoc.2018.06.039.

Amorim, A. J.; Abreu, T.; Tonelli-Neto, M.S. and Minussi, C.R. “A new formulation of multinodal short-term load forecasting based on adaptive resonance theory with reverse training”, Electric Power Systems Research, Vol. 179, 2020. Doi: 10.1016/j.epsr.2019.106096.

Carpenter, G.A. and Grossberg, S. “A self-organizing neural network for supervised learning, recognition and prediction”, IEEE Communications Magazine, Vol. 30, No. 9, pp.38-49, 1992. Doi: 10.1109/35.156802.

Grossberg, S. “A path toward explainable AI and autonomous adaptive intelligence: deep learning, adaptive resonance, and models of perception, emotion, and action”, Neurorobot, June 2020, Vol. 14, Article 36. DOI: 10.3389/fnbot.2020.00036.

Grossberg, S. “Adaptive resonance theory: how a brain learns to consciously attend, learn, and recognize a changing world, Neural Networks”, Vol. 37, pp. 1-47. 2013. https://doi.org/10.1016/j.neunet.2012.09.017.

Haykin, S. “Neural networks and learning machines”, 3rd. Edition, New Jersey, USA, Prentice-Hall, 2008.

Hochreiter, S. and Schmidhuber, J. "Long short-term memory". Neural Computation, 1997, Vol 9, No. 8, pp. 1735–1780. Doi:10.1162/neco.1997.9.8.173.

Hopfield, J.J. “Neural networks and physical systems with emergent collective computational properties”, Proc. Nat. Acad. Sci. (USA), 1982, Vol. 79, pp. 2554-2558.

LeCun, Y.; Bengio, Y. and Hinton, G. "Deep learning", Nature, Vol. 521, May-2015, pp. 436-444. Doi: 10.1038/nature14539.

LeCun, Y. and Bengio, T. (1995). Convolutional networks for images, speech, and time series. In M. A. Arbib (Ed.), The handbook of brain theory and neural networks (pp. 255–258). Cambridge, MA: MIT Press.

Marchiori, S.C.; da Silveira, M.C.G.; Lofufo, A.D.P.; Minussi, C.R. and Lopes, M.L.M. "Neural network based on adaptive resonance theory with continuous training for multi-configuration transient stability analysis of electric power systems", Applied Soft Computing, Vol. 11, No.1, pp. 701-715. 2011. DOI: 10.1016/j.asoc.2009.12.032.

Nielsen, A. "Practical time series analysis: prediction with statistics and machine learning", O'Reilly Media, Inc., Sebastopol, CA, 1st.Edition, 2019. ISBN: 9781492041658.

Ilha Solteira-SP, 29 de Setembro de 2025.

gov.br Documento assinado digitalmente
CARLOS ROBERTO DOS SANTOS JUNIOR
Data: 26/09/2025 14:58:04-0300
Verifique em https://validar.iti.gov.br

Carlos Roberto dos Santos Júnior.

gov.br Documento assinado digitalmente
MARA LUCIA MARTINS LOPES
Data: 28/09/2025 18:49:01-0300
Verifique em https://validar.iti.gov.br

Mara Lúcia Martins (Supervisora)

Ciente e de acordo.

ANEXO I – Atividades Acadêmicas e Técnicas Desenvolvidas (2023–2024)

ARTIGOS EM PERIÓDICOS

- SILVA, R. J.; SANTOS JUNIOR, C. R.; ABREU, T. A.; MINUSSI, C. R.; LOPES, M. L. M.. Machine Learning for Affordable Diagnosis of SARS-COV-2 from Hematological and Biochemical Tests. preprints202404.0956 v1, v. 7, p. 1-29, 2024.

ARTIGOS COMPLETOS E EVENTOS

- FAZZIO JUNIOR, A. J.; SANTOS JUNIOR, C. R.; LOPES, M. L. M.. Otimização de Estratégias de Negócio de Micro e Pequeno Empreendimento através de Técnicas de Data Science. In: VIII ERMAC - Encontro Regional de Matemática Aplicada e Computacional - Regional 9, 2024, Ilha Solteira.

- SILVA, R. J.; SANTOS, A. S.; ABREU, T. A.; COSTA, A. L. C.; SANTOS JUNIOR, C. R.; MORENO, A. L.; LOPES, M. L. M.. Classificação de Arritmias no Tempo de Tempo-Frequência: Uma abordagem baseada em Subproblemas. In: XLIII CNMAC, 2024, Porto de Galinhas - PE.

RESUMO EXPANDIDO

- SILVA, B. M.; ABREU, T. A.; SANTOS JUNIOR, C. R.; LOPES, M. L. M.. Dispositivo Inteligente de Mapeamento de Doenças Virais. In: VIII ERMAC, 2024, Ilha Solteira.

- SOUZA, M. H. L.; ABREU, T. A.; SANTOS JUNIOR, C. R.; SILVA, R. J.; LOPES, M. L. M.. Aplicação do Orange Data Mining para Previsão da Resistência Mecânica às Tensões Normais de Compressão. In: VIII ERMAC, 2024, Ilha Solteira.

DEMAIS TIPOS DE PRODUÇÃO TÉCNICA

- SANTOS JUNIOR, C. R.; SILVA, R. J.; ABREU, T. A.; LOPES, M. L. M.. Introdução ao Machine Learning: Conceitos Básicos e Aplicações. 2024. (Curso de curta duração ministrado).

- SANTOS JUNIOR, C. R.; ABREU, T. A.; SILVA, R. J.; LOPES, M. L. M.. Minicurso: Introdução à Ciência de Dados com Orange Data Mining, Evento: XX Semana da Matemática. 2023.

PARTICIPAÇÃO EM BANCAS

Mestrado:

- Andrés Iván Atoche Galarreta. Utilização de Modelos de Deep Learning para Detecção do Câncer de Pulmão. 2024.

- Reginaldo José da Silva. Diagnóstico da COVID-19 utilizando Redes Neurais Artificiais baseada na Teoria da Ressonância Adaptativa. 2023.

Doutorado (Qualificações):

- Camilla Nayara Santos Mota. Técnicas de Machine Learning Aplicadas na Previsão de Demanda de Prédios Públicos. 2024.

- Andréia Brasil Alves Ferreira. Previsão interpretável de carga elétrica com redes neurais de fusão temporal baseadas em transformers. 2023.

- Driely Cândido Santos. Sistema de Monitoramento e Classificação de Falhas em Estruturas Mecânicas utilizando Sistemas Imunológicos Artificiais. 2023.

Trabalhos de Conclusão de Curso (Graduação):

- Victor Suzuki Souto. Previsão de Curva de Carga Elétrica usando a Rede Neural ARTMAP Fuzzy. 2024.

- Murilo Leite de Sousa. Ciência de Dados como Ferramenta para Manutenção Preditiva em Equipamentos Industriais Sensorizados. 2023.

Estudos Especiais do Programa de Pós-Graduação em Engenharia Elétrica

- Exploração e Análise de Dados de Perdas Não Técnicas em Conjunto com Dados Demográficos. 2024.

- Otimização da Performance em Contexto de Dados Desbalanceados na Classificação Multiclasse de Arritmias. 2023.

Publicações

ARTIGOS SUBMETIDOS EM PERIÓDICOS

- MOREIRA JUNIOR, J. R.; SILVA, R. J.; SANTOS JUNIOR, C. R.; ABREU, T. A.; LOPES, M. L. M.. Analysis and Optimization of Fuzzy ARTMAP Parameters for Multinodal Electric Load Forecasting. Energies, 2025.

ARTIGOS EM PERIÓDICOS

- SILVA, R. J.; SANTOS JUNIOR, C. R.; ABREU, T. A.; MINUSSI, C. R.; LOPES, M. L. M.. Machine Learning for Affordable Diagnosis of SARS-COV-2 from Hematological and Biochemical Tests. preprints202404.0956 v1, v. 7, p. 1-29, 2024.

ARTIGOS COMPLETOS E EVENTOS

- FAZZIO JUNIOR, A. J.; SANTOS JUNIOR, C. R.; LOPES, M. L. M.. Otimização de Estratégias de Negócio de Micro e Pequeno Empreendimento através de Técnicas de Data Science. In: VIII ERMAC - Encontro Regional de Matemática Aplicada e Computacional - Regional 9, 2024, Ilha Solteira.

- SILVA, R. J.; SANTOS, A. S.; ABREU, T. A.; COSTA, A. L. C.; SANTOS JUNIOR, C. R.; MORENO, A. L.; LOPES, M. L. M.. Classificação de Arritmias no Tempo de Tempo-Frequência: Uma abordagem baseada em Subproblemas. In: XLIII CNMAC, 2024, Porto de Galinhas - PE.

RESUMO EXPANDIDO

- SILVA, B. M.; ABREU, T. A.; SANTOS JUNIOR, C. R.; LOPES, M. L. M.. Dispositivo Inteligente de Mapeamento de Doenças Virais. In: VIII ERMAC, 2024, Ilha Solteira.

- SOUZA, M. H. L.; ABREU, T. A.; SANTOS JUNIOR, C. R.; SILVA, R. J.; LOPES, M. L. M.. Aplicação do Orange Data Mining para Previsão da Resistência Mecânica às Tensões Normais de Compressão. In: VIII ERMAC, 2024, Ilha Solteira.

ARTIGOS SUBMETIDOS EM PERIÓDICOS

Gmail energies

99+

Mail

Chat

Meet

[Energies] Manuscript ID: energies-3863146 - Accepted for Publication

Externa Caixa de entrada ×

Energies Editorial Office
para Joaquim, Reginaldo, Carlos, Thays, mim, Energies, Jared

Parece que esta mensagem está em inglês
Traduzir para o português

Dear Mr. Moreira Júnior,

Congratulations on the acceptance of your manuscript, and thank you for submitting your work to Energies. Please see the relevant manuscript details below:

Manuscript ID: energies-3863146
Type of manuscript: Article
Title: Analysis and Optimization of Fuzzy ARTMAP Parameters for Multinodal Electric Load Forecasting
Authors: Joaquim Ribeiro Moreira Júnior *, Reginaldo José Silva, Carlos Roberto dos Santos Júnior, Thays Abreu, Mara Lúcia Martins Lopes
Received: 24 Aug 2025
E-mails: jr.moreira@unesp.br, reginaldo.silva@unesp.br, carlos.rsantos@ifsp.edu.br, thays.abreu@unesp.br, mara.lopes@unesp.br
F: Electrical Engineering
https://www.mdpi.com/journal/energies/sections/electrical_engineering
https://susy.mdpi.com/user/manuscripts/review_info/48471d2ce1cd1d118373780f64a013e5

We will now edit your paper; once complete, we will return it to you for your review and approval. Within the next few days, an invoice for the article processing charge (APC), required for publication, will be sent by email from the Editorial Office in Basel, Switzerland.

If, however, your manuscript requires extensive English language and grammar revisions, we will need to return the paper and request that such changes are made.

energies

MDPI

Article

Analysis and Optimization of Fuzzy ARTMAP Parameters for Multinodal Electric Load Forecasting

Joaquim Ribeiro Moreira Júnior [1,*], Reginaldo José da Silva [1], Carlos Roberto dos Santos Júnior [2], Thays Abreu [3] and Mara Lúcia Martins Lopes [3]

[1] Electrical Engineering Department, School of Engineering, São Paulo State University (UNESP), Ilha Solteira 15385-000, Brazil; reginaldo.silva@unesp.br
[2] Federal Institute of Mato Grosso do Sul (IFMS), Campus Três Lagoas, Três Lagoas 79641-162, Brazil; carlos.rsantos@ifsp.edu.br
[3] Department of Mathematics, School of Engineering, São Paulo State University (UNESP), Ilha Solteira 15385-000, Brazil; thays.abreu@unesp.br (T.A.); mara.lopes@unesp.br (M.L.M.L.)
* Correspondence: jr.moreira@unesp.br; Tel.: +55-67-981236138

Abstract

Accurate electrical load forecasting is fundamental to the efficient operation of energy systems and plays a decisive role in both generation planning and the prevention of supply interruptions. Anticipating demand with precision enables energy generation and distribution to be adjusted effectively, reducing risks for both industrial and residential consumers. However, forecasting is challenged by climatic variations, demographic changes, and evolving consumption patterns, which limit the effectiveness of traditional approaches. Advanced machine learning techniques such as artificial neural networks have demonstrated potential to address these challenges, although their performance depends strongly on hyperparameter optimization. This study applies a multinodal forecasting methodology based on the Fuzzy ARTMAP network to predict short-term electricity demand at nine substations in New Zealand. The method involves an exhaustive search for network parameters, particularly the vigilance parameters ρ_a and ρ_b and the learning rate β, which are critical to model performance. The input data were extended with statistical measures—maximum, minimum, mean, and standard deviation—to evaluate their contribution to forecast accuracy. The results showed that the standard deviation provided the most consistent improvements among the windowing techniques, reducing the Mean Absolute Percentage Error (MAPE) in most substations. Parameter analysis further indicated that specific combinations such as ρ_a and β strongly influence category formation within the network, and consequently the precision of the forecasts.

Keywords: adaptive resonance theory; artificial neural networks; short-term forecasting; electricity system distribution; machine learning; multinodal load forecasting

Academic Editor: Firstname Lastname

Received: 24 August 2025
Revised: 29 September 2025
Accepted: 12 October 2025
Published:

Citation: Moreira Júnior, J.R.; da Silva, R.J.; dos Santos Júnior, C.R.; Abreu, T.; Lopes, M.L.M. Analysis and Optimization of Fuzzy ARTMAP Parameters for Multinodal Electric Load Forecasting. *Energies* **2025**, *1*, 0. https://doi.org/

1. Introduction

For electricity companies, providing accurate load forecasts is crucial to ensuring that the grid meets demand efficiently and reliably. Accurate forecasts make it possible to optimize supply while maintaining a continuous, stable, and economically viable service that avoids system interruptions and overloads. However, utilities face growing challenges in achieving higher accuracy, particularly with the increasing complexity of the grid due to the integration of intermittent renewable sources and varying consumption patterns [1].

Electricity load forecasting can be classified into four time horizons: very short term (VSLF), covering fractions of a second up to fifteen minutes; short term (STLF), covering hours to days; medium term (MTLF), covering weeks to months; and long term (LTLF), involving annual projections [1,2]. Traditionally, most forecasting approaches focus on overall system demand, which is essential for operational functions such as economic dispatch, safety assessment, and maintenance scheduling [3].

However, with the increasing complexity of power systems, multinodal forecasting that analyzes individual loads in substations, consumption zones, bars, or specific nodes has become equally important [3,4]. While global forecasting helps with the systemic balance between supply and demand, the multinodal approach is indispensable for static and dynamic system analysis such as load flow and voltage stability assessment [4]. Despite the challenges inherent in its greater complexity, this approach enables more effective infrastructure management on a regional scale [4,5]. Both global and multinodal forecasting, however, face challenges arising from the nonlinear and nonstationary nature of load data, which are influenced by factors such as extreme weather conditions, seasonality, and socioeconomic events.

Faced with these complexities, traditional linear models such as ARIMA and linear regression often prove inadequate and unable to capture the required dynamic and non-linear relations [6,7]. To address these limitations, a wide range of advanced data-driven methods, particularly those based on machine learning and Artificial Neural Networks (ANN), have emerged as superior alternatives for modeling these intricate relationships while offering greater precision in real-world scenarios.

A study by [8] concluded that while traditional statistical and machine learning methods have their strengths, deep learning techniques are more suitable for the dynamic and nonlinear characteristics of electricity load data. Studies on the Greek electricity system have highlighted that even simple feedforward ANNs can achieve a decent level of predictive performance, though their results heavily depend on the careful selection and quality assurance of the input data [9].

The literature reveals a variety of methods for predicting electrical loads, including both classic and innovative approaches. For instance, [10] obtained promising results by combining Autoregressive Integrated Moving Average (ARIMA) with ANNs for short-term electrical load forecasting, while [11] conducted a comprehensive evaluation of various techniques based on artificial intelligence and time series analysis. [12] demonstrated the importance of feature extraction and influencing factor analysis, showing that data mining improved results when combined with regression approaches such as Random Forest.

In recent years, more sophisticated approaches have been developed. [13] proposed a Bidirectional Long Short-Term Memory (BiLSTM) architecture that reduced Mean Absolute Error (MAE) by 25% and 46% compared to unidirectional Recurrent Neural Networks (RNNs) and Long Short-Term Memory networks (LSTMs) in 24-hour forecasts. Similarly, [14] further advanced the use of BiLSTM by incorporating stochastic weight averaging to improve generalization in substation-level forecasting.

[15] integrated a deep neural network with time series analysis and feature selection, achieving an MAPE of 3.78% and RMSE of 432.4, which outperformed ARIMA, Random Forest, and Support Vector Regression. [16] employed Temporal Convolutional Networks (TCNs) within a hierarchical framework that was resilient against missing or erroneous data, achieving reliable short-term forecasts for residential loads. At the distribution level, [17] introduced a lean forecasting approach combining clustering, neural networks, and Monte Carlo methods, while [18] proposed a step-by-step framework that explicitly incorporates electric vehicle charging stations into load forecasting.

To further overcome existing limitations, a wide range of sophisticated and hybrid models has been explored. For example, [19] highlighted that while conventional models such as Autoregressive Integrated Moving Average (ARIMA) have their place, more complex approaches like Fuzzy Time Series (FTS) outperform them due to their ability to handle nonlinear and uncertain data at low computational cost. Other hybrid approaches show similar promise: [20] proposed a method for multi-energy loads using a Radial Basis Function–AutoRegressive with eXogenous inputs (RBF-ARX) model for deterministic components and a Gaussian Mixture Model (GMM) for stochastic ones, improving forecast quality by up to 50%. Likewise, [21] combined an Autoencoder (AE) for dimensionality reduction with a Radial Basis Function Neural Network (RBFNN) for load forecasting, demonstrating better accuracy and efficiency compared to a standalone RBFNN.

Additionally, [22] compared the performance of ANN and Autoregressive with eXogenous inputs (ARX) models for net demand forecasting in distribution substations, concluding that the ANN model was better for direct forecasting due to the nonlinear nature of demand. Hybrid models have proven valuable in other domains as well, as seen in the work of [23], who used a Particle Filtering–ARIMA (PF-ARIMA) fusion model to predict battery useful life, achieving a 70% improvement over other methods by handling data specificities such as capacity regeneration.

A particularly relevant advance was presented by [24] with the Fuzzy-ARTMAP (FAM-ANN) continuous learning network, specifically developed for smart grids. This innovative solution proved capable of incorporating new data without requiring complete retraining, achieving a MAPE of $\approx$2% (60% better than the static version) and maintaining a consistent performance of 2.32% MAPE over 12 months, thereby combining precision, computational efficiency, and remarkable adaptability to dynamic scenarios.

Recently, multinodal forecasts have gained special prominence for their ability to integrate global planning with detailed local analysis. In this scenario, contributions include that of [25], who proposed a single-stage forecasting method. This approach simultaneously considers scenarios with and without the load contribution factor, offering a more efficient solution compared to conventional two-stage methods.

While traditional approaches require first predicting the global load and then predicting the local loads, the proposed method significantly simplifies computational complexity by performing these steps in an integrated manner while also demonstrating improvements in the precision of the results. Another notable advance was presented by [26], who introduced a methodology for forecasting consumption at all system nodes. Their method was based on the direct determination of specific rating coefficients for each voltage level, providing a comprehensive approach that encompasses everything from substations to supply zones and other critical components of the energy infrastructure. These advances in multinodal techniques pave the way for practical applications in real systems, such as the one presented in this paper.

However, it is crucial to note that the performance of these models depends fundamentally on the proper selection and optimization of their hyperparameters, such as learning rates and the number of neurons. An inadequate configuration can lead to problems of underfitting or overfitting, compromising the generalization of the model [27,28]. In this context, parameter optimization has proven to be a crucial strategy for improving the precision of load forecasting models. Techniques such as grid search, evolutionary algorithms, and Bayesian optimization make it possible to efficiently explore the parameter space in order to identify configurations that maximize predictive performance [29]. This importance is corroborated by work such as that of [30], which showed how hyperparameter optimization is decisive in reducing errors in short-term forecasting models for urban smart grids. Similarly, [31] obtained significant performance gains by applying optimization techniques to a fuzzy ARTMAP neural network for forecasting at disaggregated levels, combining it with singular spectrum analysis for noise treatment.

Despite the advances achieved with machine learning, deep learning, and hybrid approaches, several challenges remain. Many models, including deep learning architectures such as LSTM and transformer models, are highly sensitive to hyperparameter configurations, prone to overfitting, and often require large datasets and long training times. In multinodal forecasting, where the complexity is higher and data availability may be limited, systematic strategies for parameter optimization and data enrichment are still underexplored. These gaps open space for approaches such as Fuzzy ARTMAP, derived from Adaptive Resonance Theory (ART), which offers resistance to outliers, incremental learning without catastrophic forgetting, reduced dependence on large datasets, and fast convergence [32]. These characteristics make ARTMAP a suitable alternative for scenarios that demand adaptability, accuracy, and efficiency.

This study applies and expands the methodology proposed by [33] for short-term (24 h ahead) multinodal electricity load forecasting, using data from nine substations of a system in New Zealand. The approach focuses on implementing the fuzzy ARTMAP neural network [34], emphasizing an exhaustive search for optimal parameters, detailed analysis of parameter effects, and enrichment of input data with descriptive statistics (maximum, minimum, mean, and standard deviation) calculated from the participation factors in the periods $t-1$, $t-2$, and $t-3$. Its performance is compared with well-known benchmark models, including Multilayer Perceptron (MLP), Random Forest, and Support Vector Regression (SVR), to evaluate the method's effectiveness and investigate how network configurations and input variables influence the accuracy of short-term electricity demand forecasts.

The remainder of this article is organized as follows: Section 2 outlines the key contributions of this study to the field of electrical load forecasting; Section 3 describes the methodology, including the dataset, the fundamentals of the Fuzzy ARTMAP network, the strategies for global and multinodal load forecasting, the evaluation criteria, and the windowing techniques applied; Section 4 presents and discusses the results, offering a comparative analysis of the performance of different techniques and a detailed investigation of the effect of network parameters on the forecasts; finally, Section 5 summarizes the study's conclusions and suggests future research directions.

2. Contributions

This study offers contributions to the field of electricity load forecasting, focusing on the application and optimization of the Fuzzy ARTMAP network in a multinodal context. The main contributions are as follows:

- Systematic Parameter Optimization: We present a rigorous approach based on an exhaustive search for critical Fuzzy ARTMAP network parameters (ρ_a, ρ_b, and β). This goes beyond a simple application of the model, providing a detailed analysis of how parameter interactions influence network behavior, cluster formation, and forecast accuracy.
- Statistical Feature Validation for Data Enrichment: The enrichment of input data with statistical features such as the standard deviation is shown to improve forecasting performance across multiple substations. This provides a new and effective strategy for preprocessing time series data.
- Detailed Multinodal Forecasting Analysis: A comprehensive assessment of forecasting performance at a disaggregated level across nine individual substations is provided. The multinodal approach offers insight into local complexities of power networks that are often overlooked in global forecasting studies.

- Discussion of Model Robustness and Limitations: Key limitations of the proposed method are analyzed, including its sensitivity to parameter configurations and the challenge of applying a single optimized parameter set to large-scale systems.

3. Load Forecasting

This section details the methodology used for multinodal electricity load forecasting. It starts with a description of the dataset and then presents the Fuzzy ARTMAP neural network. This section also explains how global and multinodal forecasts are made, including the mathematical formulas for the participation factor. Finally, the criteria for comparing the results are presented.

3.1. Dataset

The database was supplied by the Electricity Commission of New Zealand and collected from the Centralized Dataset (CDS) from January 2007 to March 2009. It contains active power values measured every half an hour at each substation along with indicators for the day of the month, month, year, day of the week, holidays, time, and load sample value. The substations studied are in the Waikato region, located in the northern part of New Zealand's North Island. The substations considered were Kopu, Waikino, Waihou, Hamilton 11, Hamilton 33, Cambridge, Te Awamutu, Hinuera, and Kinleith.

For the training and validation stages of the Fuzzy ARTMAP network, a specific subset of this data was used covering the period from 8 December 2007 to 7 January 2008, totaling 1488 samples. The hyperparameter optimization for all models was performed on data from 8 December 2007 to 6 January 2008, with the objective of minimizing the error on the final day, 7 January 2008. The forecast period consisted of 48 load values (half-hourly) for a 24-h day (8 January 2008).

Figure 1 highlights various substations, distribution lines, and power stations on the map of the power transmission system in the north of New Zealand's North Island.

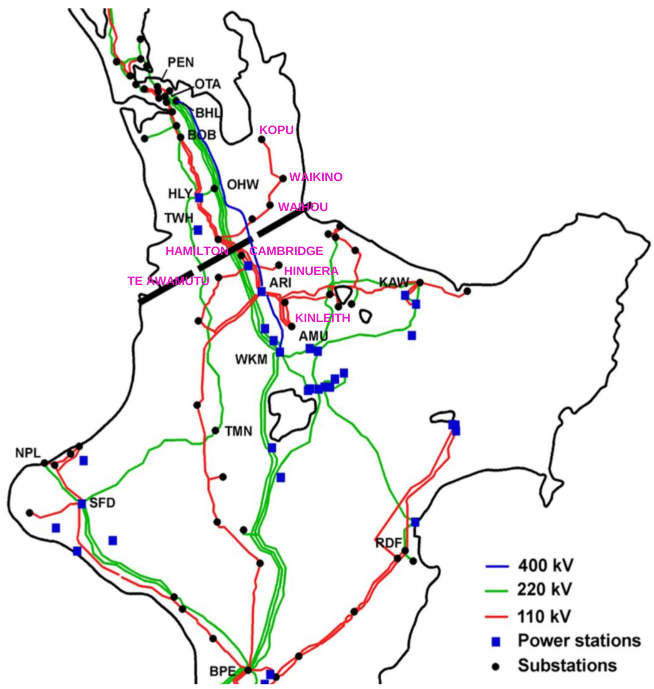

Figure 1. Map of the power transmission network in the north of New Zealand's North Island (adapted from [35]).

3.2. Fuzzy ARTMAP

The Fuzzy ARTMAP supervised learning network [34] consists of two Adaptive Resonance Theory modules, ART_a and ART_b. These modules perform calculations based on fuzzy set theory [36], specifically using the AND ($\wedge$) as defined by (1).

$$(x \wedge y)_i = \min\{x_i, y_i\} \tag{1}$$

Figure 2 illustrates the ART modules of the network. The input data and desired outputs are entered into the ART_a and ART_b modules, respectively; the inter-ART associative memory module is responsible for checking the correspondence between the input patterns and the expected output categories. A critical component of the network is the Match-Tracking used by the inter-ART module, which dynamically adjusts the vigilance parameter to achieve an optimal balance. This minimizes the prediction error while maximizing the model's overall ability to handle a variety of input patterns while at the same time producing accurate results even for unseen data. Prior to training, the weight matrices associated with the ART_a, ART_b, and inter-ART modules are initialized with values of 1, indicating that no categories are active in the network. During the training process, as the network is exposed to the input data, resonance occurs between the input patterns and the predicted output categories, leading to the activation of the corresponding categories in the network. In turn, this triggers the updating of these weight matrices to capture the relationships learned between the input patterns and the output categories. Algorithm 1 shows the pseudocode for the Fuzzy ARTMAP network.

The input data for the global forecasting model is composed of a set of 11 binary bits related to the exogenous data plus three global load values from previous time steps, resulting in a 14-dimensional input space. For each substation, the input of the Fuzzy ARTMAP network (ART_a) is composed of the global load at the current time (h) and the participation factors from three past time steps, resulting in a four-dimensional input space. It should be noted that the raw data are not preprocessed or normalized externally, as the network performs L1 normalization internally.

The Fuzzy ARTMAP network's performance is fundamentally influenced by the vigilance parameters ρ_a and ρ_b and the learning rate β. In this study, we perform an extensive hyperparameter search on these critical parameters, while other parameters such as ρ_{ab}, α, and ϵ are kept fixed. The search ranges were defined as follows: ρ_a from 0.90 to 0.99 (increment of 0.01), ρ_b from 0.980 to 0.999 (increment of 0.001), and β from 0.02 to 1.00 (increment of 0.01).

The vigilance parameter (ρ) acts as a similarity constraint for category formation. A higher ρ value enforces stricter similarity, leading to the creation of more categories (clusters). This is particularly relevant for ρ_b, which clusters the network's output. A large number of clusters results in a narrower range of values per cluster; conversely, a low ρ_b generates fewer clusters, grouping a wider range of output values. This can lead to a "discretization" or "straight-line" effect on the forecast curve, as diverse output values are mapped to a single oversimplified category. The α parameter, or learning rate, is a constant that indicates the extent to which new patterns influence a category's weight update. The β parameter, or training rate, controls the speed of learning, with a value of 1 implying faster training.

The inter-ART vigilance parameter ρ_{ab} acts as a match-tracking mechanism between the ART_a (input) and ART_b (output) modules. Its primary function is to ensure consistency between the input pattern and the expected output category. Because its role is to measure the compatibility between categories rather than to fine-tune the forecast precision itself, we considered its optimization to be non-critical for this study, and consequently kept its value fixed.

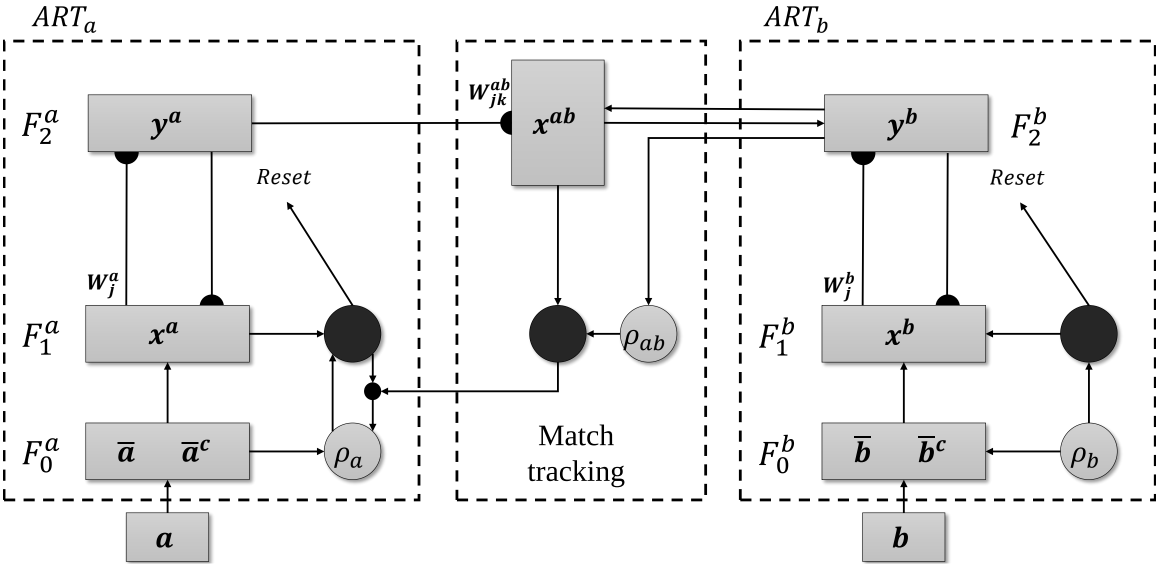

Figure 2. Fuzzy ARTMAP architecture.

Algorithm 1 Pseudocode for training the Fuzzy ARTMAP neural network.

Input: a: Input Data;
b: Desired output;
α: Learning Rate ($\alpha > 0$);
β: Training Parameter ($0 < \beta \leq 1$);
ρ_a: Vigilance Parameter Module A ($0 < \rho_a \leq 1$);
ρ_b: Vigilance Parameter Module B ($0 < \rho_b \leq 1$);
ρ_{ab}: Vigilance Parameter Inter-ART Module ($0 < \rho_{ab} \leq 1$);
ϵ: Increase.
Output: W^{ab}

procedure
$\boldsymbol{W}^a = 1 \quad \boldsymbol{W}^b = 1 \quad \boldsymbol{W}^{ab} = 1$
$\bar{\boldsymbol{a}} = \dfrac{\boldsymbol{a}}{\left|\sum_i^M a_i\right|} \quad \bar{\boldsymbol{b}} = \dfrac{\boldsymbol{b}}{\left|\sum_i^M b_i\right|}$
$\bar{a}_i^c = 1 - \bar{a}_i \quad \boldsymbol{I}_a = [\bar{\boldsymbol{a}} \quad \bar{\boldsymbol{a}}^c] \quad \bar{b}_i^c = 1 - \bar{b}_i \quad \boldsymbol{I}_b = \left[\bar{\boldsymbol{b}} \quad \bar{\boldsymbol{b}}^c\right]$
while Data for training exists **do**
  for all clusters W_k^b **do**
    $T_k^b = \dfrac{|\boldsymbol{I}_b \wedge \boldsymbol{W}_k^b|}{\alpha + |\boldsymbol{W}_k^b|}$
  $flag = True$
  while flag = True **do**
    $K = \max\{T_k^b : k = 1, \ldots, N_b\}$
    if $\dfrac{|\boldsymbol{I}_b \wedge \boldsymbol{W}_K^b|}{|\boldsymbol{I}_b|} \geq \rho_b$ **then**
      $\boldsymbol{W}_K^b = \beta(\boldsymbol{I}_b \wedge \boldsymbol{W}_K^b) + (1 - \beta) \cdot \boldsymbol{W}_K^b$
      $y^b = \begin{cases} 0, & k \neq K, \\ 1, & k = K. \end{cases}$
      $flag = False$

Algorithm 1 *Cont.*

else
$T_J^b = 0$
for all clusters W_k^a **do**
$$T_j^a = \frac{|\boldsymbol{I}_a \wedge \boldsymbol{W}_j^a|}{\alpha + |\boldsymbol{W}_j^a|}$$
$flag = True$
while flag = True **do**
$J = \max\{T_j^a : j = 1, ..., N_a\}$
if $\frac{|\boldsymbol{I}_a \wedge \boldsymbol{W}_J^a|}{|\boldsymbol{I}_a|} \geq \rho_a$ **then**
if $\frac{|\boldsymbol{y}^b \wedge \boldsymbol{W}_J^{ab}|}{|\boldsymbol{y}^b|} \geq \rho_{ab}$ **then**
$\boldsymbol{W}_J^a = \beta(\boldsymbol{I}_a \wedge \boldsymbol{W}_J^a) + (1-\beta) \cdot \boldsymbol{W}_J^a$
$$W_{JK}^{ab} = \begin{cases} 0, & j \neq J, k \neq K, \\ 1, & j = J, k = K. \end{cases}$$
$flag = False$
else
$T_J^a = 0$
$$\rho_a = \frac{|\boldsymbol{I}_a \wedge \boldsymbol{W}_J^a|}{|\boldsymbol{I}_a|} + \epsilon$$
$T_J^a = 0$

3.3. Global Load Forecasting

To forecast the multinodal load, it is necessary to obtain the global (forecast) load; in turn, this is used to calculate the participation factor provided by Equation (2), which is fundamental to multinodal forecasting. Global forecasting is carried out by a system called the global load forecasting system, which is based on the Fuzzy ARTMAP neural network [33]. The input data set of the ART$_a$ module in this system contains exogenous data such as time of day, day of the week, month, holidays, daylight savings time, and global load (CG) at three previous time instants ($t-1$, $t-2$, and $t-3$). This representation of the global load includes the "sliding window" technique proposed by [37] and aims to identify the behavior of the load profile. The forecasting result consists of the CG at time t, which is provided by the output of the ART$_b$ module of the Fuzzy ARTMAP network. The exogenous variables are described in detail in Table 1, and are composed of 11 binary bits related to the exogenous data plus the three global load values from previous time steps, resulting in a 14-dimensional input space. Figure 3 details the global load forecasting strategy with the Fuzzy ARTMAP network.

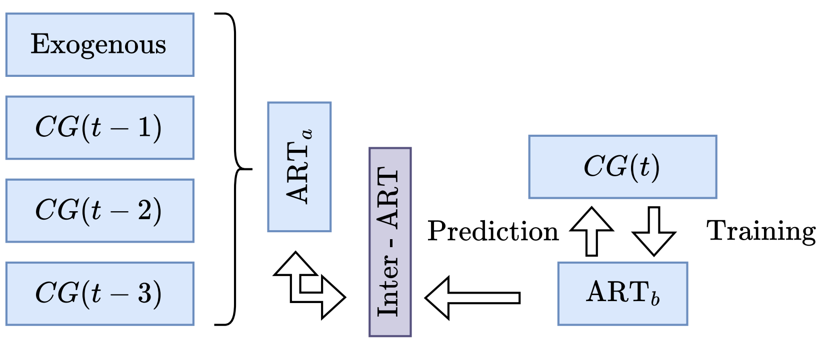

Figure 3. Strategy for global load forecasting with FAM-ANN.

Table 1. Encoding of exogenous variables.

Variable	Bits	Encoding
Day of the Week	3 bits	001—Monday 010—Tuesday 011—Wednesday 100—Thursday 101—Friday 110—Saturday 111—Sunday
Time of Day	6 bits	[000001] to [110000] (representing 48 half-hour values)
Holiday	1 bit	1—holiday 0—not a holiday
Daylight Saving Time	1 bit	1—daylight saving time 0—not in daylight saving time

3.4. Multinodal Load Forecasting

The multinodal load forecasting system (PCM) is based on the Fuzzy ARTMAP neural network. Forecasting in this system is carried out in modules, where each module contains a neural network responsible for predicting the load at individual locations such as substations, transformers, and feeders. To perform substation load forecasting, the multinodal load forecasting system uses the global participation factor (FPG), defined as the percentage of each substation's load within the total system load, as specified in (2) [37,38]:

$$FPG_j(t) = \frac{CM_j(t)}{CG(t)} \tag{2}$$

in which:

- $CM_j(t)$ is the multinodal load associated with substation j at time t.
- $CG(t)$ is the global load, which corresponds to the addition of the loads of each substation at time t.

For each substation, the load forecast is obtained by the multinodal forecast. The input dataset for the Fuzzy ARTMAP network for each substation j consists of the global load at time t, $CG(t)$, and the participation factors of substation j at times $t-1$, $t-2$, and $t-3$. The network output in the PCM system corresponds to the predicted participation factor at time t. The flowchart of the multinodal forecasting system is shown in Figure 4.

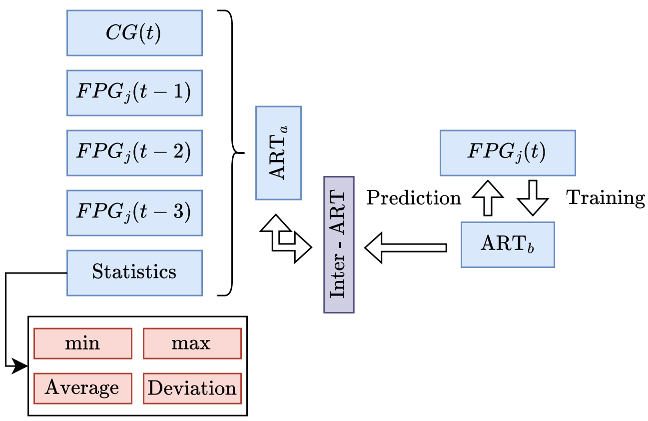

Figure 4. Multinodal load forecasting system.

Within this system, statistical features derived from the global participation factors (FPG_j) at times $t-1$, $t-2$, and $t-3$ were evaluated as potential input extensions to the network. The considered statistics included the mean, standard deviation, maximum, and minimum values, which were assessed individually in order to determine their impact on forecasting performance.

These statistical features are part of a feature engineering strategy. Feature engineering aims to transform raw data into informative input variables that help the model to capture relevant patterns. By deriving statistics from the recent participation factors, each feature provides a distinct perspective on the substation's recent load behavior, such as its central tendency, variability, or extreme values [39–41]. Evaluating these features separately allows the most effective input to be identified for each substation and forecasting horizon.

From a theoretical perspective, each derived feature adds a new dimension to the input space. For example, using only the mean of the past three FPG_j values extends the original three-dimensional lag space by one dimension. This dimensionality increase provides the Fuzzy ARTMAP network with richer information, enhancing its ability to separate patterns corresponding to different load behaviors and improving generalization [42,43].

The mean is obtained as described by (3):

$$\overline{FPG}_j = \frac{1}{N}\sum_{i=1}^{N} FPG_j(t-i) \tag{3}$$

in which:

- $N = 3$ (considering the values at $t-1$, $t-2$, and $t-3$).
- $FPG_j(t-i)$ is the global participation factor of substation j at time $t-i$.

The standard deviation, which measures the variability of the data around the mean, is calculated by (4).

$$s_{FPG_j} = \sqrt{\frac{1}{N}\sum_{i=1}^{N}\left(FPG_j(t-i) - \overline{FPG}_j\right)^2} \tag{4}$$

The maximum and minimum values are determined by Equations (5) and (6).

$$FPG_j^{\max} = \max\left(FPG_j(t-1), FPG_j(t-2), FPG_j(t-3)\right) \tag{5}$$

$$FPG_j^{\min} = \min\left(FPG_j(t-1), FPG_j(t-2), FPG_j(t-3)\right) \tag{6}$$

By evaluating each statistic individually, the most informative feature can be selected for each substation, thereby optimizing the network's predictive performance. Empirical studies indicate that networks using feature-augmented inputs outperform those trained solely on raw lagged values, particularly in capturing trends, variability, and extreme events.

After the participation factor has been predicted at time t, the substation load $PCM_j(t)$ is obtained by multiplying the predicted participation factor $\widehat{FPG}_j(t)$ by the predicted global load $\widehat{CG}(t)$ (7) [33,37]:

$$PCM_j(t) = \widehat{FPG}_j(t) \times \widehat{CG}_j(t). \tag{7}$$

3.5. Benchmark Models and Hyperparameter Optimization

To validate the effectiveness of our proposed Fuzzy ARTMAP methodology, we compared its performance with three widely used machine learning models implemented in the Scikit-learn library in Python [44]: Multi-layer Perceptron (MLP), Random Forest, and Support Vector Regression (SVR). For a fair comparison, each model went through a hyperparameter optimization process to find its best configuration, using the same training and validation period as Fuzzy ARTMAP. The optimization used a grid search, with MAPE as the main criterion for selecting the best model.

These models were chosen because they represent different approaches to time series forecasting. MLP is a type of artificial neural network that captures nonlinear relationships by learning patterns across multiple layers of neurons, making it a stronger alternative to linear models [45,46]. Random Forest combines many decision trees built from random subsets of the data, which lowers the risk of overfitting and produces more stable predictions [47]. SVR, an extension of Support Vector Machines, models nonlinear relationships through kernels, is less sensitive to outliers, and balances model complexity with generalization by defining a margin of tolerance around the regression function [48].

The hyperparameter search spaces for each model were defined as follows:

- MLP
  - Hidden layer sizes: (5), (10), (5, 5), (10, 5), (5, 10), (20), (20, 15), (20, 30), (100), (200), (100, 50)
  - Maximum number of iterations: 1500
  - Activation function: 'logistic', 'tanh', 'relu'
  - Optimization method (solver):
    - 'LBFGS' (Limited-memory Broyden–Fletcher–Goldfarb–Shanno)
    - 'SGD' (Stochastic Gradient Descent)
    - 'ADAM' (Adaptive Moment Estimation)
- Random Forest
  - Number of trees (estimators): 50, 100, 200
  - Maximum depth: 2, 5, 8, 10, 15, 20, 25, 30, None
  - Minimum samples required to split: 2, 5, 10
  - Splitting criterion: 'squared_error', 'absolute_error', 'friedman_mse', 'poisson'
- SVR
  - Kernel type: 'RBF', 'poly', 'sigmoid'
  - Regularization parameter (C): 1, 10, 100
  - Tolerance margin (epsilon): 0.01, 0.1, 0.5

3.6. Criteria for Comparing Results

The Mean Absolute Percentage Error (MAPE) is a metric that is commonly used to assess the precision of forecasting models. It is calculated by taking the mean of the absolute percentage errors between the predicted values and the actual values. The MAPE formula is provided by (8):

$$\text{MAPE} = \frac{1}{n}\sum_{t=1}^{n}\left|\frac{FPG_t - \widehat{FPG}_t}{FPG_t}\right| \times 100 \quad (8)$$

in which:

- FPG_t represents the actual value of the participation factor at time t.
- $\widehat{FPG}_t$ represents the predicted value of the participation factor at time t.
- n is the number of hours, with a reading every half hour.

MAPE is widely used due to its interpretability; it expresses the error as a percentage, which makes it easier to understand the model's performance [49]. Smaller MAPE values indicate more precise forecasts. The use of MAPE is particularly well suited for this study, as it provides a normalized error measure across different substations and load profiles. This allows for a direct comparison of forecasting quality between substations with varying load levels, since the metric is not biased by the scale of the load. Lower MAPE values mean better forecasts.

4. Load Forecast Result

This section presents and discusses the results obtained from the multinodal electricity load forecasting. It begins with a detailed analysis of the MAPE values for the nine substations, comparing the performance of different windowing techniques, followed by an in-depth look at the behavior of the Fuzzy ARTMAP parameters and their impact on forecasting precision.

4.1. Results

The results presented in Table 2 provide a detailed analysis of the MAPE values for nine substations, using windowing methods that consider the maximum, minimum, mean, and standard deviation values of the samples calculated considering the participation factor at times $t-1$, $t-2$, and $t-3$.

Table 2. Results by substation.

Substation	MAPE (%)			
	Maximum	Minimum	Mean	Standard Deviation
Kopu	10.35	9.68	9.64	4.79
Waikino	6.93	5.24	7.11	5.00
Waihou	3.96	3.99	3.68	3.72
Hamilton 11	4.05	3.79	3.68	4.25
Hamilton 33	3.57	3.35	3.21	3.46
Cambridge	3.16	2.72	3.08	3.07
Te Awamutu	4.34	3.07	3.13	3.5
Hinuera	3.39	3.44	3.47	3.60
Kinleith	5.40	5.40	5.40	5.15

Analysis of the results reveals different behavior between the substations. The Kopu substation showed relatively stable performance in terms of MAPE, with values of 10.35% (maximum), 9.68% (minimum), and 9.64% (mean). On the other hand, the standard deviation introduced a significant improvement, reducing the MAPE to 4.79%. This indicates a considerable improvement in the forecast. Figure 5 shows the load curve, where it can be seen that the predicted values follow the actual load well throughout the day. The range around the forecast curve is relatively narrow, indicating that the variability within the cluster of the forecast values is low.

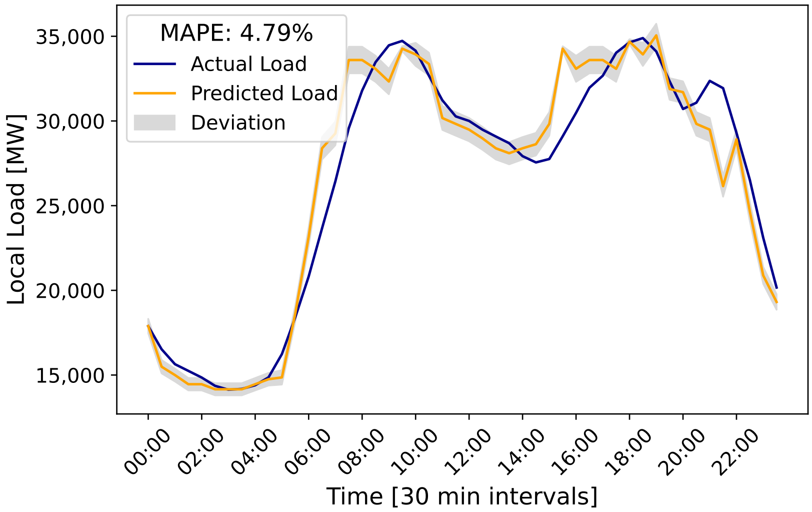

Figure 5. Actual and forecast values for Kopu substation.

Waikino, on the other hand, revealed a trend of continuous improvement in forecasts when using different windowing techniques. The MAPE showed a significant reduction when using the minimum value (5.24%) compared to the maximum value (6.93%) and the mean (7.11%). In addition, using the standard deviation resulted in an MAPE of 5.00%, the lowest value observed for Waikino. Figure 6 shows the forecast and actual load curves as well as the range obtained by the standard deviation within the cluster of forecasts. This range is slightly wider than that observed in Kopu, suggesting greater variability in the predicted values. However, the predictions still align well with the actual load, demonstrating the model's effectiveness even in the face of this variability.

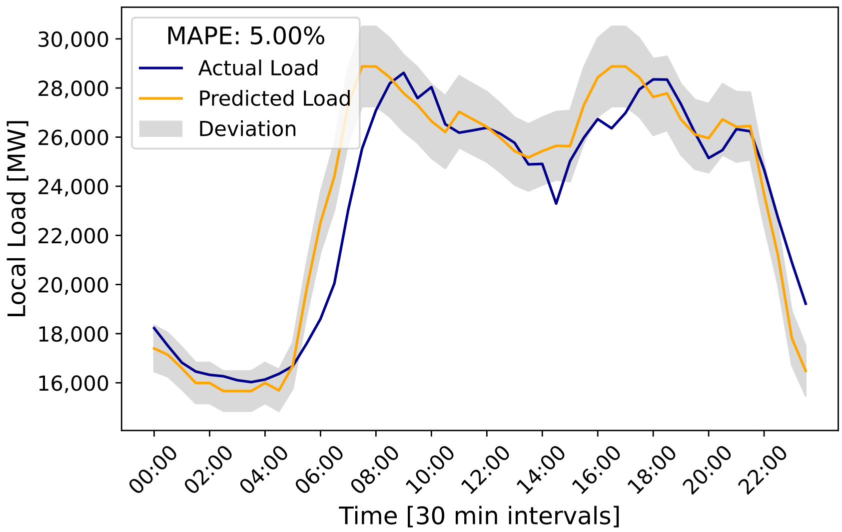

Figure 6. Actual and forecast values for Waikino substation.

For Waihou, the MAPE results varied from 3.99% (minimum) to 3.68% (mean). This variation suggests that the different windowing techniques do not have a significant impact on the precision of the forecasts for this substation. The mean showed the best result, with an MAPE of 3.68%. The forecast curve in the Figure 7 closely follows the actual load and the range around the forecast is relatively narrow, indicating that the model captures load fluctuations well and has low variability in the forecast clusters.

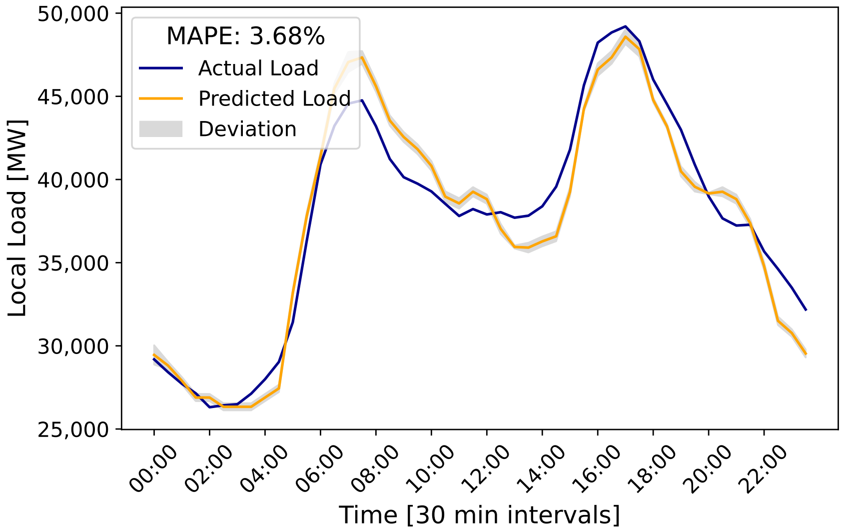

Figure 7. Actual and forecast values for Waihou substation.

Hamilton 11 showed a moderate variation in MAPE values, with a maximum difference of 0.57% between the different methods. The best result was obtained using the mean (3.68%), followed by the minimum (3.79%). The moderate variation suggests that all the windowing techniques offer relatively accurate prediction, although the mean was able to better capture the trend of the data in this substation. As shown in Figure 8, the confidence interval around the forecasts is narrow, indicating that the forecast is quite accurate and that the variability in the forecasts is low.

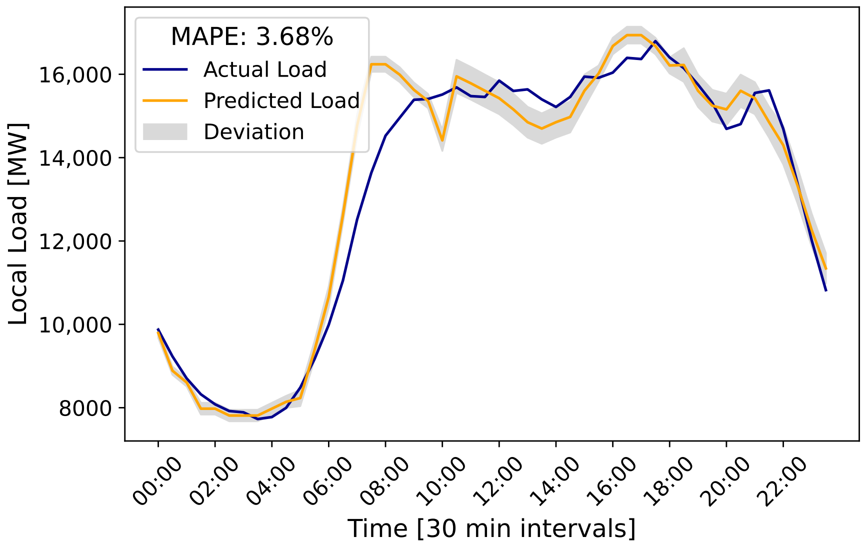

Figure 8. Actual and forecast values for Hamilton 11 substation.

For Hamilton 33, all MAPE values were lower than 4.00%, with the best result obtained by the mean (3.21%). The corresponding prediction curve can be seen in Figure 9. The consistency of the results suggests that windowing techniques are highly effective for this substation. In particular, inclusion of the mean seems to capture important characteristics that contribute to more precise predictions.

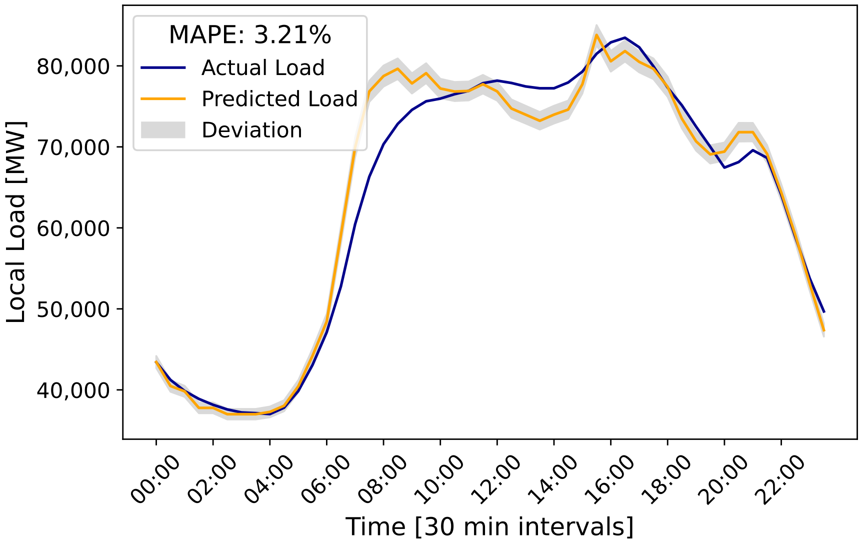

Figure 9. Actual and forecast values for Hamilton 33 substation.

Cambridge showed a smooth and constant variation in MAPE values, from 3.16% (maximum) to 2.72% (minimum), with the minimum providing the best result, as shown in Figure 10. It is worth noting that the minimum in Cambridge was not only the best result among all the substations but also had the lowest MAPE among the four techniques used, showing uniform and accurate performance. The forecast curve followed the actual curve well, with a slight divergence observed between 5:30 and 8:30. The interval around the forecast is quite narrow as a result of the low variability of the clusters.

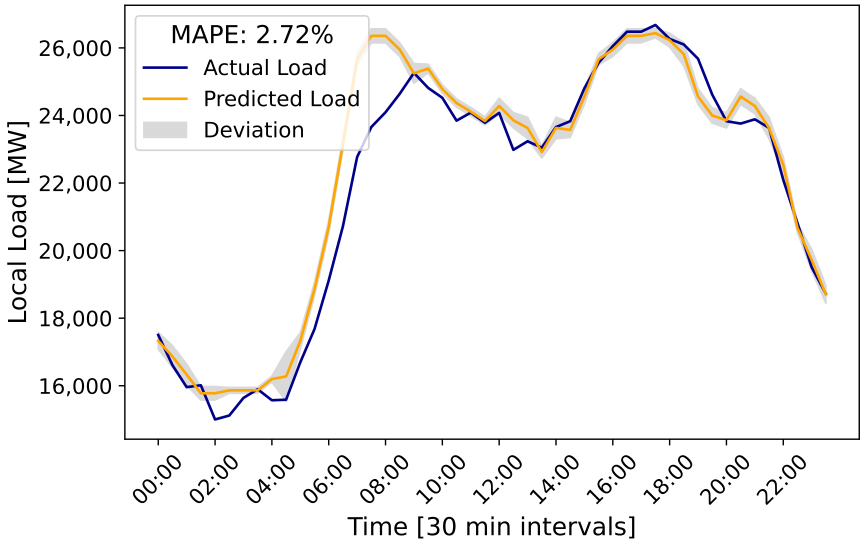

Figure 10. Actual and forecast values for the Cambridge substation.

Te Awamutu showed MAPE values of less than 4.5%, with the best result obtained with the minimum value (3.07%) and the highest with the maximum (4.34%). The forecast curve shown in Figure 11 shows predicted behavior very close to the real values. In addition, the forecast showed no variability within the clusters, suggesting that for this substation there were no significant differences between the load values within the clusters.

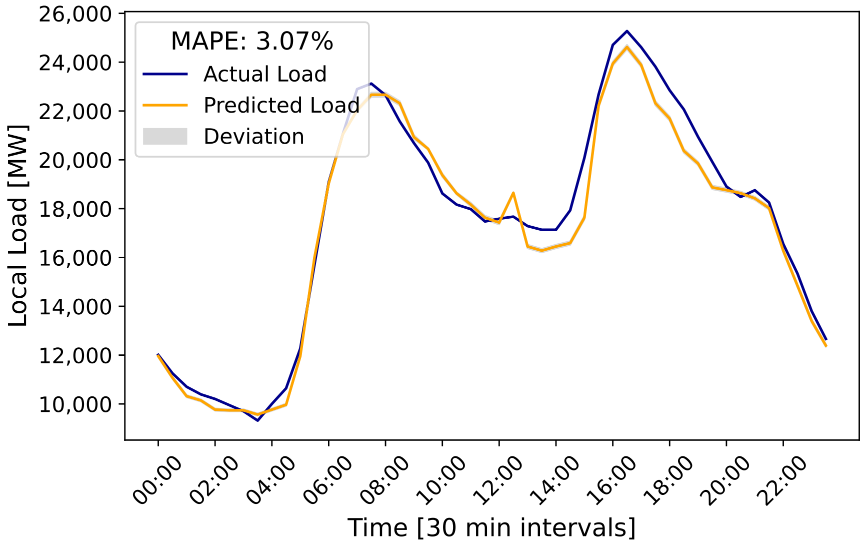

Figure 11. Actual and forecast figures for the Te Awamutu substation.

Hinuera maintained a similar variation in MAPE values, between 3.39% and 3.60%, showing consistent performance across the different windowing techniques. This performance reveals that all the techniques offer relatively accurate predictions, with the standard deviation being slightly more effective in this substation. The range around the prediction is slightly wider, as shown in Figure 12, indicating more variability in the predicted values; however, the predictions still follow the actual load well.

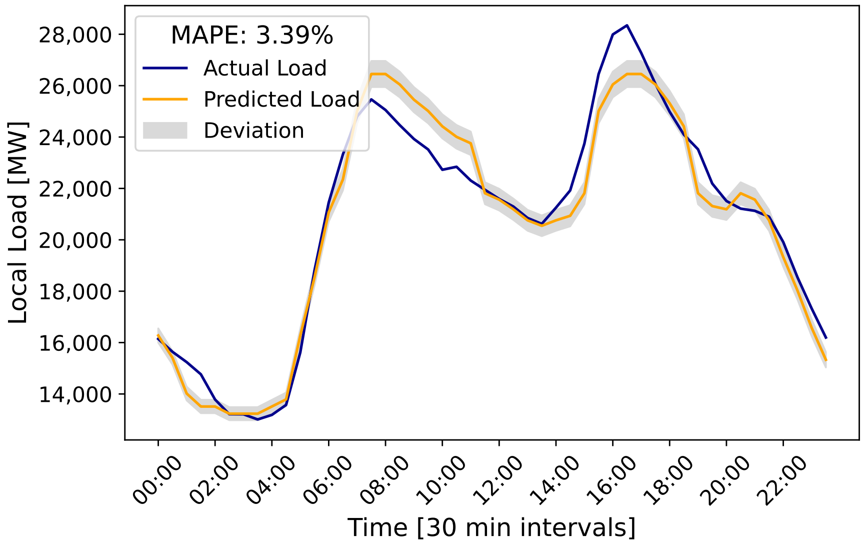

Figure 12. Actual and forecast figures for the Hinuera substation.

Finally, Kinleith showed an improvement in MAPE with the standard deviation (5.15%), standing out from the other techniques that kept MAPE constant at 5.40%. The prediction curve can be seen in Figure 13. It shows greater variability in the interval around the prediction curve, indicating that there was a greater variety of values within the clusters.

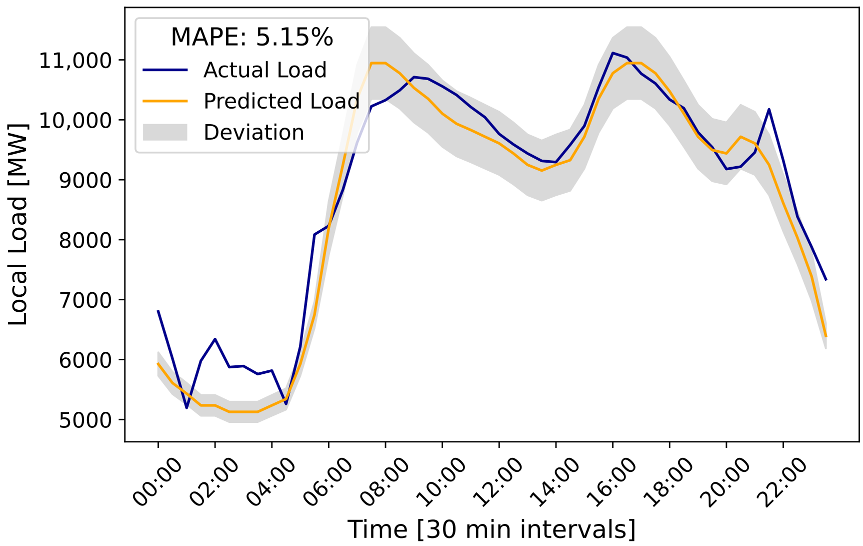

Figure 13. Actual and forecast values for the Kinleith substation.

In general, substations such as Kopu, Waikino and Kinleith stand out in the forecasts when using the standard deviation. On the other hand, Waihou, Hamilton 11, and Hamilton 33 showed better results when using the minimum value. Other substations such as Cambridge, Te Awamutu, and Hinuera also showed improvements with different strategies.

The standard deviation and minimum value proved to be effective techniques in most cases, with each offering its own advantages for predicting electrical load. The combination of parameters that produced the best results can be analyzed in Table 3.

When analyzing the table with the configuration of parameters that obtained the best results for each substation, we observed a relationship between these parameters and those substations that showed the greatest variability in the intervals around the prediction curve. The Kopu, Waikino, Hamilton 11, and Kinleith substations showed the greatest variations. This is directly related to the ρ_b parameter, which controls the required similarity for a given piece of data to belong to the cluster. Lower values of ρ_b relax this restriction, allowing slightly different values to be included. On the other hand, values closer to 1 restrict similarity so that relatively close data does not fit into the cluster, which can result in the creation of a new cluster to house it. The Kinleith substation, although it had a wider range with ρ_b close to 1, had high variability due to the β parameter responsible for the learning rate being close to zero. This reduced the creation of new categories, increasing the variability within the existing clusters.

Table 3. Setting parameters for the best results.

Substation	Statistics	Parameters
Kopu	Standard Deviation	$\rho_a = 0.91$, $\beta = 0.96$, $\rho_b = 0.991$
Waikino	Standard Deviation	$\rho_a = 0.95$, $\beta = 0.40$, $\rho_b = 0.996$
Waihou	Mean	$\rho_a = 0.99$, $\beta = 0.92$, $\rho_b = 0.996$
Hamilton 11	Mean	$\rho_a = 0.91$, $\beta = 0.40$, $\rho_b = 0.998$
Hamilton 33	Mean	$\rho_a = 0.91$, $\beta = 0.98$, $\rho_b = 0.997$
Cambridge	Minimum	$\rho_a = 0.95$, $\beta = 0.78$, $\rho_b = 0.999$
Te Awamutu	Minimum	$\rho_a = 0.99$, $\beta = 1.00$, $\rho_b = 0.999$
Hinuera	Maximum	$\rho_a = 0.91$, $\beta = 0.44$, $\rho_b = 0.994$
Kinleith	Standard Deviation	$\rho_a = 0.97$, $\beta = 0.02$, $\rho_b = 0.999$
Fixed parameters: $\rho_{ab} = 1.00$, $\alpha = 0.001$, $\epsilon = 0.0005$		

It can be seen that the Waihou, Hamilton 33, Cambridge, and Te Awamutu substations have high values for ρ_a, ρ_b, and β, which is directly related to greater variability and standard deviation within the clusters formed by the prediction labels that represent the actual load. These parameters indicate greater rigidity in the formation of these clusters, ensuring that only values with high similarity are grouped together. On the other hand, substations such as Waikino, Hamilton 11, and Kinleith have lower ρ_a and β values and show greater variability, as reflected in larger shaded areas around the prediction curves.

The results show notable differences in forecasting performance across the nine substations, reflecting the unique characteristics of each substation's load profile. Substations such as Kopu and Kinleith benefited most from including the standard deviation as an input, suggesting more volatile or irregular load patterns; in contrast, Waihou and Hamilton 33 performed best when the mean was used, indicating more stable and predictable consumption. This demonstrates that the Fuzzy ARTMAP model adapts to the most informative statistical feature for each case, thereby maximizing prediction accuracy. A single forecasting strategy does not fit all substations in a multinodal system; tailoring the approach to each substation's characteristics is necessary to achieve the best results.

4.2. Computational Performance and Method Practicality

The computational performance of the Fuzzy ARTMAP method was evaluated during the forecasting phase to assess its practical applicability. Figure 14 shows the prediction time per sample (measured in microseconds, µs) for each substation and each statistical windowing technique.

The results indicate that the proposed method is highly efficient. For most substations and windowing approaches, the prediction time per sample remains below 1 µs. The mean, maximum, and minimum techniques consistently show the lowest computational cost across all substations.

The standard deviation approach, which often yields the most accurate forecasts, requires slightly more computation. Notable increases in prediction time occur at the Waihou and Te Awamutu substations, reaching approximately 4 µs and 2 µs per sample, respectively. Despite these peaks, the times remain in the microsecond range, supporting real-time application.

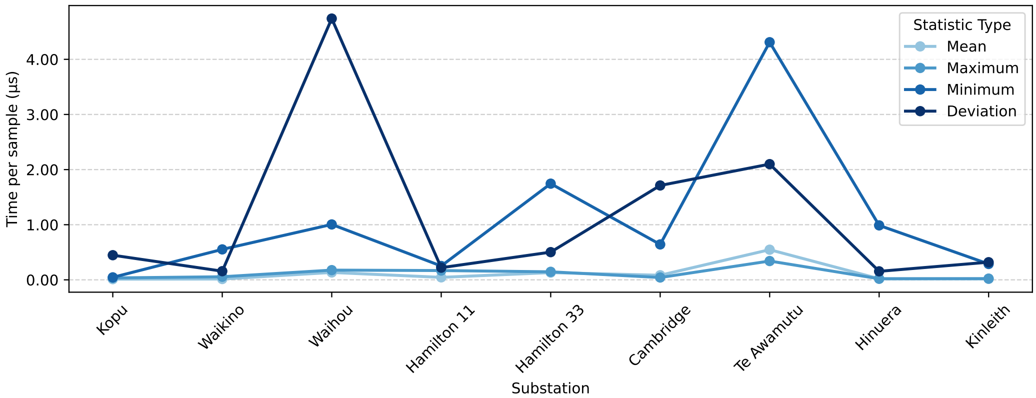

Figure 14. Prediction time per sample for all substations and windowing techniques.

This efficiency highlights an advantage of the Fuzzy ARTMAP architecture. Unlike complex deep learning models, which demand extended training and specialized hardware, this method provides fast predictions with minimal computational resources. The combination of rapid training and prediction times makes the Fuzzy ARTMAP model suitable for scalable real-time load forecasting in dynamic smart grid environments.

4.3. Analysis of Parameters

Analysis of the parameters of the Fuzzy ARTMAP network applied to predicting electrical loads in substations is crucial to optimizing its performance, since it is an architecture that is sensitive to changes in parameters. To adjust the parameters, β was varied from 0.02 to 1.00 with an increment of 0.02, ρ_a of the ART_a module from 0.91 to 0.99 with an increment of 0.02, and ρ_b of the ART_b module from 0.98 to 0.999 with an increment of 0.001. This analysis was applied to all substations, taking into account the expansion of the input data dimension with the maximum, minimum, mean, and standard deviation values of the load participation factor at times $t-1$, $t-2$, and $t-3$. The discussion on the behavior of the parameters is reported for the Kopu substation; similar behavior was observed for the other substations, especially in relation to the parameters ρ_a, ρ_b, β, and the number of categories in the ART_a and ART_b modules of Fuzzy ARTMAP.

Figure 15 illustrates the three-dimensional relationship between the parameters ρ_a, β, and the number of categories (neurons) created in module A of the Fuzzy ARTMAP network. In Figure 15a, it can be observed that high values of ρ_a combined with high values of β result in a greater number of categories. This combination of parameters makes the network more prone to creating multiple categories due to the greater restriction imposed by ρ_a, which prevents new data from being allocated to existing clusters, necessitating the creation of new categories to accommodate them whenever the similarity does not reach the stipulated threshold (ρ). In contrast, although the β parameter allows for fast learning without many training cycles when $\beta = 1$, it prevents the old information contained in the clusters from remaining. Instead, this information is replaced by the current information, leading to the creation of more categories. Similar behavior is observed for Figure 15b–d, which illustrates the same relationship with the insertion of the minimum, mean, and standard deviation of the three previous loads.

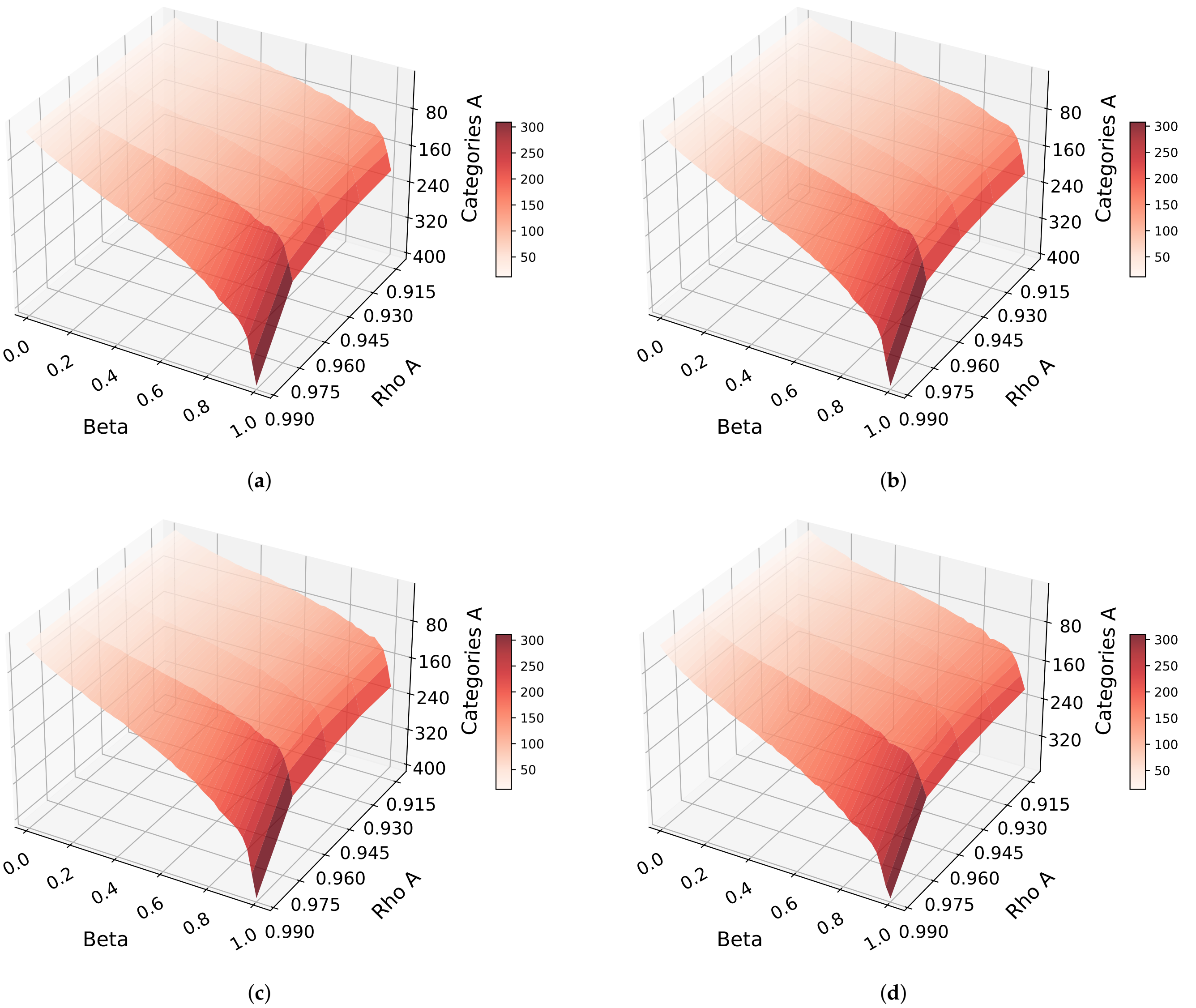

Figure 15. Three-dimensional visualization of the relation between the parameters ρ_a, β, and number of categories in module A: (**a**) maximum, (**b**) minimum, (**c**) mean, and (**d**) standard deviation.

Figure 16 follows a similar structure to Figure 15 but focuses on module B of the Fuzzy ARTMAP network. In Figure 16a, it can be observed that high values of ρ_b combined with high values of β favor the creation of a greater number of categories, similar to what was observed in Figure 16a, but generating a smaller number of clusters because these clusters are responsible for housing the network's output information.

The interaction between the parameters ρ_b, β, and the Mean Absolute Percentage Error (MAPE) can be seen in Figure 17 when inserting the maximum, minimum, mean, and standard deviation of the three previous loads into the input data. This makes it easier to understand which values of β and ρ_b produced the best results.

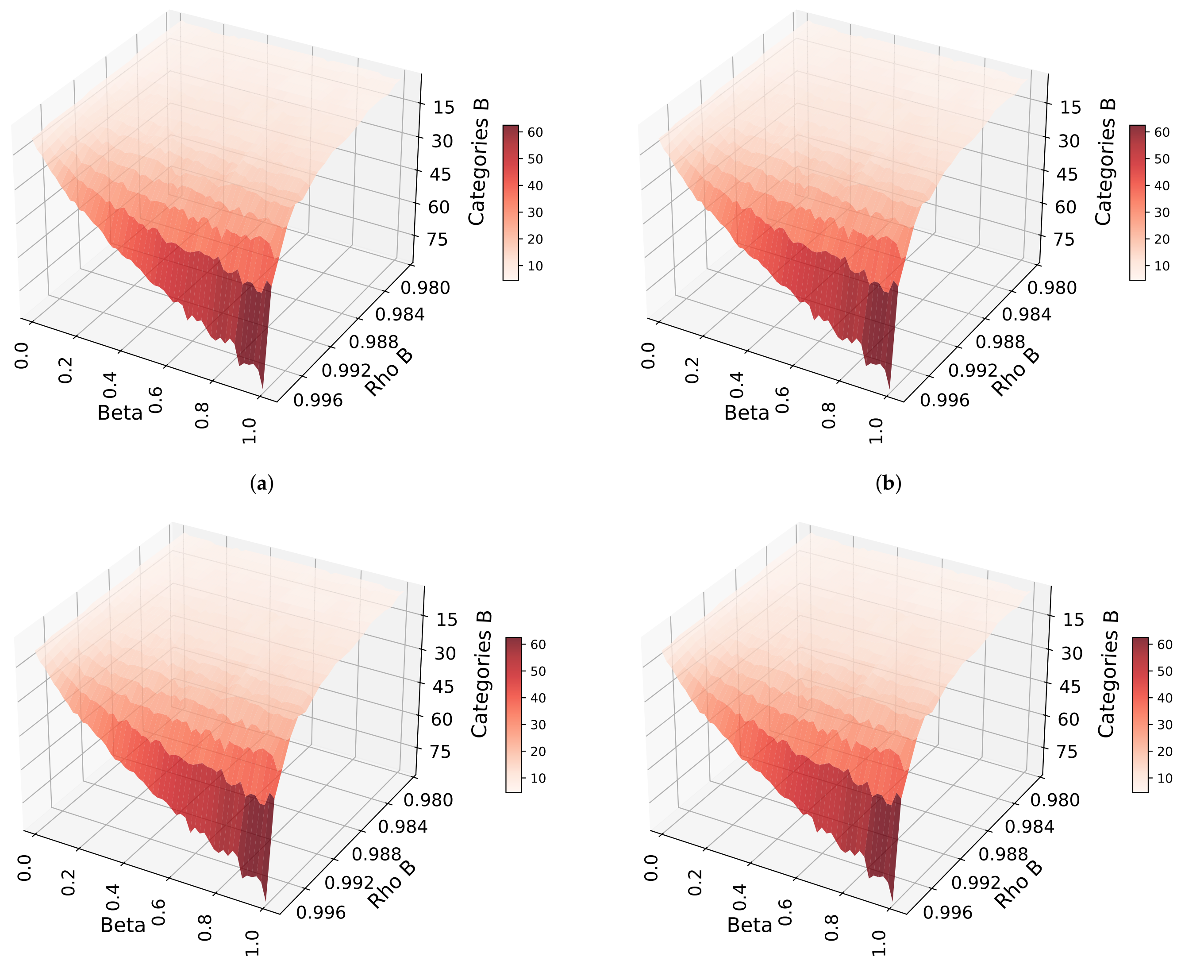

(**a**) (**b**) (**c**) (**d**)

Figure 16. Three-dimensional visualization of the relation between the parameters ρ_b, β, and number of categories in module B: (**a**) maximum, (**b**) minimum, (**c**) mean, and (**d**) standard deviation.

In Figure 17a, the lowest MAPE values are observed for combinations of high ρ_b values, while β shows more flexibility, oscillating within the $[0, 1]$ range. This relationship between low MAPE values and high ρ_b values indicates that the network needs to create a considerable number of categories in module B during training in order to obtain good results. This allows the network to predict results more accurately when it comes to forecasting. However, the value of β does not seem to have a significant impact on the result, unlike its influence on the creation of clusters reported in Figure 16.

Similar behavior is observed when the other statistics are used to expand the input dimension of the data, as shown in Figure 17b–d. In addition, it can be seen that for Figure 17d there is a greater fluctuation of the MAPE for the walls, causing more irregularities on the surface compared to the others. This unevenness indicates that the model's response is more unstable when the standard deviation is used as one of the inputs, reflecting greater sensitivity to variations in the data. The more uneven surface also reveals that small adjustments to the ρ_b and β parameters can lead to significant changes in MAPE.

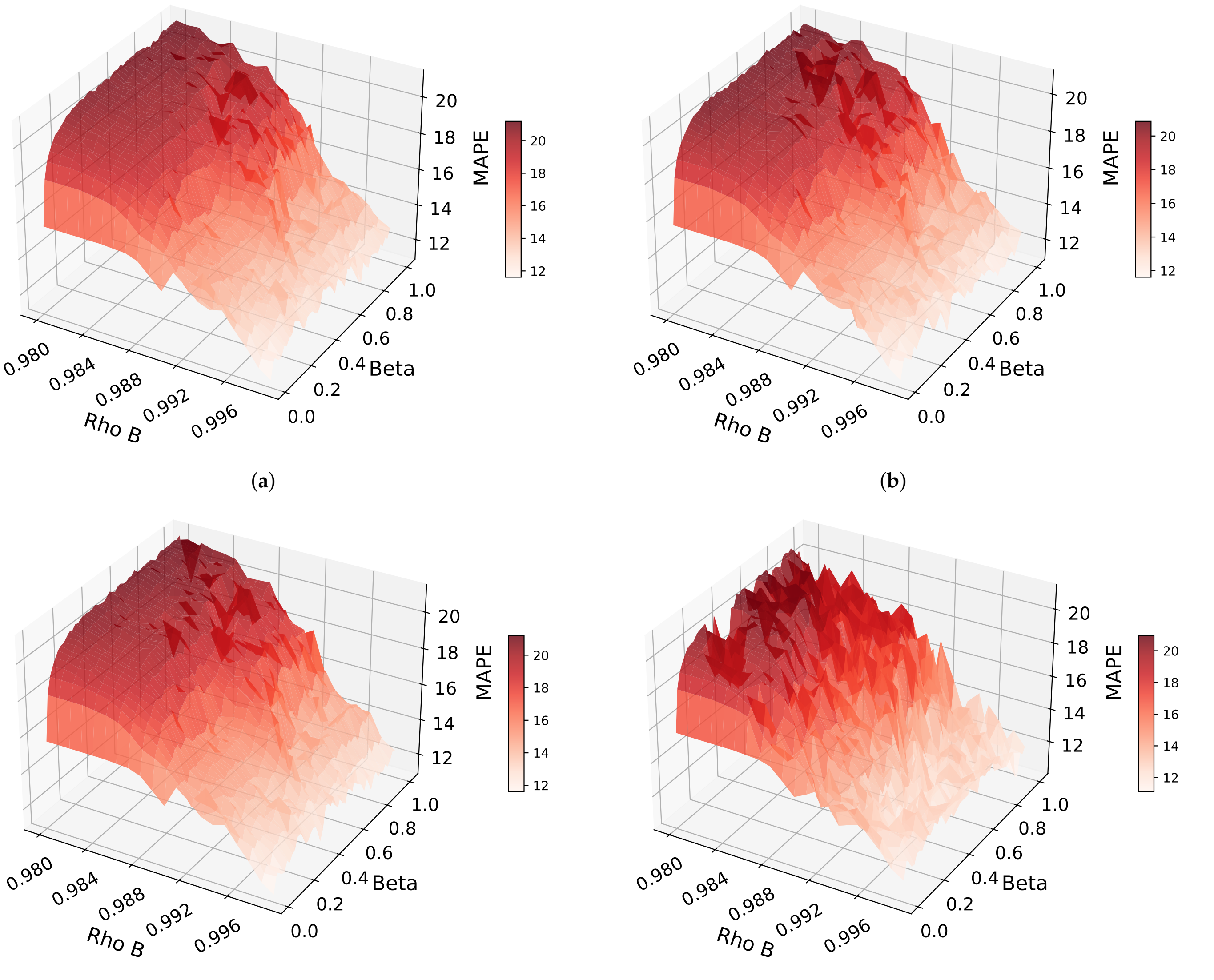

(**a**) (**b**)

(**c**) (**d**)

Figure 17. Three-dimensional visualization of the relation between parameters β, ρ_b, and MAPE: (**a**) maximum, (**b**) minimum, (**c**) mean, and (**d**) standard deviation.

Despite this irregularity, the standard deviation produced the best results for most substations, as shown in Table 2. This is because the standard deviation captures the variability of the data more effectively, allowing the model to better adjust to fluctuations and make more precise predictions. This highlights the importance of selecting the appropriate statistical feature for each unique dataset, which is a key contribution of this work.

Figure 18 explores the relationship between ρ_a, β, and MAPE. Analyzing Figure 18a,b,d, it can be seen that the highest error rates occur in regions where ρ_a and β are high; in other words, a low constraint in module A (low ρ_a) combined with a high learning rate (high β) can lead to greater imprecision in predictions.

However, a different behavior is observed when using the standard deviation to scale the input data, as shown in Figure 18d, where it can be seen that the lowest prediction errors are achieved when ρ_a is medium or low and β oscillates throughout the range, with values close to 0.6 obtaining the lowest MAPE.

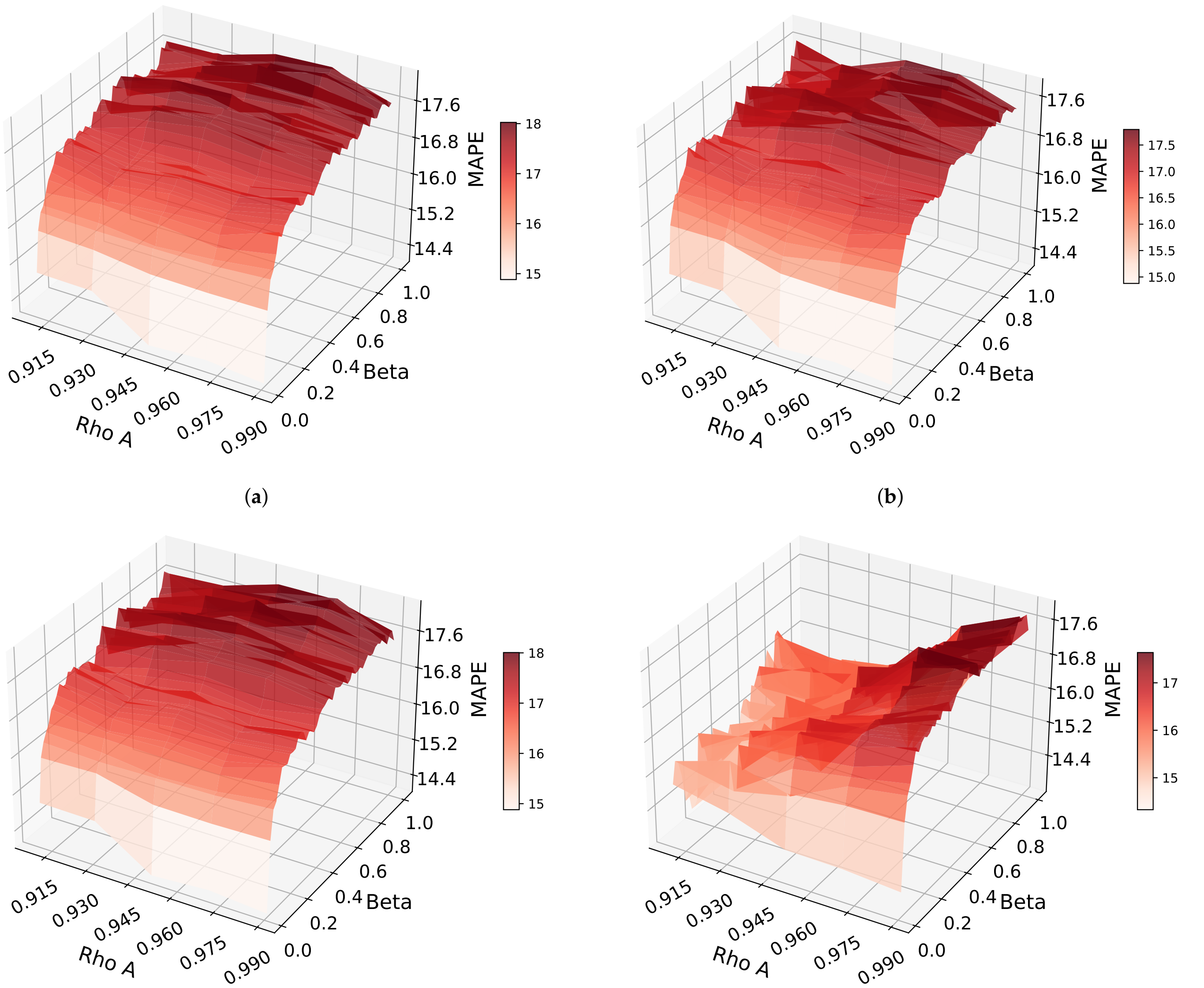

(**a**) (**b**)

(**c**) (**d**)

Figure 18. Three-dimensional visualization of the relation between the parameters β, ρ_a, and MAPE: (**a**) maximum, (**b**) minimum, (**c**) mean, and (**d**) standard deviation.

Finally, Figure 19 shows the relationship between the parameters ρ_a, ρ_b, and MAPE. Figure 19a–c illustrates that the highest error rates occur when both ρ_a and ρ_b are low. In other words, relaxing the similarity of modules A and B can lead to greater inaccuracy in predictions. On the other hand, Figure 19d reveals that by including the standard deviation, the behavior of ρ_b is modified. Higher values of ρ_b tend to reduce the model's performance, which means that a greater restriction on ρ_b (resulting in a greater number of categories) compromises the precision of the forecasts when the standard deviation is taken into account.

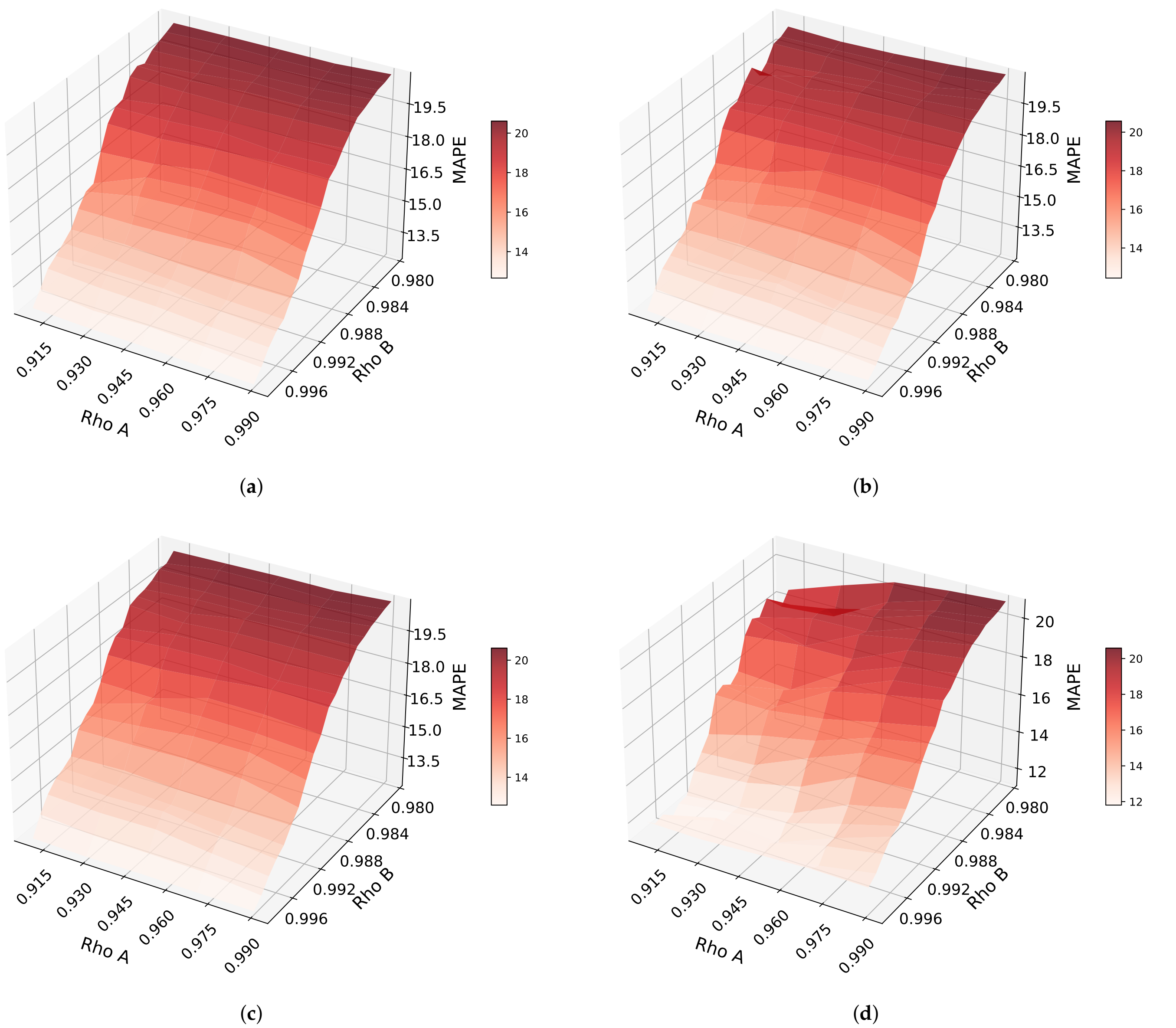

Figure 19. Three-dimensional visualization of the relation between the parameters ρ_a, ρ_b, and MAPE: (**a**) maximum, (**b**) minimum, (**c**) mean, and (**d**) standard deviation.

4.4. Global Parameter Optimization Analysis

A global optimization was performed to evaluate whether a single set of parameters could provide satisfactory performance across all nine substations. The results are shown in Table 4. Using the standard deviation as the windowing feature yielded the lowest global MAPE of 9.98%.

Table 4. Global parameters for all substations.

Windowing Type	ρ_a	β	ρ_a	MAPE
Mean	0.99	0.94	0.999	13.44%
Maximum	0.95	0.54	0.998	13.43%
Minimum	0.99	0.84	0.997	12.41%
Standard Deviation	0.91	0.42	0.996	9.98%
Best Overall Global Set	0.91	0.02	0.99	14.85%

The single best global parameter set optimized across all substations resulted in an MAPE of 14.85%. This is considerably higher than the substation-specific results, where some values reached 2.72% (Table 2). This outcome confirms that the load characteristics varied significantly between substations.

Although the global approach is less computationally demanding and may be suitable for large-scale grids, local optimization for each substation provides higher forecasting accuracy.

4.5. Comparison with Other Models

The Fuzzy ARTMAP model was evaluated against three established machine learning techniques: Multi-Layer Perceptron (MLP), Support Vector Regression (SVR), and Random Forest (RF). All models were applied to the same dataset using identical statistical windowing techniques, with performance assessed by MAPE as reported in Table 5.

Table 5. MAPE (%) statistics by substation for MLP, SVR, and RF.

Substation	MLP				SVR				Random Forest			
	Mean	**Max**	**Min**	**Std**	**Mean**	**Max**	**Min**	**Std**	**Mean**	**Max**	**Min**	**Std**
Kopu	11.13	9.72	14.75	9.05	9.04	9.01	12.02	6.71	9.54	11.28	9.85	6.69
Waikino	9.04	9.04	9.04	9.04	8.70	9.09	9.17	9.01	7.09	7.03	6.19	6.69
Waihou	5.43	7.74	7.89	6.78	4.60	4.70	4.51	4.44	4.66	4.65	4.76	4.59
Hamilton 11	7.49	7.49	7.49	7.49	6.78	6.70	6.71	6.76	7.10	7.07	7.11	7.15
Hamilton 33	5.76	5.79	5.86	7.91	5.08	7.08	7.08	7.09	5.35	5.12	5.78	5.35
Cambridge	5.63	5.63	5.63	5.33	3.10	3.39	3.39	3.10	8.48	8.48	8.48	6.99
Te Awamutu	7.24	7.24	7.23	7.24	7.24	6.69	7.24	6.73	6.79	6.79	6.79	6.79
Hinuera	15.57	16.84	15.45	15.79	16.41	16.22	16.54	13.04	4.99	4.99	4.99	4.99
Kinleith	6.30	6.30	6.30	6.30	6.12	6.11	6.12	3.99	6.44	6.44	6.42	6.43

Fuzzy ARTMAP achieved the lowest error in several substations. For example, at Waihou and Hamilton 11, the mean windowing method yielded MAPEs of 3.68%, outperforming all other models. Cambridge and Te Awamutu achieved the best results with the minimum windowing method, reaching 2.72% and 3.07%, respectively. For Kopu and Waikino, the standard deviation windowing method provided the lowest errors.

These characteristics make Fuzzy ARTMAP a reliable alternative for multinodal electrical load forecasting, consistently providing accurate predictions across substations with diverse load profiles. Its ability to adjust to different statistical features allows it to maintain high precision while remaining computationally efficient, confirming its suitability for real-time forecasting in multinodal power systems.

4.6. Advantages and Limitations of the Study

The methodology presented in this paper combines data enrichment with the Fuzzy ARTMAP network. Using statistical features such as the mean, standard deviation, maximum, and minimum to expand the input data allows the model to adjust to different load profiles, improving the precision of predictions. This feature enables more stable loads to benefit from the mean, while more volatile loads benefit from the standard deviation. These results demonstrate the method's adaptability to various conditions. Comparisons with other techniques such as MLP, SVR, and Random Forest show that Fuzzy ARTMAP achieves smaller errors in several substations.

Another clear advantage is its computational efficiency. The model makes predictions in microseconds without requiring specialized hardware or long training periods, which ensures its viability in real-time applications and scenarios with limited computational resources.

The flexibility gained from using statistics to enrich the data suggests that the proposed approach can be applied to other types of time series beyond electrical load data.

There is potential for use in predicting vibrations in mechanical systems, as part of an equipment's useful life analysis, or in other data series such as network traffic or financial indicators. The ability to recognize patterns and group information in an adaptive way allows the proposed method to be explored in different domains with internal variability and dynamic behavior.

Despite its advantages, this study has limitations that open the door for new work. The dataset we used is from 2010, a period before the widespread adoption of renewable energy and smart meters, which have altered consumption patterns. This means that application of the proposed method in modern grids still needs validation. In addition, the work was performed on a limited number of substations, which raises the challenge of scalability. For larger networks, optimization by exhaustive search becomes unfeasible. An exploration of distributed computing or other more efficient adjustment methods to process data in parallel could be a solution.

Another point is that the model's performance on abnormal days such as holidays or under extreme weather conditions was not evaluated. These events generate load patterns that deviate from regular behavior. An analysis in these scenarios would be important to verifying the model's reliability. It is also relevant to note that while using multiple statistics enriches the data, it also increases the complexity of the input set. Future work could investigate which combinations of statistics are the most relevant for different load types, thereby reducing redundancies and maintaining efficiency.

Finally, integration with probabilistic methods which can provide confidence intervals for predictions would be a valuable enhancement. Expanding the study to larger networks or other time series domains would help to evaluate the generality of the proposed approach as well as the adjustments needed for different contexts.

5. Conclusions

Precise forecasting of electricity demand is an essential tool for the efficient and sustainable management of today's energy systems. This study applied the Fuzzy ARTMAP network to multinodal short-term electricity load forecasting at nine substations in New Zealand, presenting an approach that includes exhaustive parameter analysis and search along with the incorporation of statistics such as maximum, minimum, mean, and standard deviation.

The results showed that standard deviation was the most effective among the windowing techniques we explored in improving the precision of the forecasts, resulting in a reduction in Mean Absolute Percentage Error (MAPE) for most of the substations. In addition, our analysis of the Fuzzy ARTMAP parameters highlighted that the combination of the ρ_a and β parameters has a significant impact on the creation of categories, and consequently on the precision of forecasts.

The shaded area around the load curve, which represents the variability of the data and the uncertainty of the forecasts, was particularly impacted by the configuration of the parameters. Substations with higher values of ρ_a, β, and ρ_b, such as Waihou, Hamilton 33, Cambridge, and Te Awamutu, showed a significant reduction in the shaded area of the load curve, indicating greater stability in the demand forecast. On the other hand, stations with lower parameters, such as Waikino, Hamilton 11, and Kinleith, showed greater dispersion, reflecting a larger shaded area and less accurate forecasting.

This information indicates that fine adjustments to parameter settings, especially those such as ρ_b that are responsible for checking the similarity of data within clusters, have a direct effect on the model's ability. When ρ_a and ρ_b are lower, this allows for greater variation in the data, resulting in greater imprecision and a larger shaded area.

To assess its scalability and robustness of this methodology in different contexts, future work could explore its application to other data types, such as demand from industrial consumers or individual households. Furthermore, a comparative analysis with other advanced machine learning models such as transformers or hybrid models could be conducted to more comprehensively evaluate the performance of Fuzzy ARTMAP.

Author Contributions: Conceptualization, J.R.M.J., R.J.d.S., C.R.d.S.J., and M.L.M.L.; methodology, J.R.M.J. and R.J.d.S.; software, J.R.M.J. and R.J.d.S.; validation, J.R.M.J., R.J.d.S., C.R.d.S.J., T.A., and M.L.M.L.; formal analysis, J.R.M.J., R.J.d.S., C.R.d.S.J., T.A., and M.L.M.L.; investigation, J.R.M.J., R.J.d.S., and M.L.M.L.; resources, J.R.M.J., R.J.d.S., and M.L.M.L.; data curation, J.R.M.J. and R.J.d.S.; writing—original draft preparation, J.R.M.J. and R.J.d.S.; writing—review and editing, J.R.M.J., R.J.d.S., C.R.d.S.J., T.A., and M.L.M.L.; visualization, J.R.M.J.; supervision, M.L.M.L.; project administration, M.L.M.L.; funding acquisition, M.L.M.L. All authors have read and agreed to the published version of the manuscript..

Funding: This study was financed in part by the Coordenação de Aperfeiçoamento de Pessoal de Nível Superior—Brasil (CAPES)—Finance Code 001.

Data Availability Statement: The data used to support the findings of this study are available from the corresponding author upon request.

Conflicts of Interest: The authors declare no conflicts of interest.

References

1. Hong, T.; Fan, S. Probabilistic electric load forecasting: A tutorial review. *Int. J. Forecast.* **2016**, *32*, 914–938. https://doi.org/10.1016/j.ijforecast.2015.11.011.
2. Alfares, H.K.; and, M.N. Electric load forecasting: Literature survey and classification of methods. *Int. J. Syst. Sci.* **2002**, *33*, 23–34. https://doi.org/10.1080/00207720110067421.
3. Amjady, N. Short-Term Bus Load Forecasting of Power Systems by a New Hybrid Method. *IEEE Trans. Power Syst.* **2007**, *22*, 333–341. https://doi.org/10.1109/TPWRS.2006.889130.
4. Amorim, A.J.; Abreu, T.A.; Tonelli-Neto, M.S.; Minussi, C.R. A new formulation of multinodal short-term load forecasting based on adaptive resonance theory with reverse training. *Electr. Power Syst. Res.* **2020**, *179*, 106096. https://doi.org/10.1016/j.epsr.2019.106096.
5. Panapakidis, I.P. Clustering based day-ahead and hour-ahead bus load forecasting models. *Int. J. Electr. Power Energy Syst.* **2016**, *80*, 171–178. https://doi.org/10.1016/j.ijepes.2016.01.035.
6. Liu, D.; Zeng, L.; Li, C.; Ma, K.; Chen, Y.; Cao, Y. A Distributed Short-Term Load Forecasting Method Based on Local Weather Information. *IEEE Syst. J.* **2018**, *12*, 208–215. https://doi.org/10.1109/JSYST.2016.2594208.
7. Hussain, A.; Rahman, M.; Memon, J.A. Forecasting electricity consumption in Pakistan: The way forward. *Energy Policy* **2016**, *90*, 73–80. https://doi.org/10.1016/j.enpol.2015.11.028.
8. Dong, Q.; Huang, R.; Cui, C.; Towey, D.; Zhou, L.; Tian, J.; Wang, J. Short-Term Electricity-Load Forecasting by Deep Learning: A Comprehensive Survey. *arXiv* **2024**, arXiv:2408.16202. Available online: http://arxiv.org/abs/2408.16202 (accessed on 7 April 2025).
9. Stamatellos, G.; Stamatelos, T. Short-Term Load Forecasting of the Greek Electricity System. *Appl. Sci.* **2023**, *13*, 2719. https://doi.org/10.3390/app13042719.
10. Tarmanini, C.; Sarma, N.; Gezegin, C.; Ozgonenel, O. Short term load forecasting based on ARIMA and ANN approaches. *Energy Rep.* **2023**, *9*, 550–557. https://doi.org/10.1016/j.egyr.2023.01.060.
11. Habbak, H.; Mahmoud, M.; Metwally, K.; Fouda, M.M.; Ibrahem, M.I. Load Forecasting Techniques and Their Applications in Smart Grids. *Energies* **2023**, *16*, 1480. https://doi.org/10.3390/en16031480.
12. Kamath, A.K.; Rajalakshmi, S.B.L. Data Mining and Identification of Influencing Factors for Effective Load Forecasting of A Substation Using Machine Learning Regressors. In Proceedings of the 2024 IEEE International Conference on Distributed Computing, VLSI, Electrical Circuits and Robotics (DISCOVER), Mangalore, India, 18–19 October 2024; pp. 14–19. https://doi.org/10.1109/DISCOVER62353.2024.10750610.
13. Pavlatos, C.; Makris, E.; Fotis, G.; Vita, V.; Mladenov, V. Enhancing Electrical Load Prediction Using a Bidirectional LSTM Neural Network. *Electronics* **2023**, *12*, 4652. https://doi.org/10.3390/electronics12224652.

14. Zhu, Q.; Zeng, S.; Chen, M.; Wang, F.; Zhang, Z. Short-Term Load Forecasting Method Based on Bidirectional Long Short-Term Memory Model with Stochastic Weight Averaging Algorithm. *Electronics* **2024**, *13*, 3098. https://doi.org/10.3390/electronics13153098.
15. Waheed, W.; Xu, Q. Data-driven short term load forecasting with deep neural networks: Unlocking insights for sustainable energy management. *Electr. Power Syst. Res.* **2024**, *232*, 110376. https://doi.org/10.1016/j.epsr.2024.110376.
16. Türkoğlu, A.S.; Erkmen, B.; Eren, Y.; Erdinç, O.; İbrahim Küçükdemiral. Integrated Approaches in Resilient Hierarchical Load Forecasting via TCN and Optimal Valley Filling Based Demand Response Application. *Appl. Energy* **2024**, *360*, 122722. https://doi.org/10.1016/j.apenergy.2024.122722.
17. Wen, H.; Li, X.; Chen, B.; Chen, J.; Yang, S.; Wu, Q. Lean load forecasting method for distribution substation area. In Proceedings of the 2024 3rd International Conference on Energy, Power and Electrical Technology (ICEPET), Chengdu, China, 17–19 May 2024; pp. 1320–1324. https://doi.org/10.1109/ICEPET61938.2024.10627540.
18. Huang, J.; Zhu, C.; Liang, Q.; Jiang, N.; Luo, S.; Wu, Q. A step-by-step load forecasting method considering electric vehicle charging stations. In Proceedings of the 2024 3rd International Conference on Energy, Power and Electrical Technology (ICEPET), Chengdu, China, 17–19 May 2024; pp. 1325–1329. https://doi.org/10.1109/ICEPET61938.2024.10627620.
19. Züge, C.V.; Coelho, L.d.S. Granular Weighted Fuzzy Approach Applied to Short-Term Load Demand Forecasting. *Technologies* **2024**, *12*, 182. https://doi.org/10.3390/technologies12100182.
20. Xie, X.; Ding, Y.; Sun, Y.; Zhang, Z.; Fan, J. A novel time-series probabilistic forecasting method for multi-energy loads. *Energy* **2024**, *306*, 132456. https://doi.org/10.1016/j.energy.2024.132456.
21. Veeramsetty, V.; Konda, P.K.; Dongari, R.C.; Salkuti, S.R. Short-Term Load Forecasting in Distribution Substation Using Autoencoder and Radial Basis Function Neural Networks: A Case Study in India. *Computation* **2025**, *13*, 75. https://doi.org/10.3390/computation13030075.
22. Garcia-Garrido, E.; Mendoza-Villena, M.; Lara-Santillan, P.M.; Zorzano-Alba, E.; Falces, A. Net demand short-term forecasting in a distribution substation with PV power generation. *E3S Web Conf.* **2020**, *152*, 01001. https://doi.org/10.1051/e3sconf/202015201001.
23. He, N.; Yang, Z.; Qian, C.; Li, R.; Gao, F.; Cheng, F. Remaining useful life prediction of lithium-ion battery based on fusion model considering capacity regeneration phenomenon. *J. Energy Storage* **2024**, *85*, 111068. https://doi.org/10.1016/j.est.2024.111068.
24. da Silva, M.A.; Abreu, T.; Santos-Júnior, C.R.; Minussi, C.R. Load forecasting for smart grid based on continuous-learning neural network. *Electr. Power Syst. Res.* **2021**, *201*, 107545. https://doi.org/10.1016/j.epsr.2021.107545.
25. Rai, S.; De, M. NARX: Contribution-factor-based short-term multinodal load forecasting for smart grid. *Int. Trans. Electr. Energy Syst.* **2021**, *31*, e12726. https://doi.org/10.1002/2050-7038.12726.
26. Osgonbaatar, T.; Matrenin, P.; Safaraliev, M.; Zicmane, I.; Rusina, A.; Kokin, S. A Rank Analysis and Ensemble Machine Learning Model for Load Forecasting in the Nodes of the Central Mongolian Power System. *Inventions* **2023**, *8*, 114. https://doi.org/10.3390/inventions8050114.
27. Bergstra, J.; Bengio, Y. Random Search for Hyper-Parameter Optimization. *J. Mach. Learn. Res.* **2012**, *13*, 281–305.
28. Probst, P.; Boulesteix, A.L.; Bischl, B. Tunability: Importance of Hyperparameters of Machine Learning Algorithms. *J. Mach. Learn. Res.* **2019**, *20*, 1–32.
29. Yang, L.; Shami, A. On hyperparameter optimization of machine learning algorithms: Theory and practice. *Neurocomputing* **2020**, *415*, 295–316. https://doi.org/10.1016/j.neucom.2020.07.061.
30. Li, C. Designing a short-term load forecasting model in the urban smart grid system. *Appl. Energy* **2020**, *266*, 114850. https://doi.org/10.1016/j.apenergy.2020.114850.
31. Müller, M.R.; Gaio, G.; Carreno, E.M.; Lotufo, A.D.P.; Teixeira, L.A. Electrical load forecasting in disaggregated levels using Fuzzy ARTMAP artificial neural network and noise removal by singular spectrum analysis. *SN Appl. Sci.* **2020**, *2*, 1218. https://doi.org/10.1007/s42452-020-2988-5.
32. Grossberg, S. A Path Toward Explainable AI and Autonomous Adaptive Intelligence: Deep Learning, Adaptive Resonance, and Models of Perception, Emotion, and Action. *Front. Neurorobotics* **2020**, *14*, 36. https://doi.org/10.3389/fnbot.2020.00036.
33. Abreu, T.; Amorim, A.J.; Santos-Junior, C.R.; Lotufo, A.D.; Minussi, C.R. Multinodal load forecasting for distribution systems using a fuzzy-artmap neural network. *Appl. Soft Comput.* **2018**, *71*, 307–316. https://doi.org/10.1016/j.asoc.2018.06.039.
34. Carpenter, G.A.; Grossberg, S.; Markuzon, N.; Reynolds, J.H.; Rosen, D.B. Fuzzy ARTMAP: A neural network architecture for incremental supervised learning of analog multidimensional maps. *IEEE Trans. Neural Netw.* **1992**, *3*, 698–713. https://doi.org/10.1109/72.159059.
35. Mukhtar, K.; Ingham, M.; Rodger, C.J.; Mac Manus, D.H.; Divett, T.; Heise, W.; Bertrand, E.; Dalzell, M.; Petersen, T. Calculation of GIC in the North Island of New Zealand Using MT Data and Thin-Sheet Modeling. *Space Weather* **2020**, *18*, e2020SW002580. e2020SW002580 2020SW002580, https://doi.org/10.1029/2020SW002580.
36. Zadeh, L.A. Fuzzy sets. *Inf. Control* **1965**, *8*, 338–353. https://doi.org/10.1016/S0019-9958(65)90241-X.

37. Altran, A.B. Sistema Inteligente Para Previsão de Carga Multinodal em Sistemas Elétricos de Potência. Ph.D. Thesis, Departamento de Engenharia Elétrica, Universidade Estadual Paulista, Ilha Solteira, Brazil, 2010.
38. Nose-Filho, K.; Lotufo, A.D.P.; Minussi, C.R. Short-Term Multinodal Load Forecasting Using a Modified General Regression Neural Network. *IEEE Trans. Power Deliv.* **2011**, *26*, 2862–2869. https://doi.org/10.1109/TPWRD.2011.2166566.
39. Christ, M.; Braun, N.; Neuffer, J.; Kempa-Liehr, A.W. Time Series FeatuRe Extraction on basis of Scalable Hypothesis tests (tsfresh – A Python package). *Neurocomputing* **2018**, *307*, 72–77. https://doi.org/10.1016/j.neucom.2018.03.067.
40. Hochma, Y.; Felendler, Y.; Last, M. Efficient Feature Ranking and Selection Using Statistical Moments. *IEEE Access* **2024**, *12*, 105573–105587. https://doi.org/10.1109/ACCESS.2024.3412851.
41. Felice, F.; Ley, C.; Bordas, S.P.A.; Groll, A. Boosting any learning algorithm with Statistically Enhanced Learning. *Sci. Rep.* **2025**, *15*, 1605. https://doi.org/10.1038/s41598-024-84702-8.
42. Bishop, C.M. *Pattern Recognition and Machine Learning (Information Science and Statistics)*; Springer: Berlin/Heidelberg, Germany, 2006.
43. Zheng, A.; Casari, A. *Feature Engineering for Machine Learning: Principles and Techniques for Data Scientists*, 1st ed.; O'Reilly Media, Inc.: Sebastopol, CA, USA, 2018.
44. Pedregosa, F.; Varoquaux, G.; Gramfort, A.; Michel, V.; Thirion, B.; Grisel, O.; Blondel, M.; Prettenhofer, P.; Weiss, R.; Dubourg, V.; et al. Scikit-learn: Machine Learning in Python. *J. Mach. Learn. Res.* **2011**, *12*, 2825–2830.
45. Mouloodi, S.; Rahmanpanah, H.; Gohery, S.; Burvill, C.; Davies, H.M. Feedforward backpropagation artificial neural networks for predicting mechanical responses in complex nonlinear structures: A study on a long bone. *J. Mech. Behav. Biomed. Mater.* **2022**, *128*, 105079. https://doi.org/10.1016/j.jmbbm.2022.105079.
46. Shrestha, A.; Mahmood, A. Review of Deep Learning Algorithms and Architectures. *IEEE Access* **2019**, *7*, 53040–53065. https://doi.org/10.1109/ACCESS.2019.2912200.
47. Breiman, L. Random Forests. *Mach. Learn.* **2001**, *45*, 5–32. https://doi.org/10.1023/A:1010933404324.
48. Drucker, H.; Burges, C.J.C.; Kaufman, L.; Smola, A.; Vapnik, V. Support vector regression machines. In Proceedings of the 10th International Conference on Neural Information Processing Systems (NIPS'96), Cambridge, MA, USA, 2–5 December 1996; pp. 155–161.
49. de Myttenaere, A.; Golden, B.; Le Grand, B.; Rossi, F. Mean Absolute Percentage Error for regression models. *Neurocomputing* **2016**, *192*, 38–48. https://doi.org/10.1016/j.neucom.2015.12.114.

ARTIGOS EM PERIÓDICOS

Article

Not peer-reviewed version

Machine Learning for Affordable Diagnosis of SARS-COV-2 from Hematological and Biochemical Tests

Reginaldo José da Silva , Carlos Roberto dos Santos Júnior , Thays Abreu , Carlos Roberto Minussi * , Mara Lúcia Martins Lopes

Posted Date: 15 April 2024

doi: 10.20944/preprints202404.0956.v1

Keywords: Adaptive Resonance Theory; Artificial Neural Networks; Blood tests; Coronavirus; COVID-19

Article

Machine Learning for Affordable Diagnosis of SARS-COV-2 from Hematological and Biochemical Tests

Reginaldo José da Silva [1], Carlos Roberto dos Santos Júnior [2], Thays Abreu [3], Carlos Roberto Minussi [1,*] and Mara Lúcia Martins Lopes [3]

[1] São Paulo State University (UNESP), School of Engineering, Electrical Engineering Department, 15385-000 Ilha Solteira, Brazil; reginaldo.silva@unesp.br; minussi@dee.feis.unesp.br
[2] Federal Institute of São Paulo (IFSP), Campus Hortolândia, 13183-091 Hortolândia, Brazil; carlos.rsantos@ifsp.edu.br
[3] São Paulo State University (UNESP), School of Engineering, Department of Mathematics, 15385-000 Ilha Solteira, Brazil; thays.abreu@unesp.br; mara.lopes@unesp.br
* Correspondence: minussi@dee.feis.unesp.br; Tel. +55-183743-1225

Abstract: COVID-19, caused by the SARS-CoV-2 virus, has spread around the world and killed around 6.9 million people. Rapid and accurate diagnosis is essential for preventing and controlling the disease, reducing transmission and consequently saving lives. RT-PCR is the gold standard test used to detect the disease. However, the test is expensive and the result is time-consuming, which makes mass testing difficult, especially in countries with limited resources. In addition, the test has high analytical specificity and low diagnostic sensitivity, which leads to false-negative results. Several studies in the literature report the presence of hematological and biochemical alterations in infected patients and use these alterations with machine learning algorithms to help diagnose the disease. Therefore, this article presents the results obtained by different neural network architectures based on Adaptive Resonance Theory (ART) for the diagnosis of COVID-19. The study was conducted in two distinct stages: the first consisted of selecting the best ART network among several, using three open-access datasets and comparing the results with the literature. In the second stage, the chosen model was tested on a dataset containing patients from various hospitals in four countries. In addition, the model was subjected to external validation, including data from a country not present during the training and adjustment of the model, in order to validate the robustness and generalization capacity of the model. The results obtained by the ART networks in this study are promising, outperforming not only classical models, but also the deep learning models often used in the literature. Validation on data from different countries strengthens the model's reliability and effectiveness.

Keywords: adaptive resonance theory; Artificial Neural Networks; blood tests; coronavirus; COVID-19

---

1. Introduction

On Dec. 31 2019, the severe acute respiratory syndrome coronavirus 2 (SARS-CoV-2) causing coronavirus disease (COVID-19) was discovered in Wuhan in China. The virus has spread rapidly around the world and as of Apr. 21 2020 there were more than 2.3 million confirmed cases and a total of 162.000 deaths [1]. Currently, the virus has infected more than 775 million people and caused the deaths of 7 million worldwide [2]. Despite the high number of recorded deaths, the World Health Organization estimates the total number of deaths directly or indirectly from COVID-19 to be 14.9 million people [3], three times higher than recorded.

The symptoms of COVID-19 can be divided into three categories being common symptoms such as fever, cough, tiredness and loss of taste or smell, less common symptoms such as sore throat, headache, myalgia and diarrhea, and the critical symptoms which are dyspnea, loss of speech, mobility or confusion and chest pain [4]. Despite having several symptoms, a large proportion of infected people do not experience them. According to Wang et al. [5] the proportion of asymptomatic people may represent about a third or a fifth of the total number of cases.

 doi:10.20944/preprints202404.0956.v1

Although infected individuals develop mild or moderate disease and recover without hospitalization, a proportion of those infected may have severe symptoms, requiring hospitalization or intensive care unit (ICU) treatment.

To ensure the prevention of COVID-19, it is crucial to implement effective measures of detection, isolation and immediate medical care for infected people, in order to contain the spread of the virus [6–9]. This approach has proved effective in combating the spread of COVID-19. It is worth noting that, in addition to overloading the health system, the spread of the virus can have considerable economic impacts [10]. The costs associated with treating infected patients put significant pressure on health systems, especially in regions with limited resources [10]. Infected patients may require a diverse range of medical resources, from hospitalization in wards and ITUs to specialized interventions [11,12].

Among the various tests available to detect the disease, the reverse transcription polymerase chain reaction (RT-PCR) test, which detects the genetic material of the virus, is considered the gold standard for detecting COVID-19 and is carried out by collecting nasopharyngeal and/or oropharyngeal secretions [13]. Although RT-PCR has high analytical specificity, its diagnostic sensitivity is limited, especially in the early stages of infection, when the viral concentration may not be high enough to produce accurate results, leading to possible false negative results [14–17]. In addition, SARS-CoV-2 is an RNA virus prone to mutations, and since the beginning of the spread of the virus we have seen the emergence of several variants with different replication capacities and clinical manifestations [18]. Furthermore, the test has some limitations for testing patients on a large scale, requiring certified laboratories, expensive equipment and trained personnel, as well as the delay in obtaining results [19,20]. These limitations become even more serious in countries with limited resources, such as underdeveloped countries [21].

In addition to the RT-PCR mentioned above, computed tomography (CT) and X-ray have also been proposed to aid in the detection of COVID-19, playing a powerful role in detecting and judging the progression of the disease [22–27]. However, these tests are not efficient for the proper management of patients and the control of the spread of the virus, as their sensitivity and specificity are higher only in advanced stages of COVID-19 or other diseases [28–30], as these tests detect characteristics associated with COVID-19, such as lesions and lung inflammation, when the disease is already at an advanced stage of lung involvement. This is because the virus needs to replicate and cause significant damage to the lungs before changes are visible on the images. In addition, these exams subject patients to significant doses of ionizing radiation, which can pose major health risks [31,32].

Currently, machine learning has been an important tool to help doctors diagnose various diseases [33,34], including COVID-19 [35–37]. Studies have made use of this technology to detect COVID-19, either through images such as x-rays or CT scans, or through laboratory tests [38–40], since many clinical studies have shown hematological changes in infected patients [41–44]. While others focus on analyzing how these parameters vary throughout the course of the disease and their relationship with more serious clinical outcomes [45–47]. Given the need for efficient and more accurate diagnoses in the early stages of COVID-19, the relevant attributes of laboratory tests can be used to train machine learning algorithms, making it possible to predict the risk and evolution of the disease, as well as the early classification of infected patients. It is worth noting that laboratory tests have the advantage of being relatively more accessible in terms of cost compared to RT-PCR and imaging tests such as x-rays and CT scans, as well as avoiding exposure to radiation. This approach, based on hematological evaluations, could enable its use on a large scale, with specialist algorithms, which is especially relevant for developing countries with limited resources to carry out RT-PCR tests on the entire population, thus avoiding adverse social and economic impacts.

Several studies in the literature have used machine learning to detect COVID-19 from laboratory tests. One of the first articles, by Wu et al. [35], used the Random Forest (RF) algorithm with data collected from hospitals in China, achieving an AUC-ROC of 0.9926 in predicting patients with COVID-19. However, the model underperformed when tested with external samples. The authors Batista et al. [48] used data collected in a hospital in São Paulo, Brazil, and trained five algorithms for the detection of COVID-19 patients, Support Vector Machine (SVM) and RF were the ones that showed the best results, with an AUC-ROC of 0.847.

Sun et al. [36] employed the SVM algorithm to predict severe or critical cases of COVID-19 with patient data from a clinical center in China, obtaining a sensitivity of 77.5%, specificity of 78.4% and AUC-ROC of 0.9757. Tordjman et al. [49] developed a strategy using binary logistic regression (LR) to estimate the probability of a patient being diagnosed with COVID-19 before RT-PCR, achieving an AUC-ROC of 0.918, with sensitivity and specificity of 79% and 90%, respectively. Yang et al. [50] created a model using routine laboratory tests of patients at a medical center in the United States, and among the models tested, the Gradient Boosting Decision Tree (GBDT) obtained the best performance with an AUC-ROC of 0.854 in the internal validation and 0.838 in the external validation.

Joshi et al. [51] developed a decision support tool using LR to predict COVID-19 negative patients. The model achieved AUC-ROC of 0.78 for Stanford Health Care data, with AUC-ROC ranging from 0.75 to 0.81 at other centers. Goodman-Meza et al. [52] combined the probabilities of several algorithms to detect COVID-19 patients, achieving an AUC-ROC of 0.91 after adding certain tests such as ferritin, CRP and LDH. AlJame et al. [53] proposed ERLX, a model that stacks algorithms such as extremely randomized trees (ET), RF, LR and Extreme Gradient Boosting (XGB) to diagnose COVID-19 patients from blood tests, obtaining an AUC-ROC of 0.9938. Brinati et al. [21] proposed a model capable of predicting which patients were or were not infected with COVID-19, using data from patients admitted to the San Raffaele Hospital in Italy. Among the various algorithms tested, RF obtained the best performance, achieving an AUC-ROC of 0.84, sensitivity of 92% and specificity of 65%.

Alakus and Turkoglu [54] used a dataset containing hematological and biochemical attributes of patients from the Hospital Israelita Albert Einstein in São Paulo, Brazil, to train six deep learning architectures, with the aim of detecting patients with COVID-19. The best performance was obtained with Long Short-Term Memory (LSTM), achieving AUC-ROC of 0.625 in cross-validation and AUC-ROC of 0.90 in hold-out validation. Kukar et al. [55] created Smart Blood Analytics (SBA), a model for diagnosing COVID-19 from blood tests using algorithms such as RF, Deep Neural Network (DNN) and XGB. The best result with an AUC-ROC of 0.97 was obtained by XGB.

Using patient data from the Kepler University Hospital in Linz, Austria, Tschoellitsch et al. [56] applied the RF algorithm to predict the RT-PCR result using blood tests, achieving an AUC-ROC of 0.74. Soltan et al. [57] trained three models to identify COVID-19 patients in emergency departments and verify the need for hospitalization from patient data from Oxford University Hospitals in the UK. The best performance was obtained with XGB, achieving AUC-ROC of 0.939 in detecting patients and 0.94 in predicting hospitalization.

Cabitza et al. [58] evaluated several algorithms, including RF, Naive Bayes (NB), LR, SVM and KNN, to predict COVID-19 patients using data from patients admitted to the San Raphael Hospital in Italy. The models achieved AUC-ROC between 0.74 and 0.90, and during internal-external validation, they obtained AUC-ROC between 0.75 and 0.78. Alves et al. [59] developed a decision tree-based model to aid in the diagnosis of COVID-19 and provide explanations to healthcare teams, achieving AUC-ROC of 0.87, sensitivity of 67% and specificity of 91%. Rahman et al. [60] created the QCoVSML model, which uses stacked machine learning and a nomogram scoring system to detect COVID-19 based on biomarkers. Seven different datasets were used, and the combined model achieved an AUC-ROC of 0.96 and accuracy of 91.45%. There are many other studies that make use of laboratory tests and demonstrate the ability of machine learning algorithms to assist in medical decision-making, speeding up the diagnosis of the disease.

Although the algorithms used have achieved promising results, it is essential to recognize that they have some limitations, especially those based on backpropagation. According to Grossberg [61], these limitations include offline training, catastrophic forgetting, slow learning and sensitivity to outliers. To overcome these problems, Grossberg [62] developed Adaptive Resonance Theory (ART), which is described in detail in section 2.

Therefore, this article presents the use of neural networks based on Adaptive Resonance Theory (ART) for the classification of COVID-19, using laboratory tests (blood tests) in order to improve the detection of infected patients. Comparisons were made between seven different ART architectures, including online training algorithms. The most successful architecture was subjected to a dataset containing laboratory tests from patients from different countries. This aspect is of paramount importance, as it allows us to evaluate the algorithm's ability to detect relevant patterns and characteristics in data from different sources, thus increasing its usefulness in a global detection context.

2. Adaptive Resonance Theory

Developed Adaptive resonance theory in order to solve the stability-plasticity dilemma [63], such a dilemma can be understood as the ability of the network to remain able to adapt or group input patterns, and continue learning even with the inclusion of new patterns, without catastrophically forgetting its past knowledge Carpenter and Grossberg [64], this being a fundamental characteristic of ART family networks.

The first architecture based on this theory was developed by Grossberg [62] and named Grossberg Network (GN), in 1987, the ART1 network was created with the purpose of binary grouping patterns and was based on the GN network of Grossberg [64]. In the same year, Carpenter and Grossberg [65] improved ART1 creating ART2. This new network had the purpose of processing patterns with binary or continuous values. Considering the need to solve problems with analog input patterns, in 1991 Carpenter et al. [66], based on ART1 [64], developed the ART Fuzzy neural network (Figure 1), which employs the fuzzy min operator ($\wedge$) in place of the intersection operator ($\cap$) present in ART1 network. The first ART network with supervised training was developed by Carpenter et al. [67] and has two interconnected ART modules, the ART$_a$ module receives and processes the input pattern. In contrast, the ART$_b$ module receives the desired response for the presented pattern, and the Inter-ART module is in charge of performing the "matching" between the two ART modules. The following year Carpenter et al. [68] presented the Fuzzy ARTMAP that also has supervised training. However, its calculations are based on Fuzzy Logic [69].

Different ART network architectures have been tested in order to find the one that best classifies the data. These architectures have different characteristics, whether in their topology (cluster geometry), training method (supervised or unsupervised) or online learning capacity (Continuous Training), these characteristics appear in isolation or combined in the models to optimize data classification. The networks used in this study were:

- Self-expanding Fuzzy ART Neural Network [66]
- Self-Expanding Euclidean ART neural network [70]
- Self-Expanding Fuzzy ARTMAP neural network [68]
- Self-expanding Fuzzy ART neural network with Continuous Training [71]
- Self-expanding Euclidean ART neural network with Continuous Training [71,72]
- Self-expanding Fuzzy ARTMAP neural network with Continuous Training [71]
- Self-expanding Euclidean ARTMAP neural network with Continuous Training [73]

Although the self-expanding mechanism is not present in the original structure of the first three models, it was used because it adds advantages, as will be discussed in subsection 2.5. The other characteristics will be detailed in subsection 2.1, 2.2, 2.3, 2.4 and 2.6.

In these architectures, some parameters play a fundamental role in controlling the functioning of the model, namely α, β and ρ. The α parameter, also known as the learning rate ($\alpha > 0$), is crucial, indicating the extent to which new patterns will influence the category when the weights are updated in the next training cycle. The β parameter, or training rate ($0 < \beta \leq 1$), regulates the speed of training, with lower values indicating a slower process and values close to 1 implying faster training. Finally, the ρ parameter, or vigilance parameter ($0 < \rho \leq 1$), plays a crucial role in determining the degree of similarity required to create a new category. These parameters are essential for adjusting the network's dynamics and adapting it effectively to the input data.

Preprints.org (www.preprints.org) | NOT PEER-REVIEWED | Posted: 15 April 2024 doi:10.20944/preprints202404.0956.v1

2.1. ART - Unsupervised

Unsupervised ART models are effective in environments where the training data does not need to be labeled. The model's independence from labels allows it to autonomously explore the complexity of the data and identify relevant patterns. The basic architecture of an ART network can be seen in Figure 1, and consists of three levels, the F_1 comparison level, the F_2 recognition level and the F_0 level responsible for pre-processing the data, in which the input data is normalized and encoded (Fuzzy Topology). In addition, there is a reset mechanism responsible for controlling the degree of similarity of the patterns associated with the same category.

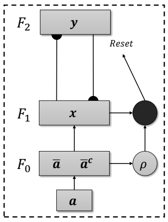

Figure 1. Fuzzy ART Architecture.

It is worth noting that, although they adopt an unsupervised approach, labels are assigned to each cluster after the model has been trained. This process is explained in detail in subsection 3.4.

Algorithm 1 Algorithm ART.

Input: Input data, parameters [β, ρ, α (Fuzzy)]

Output: Cluster

```
procedure
    if Topology for Fuzzy then
        Normalize and encode the input data by Equation 1 and 2
    end if
    while Data for training exists do
        Calculate the distance or similarity between the input data and all existing clusters
        Equation 3 or Equation 7
        while not finding a cluster to allocate the data do
            Select the cluster according to the equation Equation 4 or Equation 8
            if the Equation 5 or Equation 9 is satisfied then
                Update the weights according to Equation 6 or Equation 10
            else
                Remove the category from the search process
            end if
            The data will be allocated to the current cluster
        end while
    end while
end procedure
```

2.2. ARTMAP - Supervised

The ARTMAP model with supervised learning is made up of two ART modules, ART_a and ART_b, as shown in Figure 2. Unlike their unsupervised counterparts, these modules do not operate in the dark. They use both the input data and the corresponding labels, providing guidance during training. Furthermore, ARTMAP doesn't just passively accept information. It actively searches for meaningful connections. The inter-ART associative memory module is responsible for checking whether there is a match between the input patterns and the output. The vigilant match-tracking mechanism minimizes prediction errors and maximizes the model's ability to generalize. The weight matrices associated with the ART_a ($\boldsymbol{W}^a$), ART_b ($\boldsymbol{W}^b$) and Inter-ART ($\boldsymbol{W}^{ab}$) modules are initialized with values equal to 1, indicating the absence of active categories. However, as training takes place, there is resonance

Preprints.org (www.preprints.org) | NOT PEER-REVIEWED | Posted: 15 April 2024 doi:10.20944/preprints202404.0956.v1

between the input patterns and the output, causing specific categories to be activated. This dynamic activation process allows ARTMAP to learn and adapt in a controlled manner.

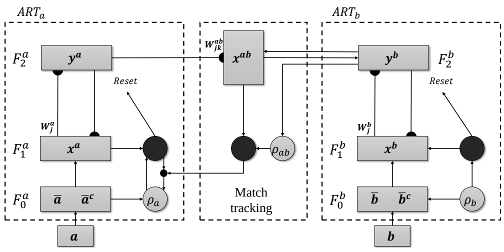

Figure 2. Architecture ARTMAP.

Although it is a powerful architecture, it is a model sensitive to noise in the labels due to supervised learning, accuracy can be compromised if the labels are inaccurate or noisy.

Algorithm 2 ARTMAP algorithm.

Input: Input data, parameters [β, ρ, α (Fuzzy)]

Output: Cluster

procedure
  if Topology for Fuzzy **then**
    Normalize and encode the input data by Equation 1 and 2
  end if
  while Data for training exists **do**
    Module B
    Calculate the distance or similarity between the input data and all existing clusters
    Equation 3 or Equation 7
    while not finding a cluster to allocate the data **do**
      Select cluster according to Equation 4 or Equation 8
      if the Equation 5 or Equation 9 is met **then**
        Update the weights of module B according to Equation 6 or Equation 10
      else
        Remove the category from the search process
      end if
    end while
    Module A
    Calculate the distance or similarity between the input data and all existing clusters
    Equation 3 or Equation 7
    while not finding a cluster to allocate the data **do**
      Select cluster according to Equation 4 or Equation 8
      if the Equation 5 or Equation 9 is met **then**
        Inter-ART module
        if The category found by module A matches the category of module B **then**
          Update the weights of module A (Equation 6 or Equation 10) and Inter-ART
        else
          Remove the category from the search process and increase the vigilance parameter of module A
        end if
      else
        Remove the category from the search process
      end if
    end while
    The data will be allocated to the current cluster
  end while
end procedure

Preprints.org (www.preprints.org) | NOT PEER-REVIEWED | Posted: 15 April 2024 doi:10.20944/preprints202404.0956.v1

2.3. Fuzzy Topology in ART Networks

In the fuzzy topology, ART networks use the fuzzy logic connectives developed by [69]. These connectives are used both to assess the similarity between input patterns and in the vigilance test. Furthermore, in this topology the data needs to be normalized and coded by complement as specified by Equation 1 and 2, in order to avoid the proliferation of categories [68].

$$\bar{\boldsymbol{a}} = \frac{\boldsymbol{a}}{\left|\sum_{i}^{M} a_i\right|}, \tag{1}$$

$$\boldsymbol{I} = [\ \bar{\boldsymbol{a}} \quad \bar{\boldsymbol{a}}^c\ ], \tag{2}$$

The Equation 3 in turn is responsible for checking the similarity between the input pattern and the existing categories, the winning category will be the one with the greatest similarity to the input data as seen in the Equation 4. The j index refers to the cluster in which the calculations are being performed, while the J index identifies the winning category in this process.

$$T_j = \frac{|\boldsymbol{I} \wedge \boldsymbol{W}_j|}{\alpha + |\boldsymbol{W}_j|}, \tag{3}$$

$$J = arg\{\max\{T_j : j = 1, ..., \text{number of clusters}\}, \tag{4}$$

Resonance occurs if the vigilance criterion given by Equation 5 is met. This process acts as a filter preventing the unbridled creation of categories. It ensures that only significantly different patterns trigger the formation of new categories, preventing the network from becoming full of redundant categories. The ρ parameter sets the threshold for this filter, determining the level of similarity required between an input pattern and the existing categories for the network to accept it or not within the cluster.

$$\frac{|\boldsymbol{I} \wedge \boldsymbol{W}_J|}{|\boldsymbol{I}|} \geq \rho, \tag{5}$$

When resonance is achieved, the network starts a weight adjustment process, as detailed in Equation 6. In this way, the weights associated with the winning category are modified to accommodate the new pattern.

$$\boldsymbol{W}_J^{new} = \beta\left(\boldsymbol{I} \wedge \boldsymbol{W}_J^{old}\right) + \left(1 - \beta\right)\boldsymbol{W}_J^{old}, \tag{6}$$

By using fuzzy logic in the network calculations, together with normalization and complement coding, the clusters take the form of hyperrectangles, giving flexibility to the complexity of the input patterns.

2.4. Euclidean Topology in ART Networks

By adopting Euclidean topology, ART networks use Euclidean distance as a metric to measure the proximity between input patterns and existing categories. As a result, the network generates hyperspheres centered on the cluster representing the class, instead of hyperectangles. This approach eliminates the need to normalize and encode the input vector, thus reducing computational costs [72]. The Equation 7 indicates how the distance between the input pattern and the existing clusters is calculated. The category chosen is the one with the smallest distance according to Equation 8, in contrast to the fuzzy approach, where the choice is based on maximum activation.

$$T_j = \sqrt{\sum_{i=1}^{M} (a_i - W_{ji})^2}, \tag{7}$$

Preprints.org (www.preprints.org) | NOT PEER-REVIEWED | Posted: 15 April 2024 doi:10.20944/preprints202404.0956.v1

$$J = arg\{\min\{T_j : j = 1, ..., numberofclusters\}\}, \tag{8}$$

The vigilance criterion will be given by Equation 9 and follows a similar pattern to that used in fuzzy topology, as detailed above in subsection 2.3.

$$\frac{T_J}{\max\left\{\sum_{i=1}^{M}(a_i)^2, \sum_{i=1}^{M}(W_{Ji})^2\right\}} \leq \rho, \tag{9}$$

Another change is in the Equation 10 responsible for the network's learning process. Here, the weight matrix ($\boldsymbol{W}_J$) is updated according to a weighted combination of the input pattern ($\boldsymbol{a}$) and the previous weight matrix ($\boldsymbol{W}_J^{old}$), controlled by the β parameter.

$$\boldsymbol{W}_J^{new} = \beta(\boldsymbol{a}) + (1-\beta)\boldsymbol{W}_J^{old}, \tag{10}$$

2.5. Self-Expanding Mechanism

The self-expanding mechanism proposed by Moreno [71,72] starts training the network by adopting the first pattern as the center of the first cluster and expands according to the need to create new clusters, i.e. as the new input patterns do not fit into the pre-existing categories, a new cluster is created to allocate that pattern. This modification reduces the processing time and, consequently, the computational expense [71,72], as it only checks the similarity of active clusters, unlike traditional architectures, in which similarity is checked with all clusters, including inactive ones. Furthermore, when inputting data that is incompatible with any of the existing clusters, the network starts a new cluster with the new pattern that is not in resonance with the input data and the empty cluster. These changes do not alter the stability of the network or compromise its ability to recognize new information in the training data.

Algorithm 3 Self-expansion mechanism algorithm.

Require: Initialization of the weight matrix with the first pattern

```
procedure
    if The surveillance criterion is not met (Equation 5 or Equation 9) then
        if There are categories to be checked then
            Remove the current category from the search process and search again
        else
            Create a new cluster to allocate the current data
            The weight for this cluster will be the input pattern itself
        end if
    end if
end procedure
```

2.6. Continuous Training in ART Neural Networks

The continuous training strategy enables networks to learn online and continuously so that prediction and training are carried out constantly, making them more efficient. This approach eliminates the need to restart training when incorporating new data, resulting in a network that constantly adjusts to changes in the environment. The inclusion of this module in ART networks is only possible due to their characteristics of stability and plasticity [72]. With online learning, there is no need to restart training when new data becomes available; this module allows new patterns to be added to the network's memory permanently [72].

In order to incorporate this module, the network needs to have temporary and definitive categories, a necessary process so that data that appears rarely is not incorporated into the network's memory. In addition, two new parameters are added: the first, called the permanence parameter ($NMIN$), defines the number of patterns needed for a temporary category to become definitive. The

Preprints.org (www.preprints.org) | NOT PEER-REVIEWED | Posted: 15 April 2024 doi:10.20944/preprints202404.0956.v1

second, called the novelty index (η), checks for the need to update the weights of the definitive category, discarding information that is not very relevant to the network, avoiding overloading the network's memory [72]. Whenever a pattern belongs to a temporary cluster, resonance will occur; on the other hand, if the category to which the pattern belongs is definitive, resonance will only occur if the distance/similarity between the entry and the center of the category is greater than the parameter (η) [72].

Thus, Equation 3 and Equation 7 are calculated for their respective topologies, for both temporary and permanent categories. The selection process remains the same. If the chosen category is definitive and passes the surveillance criterion, resonance will only occur if the condition imposed by Equation 11 (Fuzzy) or Equation 12 (Euclidean) is met, i.e. resonance will only occur if the pattern is significantly different.

$$T_J > \eta, \tag{11}$$

$$T_J < \eta, \tag{12}$$

3. Application of ART Networks in the diagnosis of COVID-19

The simulations were carried out using ten open-access datasets. These datasets contain information on clinical biomarkers collected from patients in hospitals located in Brazil, Spain, Italy and Ethiopia. The number of instances and features contained in each of the datasets can be seen in Table 1.

Table 1. Amount of data and features.

Available in:	Name	Country	Features	Positive	Negative
[21]	$Data_1$	Italy	14	177	102
[58]	$Data_2$	Italy	35	786	838
[54]	$Data_3$	Brazil	19	80	520
[74]	$Data_4$	Italy	22	163	174
[74]	$Data_5$	Italy	22	104	145
[74]	$Data_6$	Italy	22	118	106
[74]	$Data_7$	Brazil	23	334	11
[74]	$Data_8$	Brazil	23	352	949
[74]	$Data_9$	Brazil	23	375	1960
[74]	$Data_{10}$	Ethiopia	24	200	0
[74]	$Data_{11}$	Spain	24	78	42

The methodology used in this article consisted of two stages. In the first stage, the main objective was to select the best ART model from the seven architectures tested. In the second stage, the model selected in the previous stage was used to verify its generalization capacity in relation to data from different countries. Specific details of each stage are described in subsection 3.1 and subsection 3.2, respectively.

3.1. First Stage

In this stage, three different data sets were selected: $Data_1$, $Data_2$ and $Data_3$. This choice was made considering the diversity of attributes and the fact that they have been subjected to simulations with various algorithms, including deep learning models. This is to make it easier to compare the performance of the ART models with those in the literature. The Table 2 presents in detail the attributes present in each dataset used in this stage, providing an overview of the attributes used during the experiments conducted.

 doi:10.20944/preprints202404.0956.v1

Table 2. Attributes present in the data.

Data	Attributes
$Data_1$	Alanine Aminotransferase, Aspartate Aminotransferase, Basophils, Class, Eosinophils, Gamma GT, Gender, Age, Lactate Dehydrogenase, Leukocytes, Lymphocytes, Monocytes, Neutrophils, C-Reactive Protein, Platelets
$Data_2$	Alanine Aminotransferase, Aspartate Aminotransferase, Basophils ($10^9\ell^{-1}$), Basophils (%), Calcium, Average Corpuscular Hemoglobin Concentration, Creatine Kinase, Class, Creatinine, Eosinophils ($10^9\ell^{-1}$), Eosinophils (%), Alkaline Phosphatase, Gamma GT, Gender, Glucose, Average Corpuscular Hemoglobin, RBC, Hematocrit, Hemoglobin, Age, Lactate Dehydrogenase, Leukocytes, Lymphocytes ($10^9\ell^{-1}$), Lymphocytes (%), Monocytes ($10^9\ell^{-1}$), Monocytes (%), Neutrophils, Neutrophils (%), C-reactive protein, Platelets, Potassium, Suspected COVID-19, Urea, Mean Corpuscular Volume, Mean Platelet Volume
$Data_3$	Alanine Aminotransferase, Aspartate Aminotransferase, Basophils, Class, Creatinine, Eosinophils, Serum glucose, RBC, Hematocrit, Hemoglobin, Age, Leukocytes, Lymphocytes, Monocytes, Neutrophils, C-reactive protein, Platelets, Potassium, Sodium, urea

The simulations were conducted using the same attributes as those previously used by other researchers. More specifically, the $Data_1$ set underwent the same pre-processing carried out by Brinati et al. [21]. This set contains data from patients who were admitted to the IRCCS San Raffaele Hospital, located in Segrate, in the province of Milan, Italy, between February and March 2020.

The $Data_2$ set was used in the same way as in Cabitza et al.[58]. This set includes the results of routine blood tests carried out on 1925 patients admitted to the emergency room of San Raffaele Hospital between mid-February and May 2020.

For its part, the $Data_3$ set was made available pre-processed by Alakus and Turkoglu [54]. This set was obtained from data made available by the Hospital Israelita Albert Einstein[1]. The data was collected from 5644 patients and contains information from 111 laboratory tests carried out on patients treated at the hospital located in São Paulo, Brazil. It is worth noting that all datasets were used without any modification.

3.2. Second Stage

In this stage, $Data_2$, $Data_4$, $Data_5$, $Data_6$, $Data_7$, $Data_8$, $Data_9$ and $Data_{10}$ were merged to create a new dataset containing hematological information from different countries. This combination was carried out in order to provide more comprehensive information to verify the model's ability to predict COVID-19, since hematological parameters are influenced by individual factors such as age, gender and lifestyle, as well as population and ecological factors such as ethnic origin, climate, exposure to pathogens and altitude [75–77].

The Table 3 shows the averages and standard deviations of the common attributes between all the data sets. The Variance Inflation Factor (VIF) and the Mann-Whitney (MW) test [78] were used to carefully select the attributes for the simulations.

[1] The dataset is available at https://www.kaggle.com/einsteindata4u/covid19

 doi:10.20944/preprints202404.0956.v1

Table 3. Average and standard deviation of attributes.

Attributes	$Data_2$	$Data_4$	$Data_5$	$Data_6$	$Data_7$	$Data_8$	$Data_9$	$Data_{10}$
Age	60,55 ± 19,6	54,38 ± 25,0	66,35 ± 18,5	60,53 ± 20,2	54,40 ± 15,5	47,01 ± 17,4	42,87 ± 17,0	59,73 ± 13,1
BA (%)	0,34 ± 0,3	0,46 ± 0,4	0,18 ± 0,4	0,32 ± 0,3	0,30 ± 0,3	0,52 ± 0,3	0,48 ± 0,3	0,29 ± 0,4
BAT	0,02 ± 0,04	0,03 ± 0,04	0,02 ± 0,05	0,02 ± 0,04	0,02 ± 0,03	0,03 ± 0,02	0,03 ± 0,02	0,04 ± 0,1
EO (%)	0,83 ± 1,6	1,23 ± 2,1	0,74 ± 1,6	0,60 ± 1,2	1,05 ± 1,6	2,30 ± 2,4	2,27 ± 2,5	0,62 ± 1,1
EOT	0,06 ± 0,1	0,09 ± 0,2	0,06 ± 0,1	0,05 ± 0,1	0,06 ± 0,1	0,15 ± 0,2	0,17 ± 0,2	0,08 ± 0,3
HCT	39,41 ± 5,6	37,77 ± 7,4	38,20 ± 6,3	39,67 ± 6,1	40,75 ± 5,0	41,47 ± 4,0	41,18 ± 4,1	39,96 ± 7,9
HGB	13,21 ± 2,0	12,86 ± 2,7	13,21 ± 2,3	13,11 ± 2,2	13,74 ± 1,9	13,82 ± 1,5	14,11 ± 1,5	13,36 ± 3,2
LY (%)	18,54 ± 11,1	21,90 ± 14,5	16,56 ± 11,6	18,30 ± 11,9	23,14 ± 11,4	31,10 ± 11,2	27,57 ± 11,0	7,58 ± 7,1
LYT	1,37 ± 1,0	1,84 ± 4,9	1,63 ± 6,3	1,82 ± 6,1	1,31 ± 1,0	2,01 ± 1,9	2,00 ± 0,9	0,77 ± 0,6
MCH	29,20 ± 2,7	30,41 ± 2,9	29,62 ± 3,1	29,51 ± 2,4	29,60 ± 1,9	29,37 ± 1,9	29,59 ± 1,8	29,58 ± 2,8
MCHC	33,47 ± 1,4	33,98 ± 1,4	34,49 ± 1,5	33,00 ± 1,3	33,68 ± 1,1	33,31 ± 1,1	34,25 ± 1,0	33,09 ± 2,0
MCV	87,22 ± 7,1	89,44 ± 7,4	85,72 ± 8,0	89,41 ± 6,5	87,90 ± 5,1	88,19 ± 5,1	86,39 ± 4,7	88,69 ± 8,3
MO (%)	7,76 ± 3,9	8,86 ± 4,7	7,17 ± 3,9	8,13 ± 5,0	9,64 ± 4,4	9,29 ± 3,7	8,64 ± 3,2	5,74 ± 8,2
MOT	0,62 ± 0,5	0,73 ± 0,9	0,64 ± 0,4	0,64 ± 0,3	0,56 ± 0,3	0,59 ± 0,3	0,63 ± 0,3	0,63 ± 0,8
NE (%)	72,50 ± 13,3	67,54 ± 17,2	75,03 ± 14,2	72,48 ± 14,5	65,78 ± 14,1	56,79 ± 12,4	61,02 ± 12,4	85,77 ± 12,7
NET	6,47 ± 4,5	5,62 ± 4,3	7,47 ± 4,9	6,76 ± 4,3	4,35 ± 3,1	3,92 ± 2,1	4,82 ± 2,4	11,60 ± 8,5
PLT	234,49 ± 94,9	204,00 ± 113,7	220,23 ± 90,0	218,00 ± 84,8	199,81 ± 73,4	246,96 ± 70,3	239,92 ± 64,6	268,69 ± 146,8
RBC	4,55 ± 0,7	4,25 ± 0,9	4,49 ± 0,8	4,46 ± 0,8	4,65 ± 0,7	4,72 ± 0,5	4,78 ± 0,5	4,46 ± 0,9
WBC	8,69 ± 4,7	8,31 ± 7,1	9,81 ± 8,0	9,53 ± 7,5	6,30 ± 3,5	6,70 ± 3,0	7,66 ± 2,7	14,18 ± 17,8

BA: Basophils; BAT: Basophil Count; EO: Eosinophils; EOT: Eosinophil Count; HCT: Hematocrit; HGB: Hemoglobin; LY: Lymphocytes; LYT: Lymphocyte Count; MCH: *Mean Corpuscolar Hemoglobin*; MCHC: *Mean Corpuscular Hemoglobin Concentration*; MCV: *Mean Corpuscular Volume*; MO: Monocytes; MOT: Monocyte Count; NE: Neutrophils; NET: Neutrophil Count; PLT: Platelets; RBC: Red Blood Cells

The MW test is a non-parametric statistical technique used to compare the medians of two independent samples [78,79]. The test was used to check for significant differences between the classes in relation to each attribute analyzed. The determination of statistical significance was established at a confidence level of 0.05, which indicates that values of p below this threshold are considered statistically significant, indicating relevant differences between the medians of the compared groups.

On the other hand, VIF is a statistical measure used to assess multicollinearity between variables. It is obtained from the elements on the main diagonal of the inverse correlation matrix, as expressed in Equation 14 [80].

$$\boldsymbol{R}_{j\times j} = \left(\frac{1}{i-1} \cdot \boldsymbol{W}'_{j\times i} \cdot \boldsymbol{W}_{i\times j}\right), \quad (13)$$

Preprints.org (www.preprints.org) | NOT PEER-REVIEWED | Posted: 15 April 2024 doi:10.20944/preprints202404.0956.v1

$$V_{j\times j} = \left(R_{j\times j}\right)^{-1}, \tag{14}$$

Where R represents the correlation matrix, and W is the matrix of centered and reduced data. It is important to note that the R matrix will be invertible if, and only if, the rank(W) is complete, i.e. the columns/rows of W are linearly independent [81]. The literature points out that VIF values above 5.0 or 10.0 indicate the presence of multicollinearity [82]. On this basis, it was decided not to include attributes with a VIF above 8.0 in the simulations.

The results obtained after the tests are shown in Table 4. The attributes highlighted were selected for the simulations because they were relevant in both tests. It is worth noting that attributes expressed as percentages were not included in the selection, even though they were indicated as relevant by the tests. The decision to exclude these attributes was based on the consideration that absolute values have clinical significance and provide more complete information than relative values (%) [83].

Table 4. Selection of attributes by different methods.

Attributes	*p*-value MW	VIF	Attributes	*p*-value MW	VIF
Age	0.0000	1.4213	MCHC	0.0000	10.5313
BA (%)	0.0000	2.8222	MCV	0.3976	81.7446
BAT	0.0000	2.6595	MO (%)	0.7285	12.1883
EO (%)	0.0000	10.5956	MOT	0.0000	2.8672
EOT	0.0000	7.2687	NE (%)	0.0000	140.5236
HCT	0.0003	400.5673	NET	0.0000	5.4626
HGB	0.0137	351.4449	PLT	0.0627	1.2310
LY (%)	0.0000	100.8982	RBC	0.0007	59.8770
LYT	0.0000	2.1397	WBC	0.0000	3.8370
MCH	0.0136	105.2796			

The selected attributes are part of the white blood series and play a fundamental role in the immune system, helping to fight infections, viruses and bacteria. Analyzing the attributes, it was possible to see some relevant information in relation to patients affected by COVID-19, such as the reduction in cell counts, such as basophils (Figure 3b), eosinophils (Figure 3c) and lymphocytes (Figure 3d). These factors are supported in the literature by authors such as Kermali et al. [84], Samprathi and Jayashree [85] and Keykavousi et al. [86].

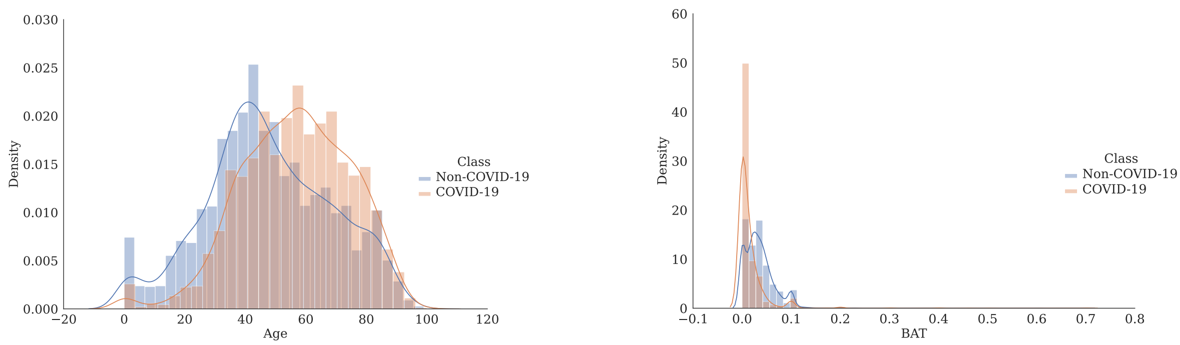

(a) Age **(b)** Basophiles

Figure 3. *Cont.*

Preprints.org (www.preprints.org) | NOT PEER-REVIEWED | Posted: 15 April 2024 doi:10.20944/preprints202404.0956.v1

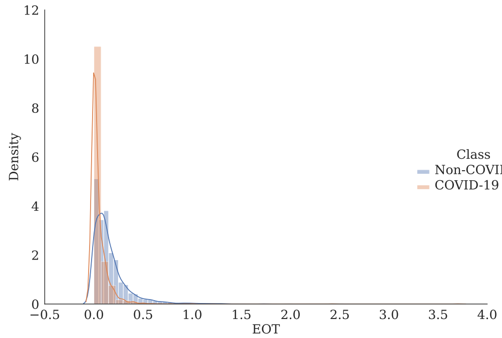

(c) Eosinophils

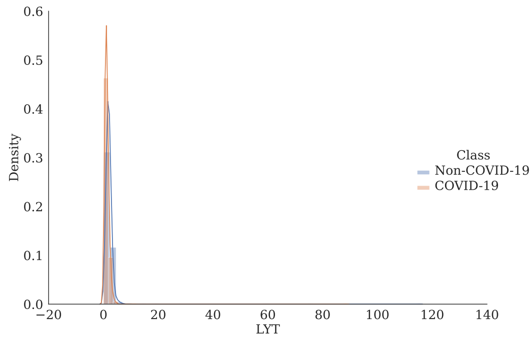

(d) Lymphocytes

Figure 3. Histogram and estimate of the probability density function for each of the attributes separated by class.

After using the combined data set to train and test the model, it was subjected to an external validation process using the Data_1 and Data_{11} sets to assess its ability to generalize on data never before seen by the model. It is worth noting that the same attributes used in training and testing were also used in the external validation phase. Data1 was chosen because it comes from Italy, a country already present in the training data, but with data collected in a different period, while Data11 was selected because it comes from Spain, a different country to those included in the training.

3.3. Evaluation Metrics

To evaluate the performance obtained by each network some metrics frequently present in the literature were used such as accuracy (ACC), sensitivity (Se), specificity (Sp), F_1-Score (F_1), Matthews correlation coefficient (MCC) given respectively by (15), (16), (17), (18), and (19) [87–89].

$$\text{ACC} = \frac{TP + TN}{TP + TN + FP + FN} \tag{15}$$

$$\text{Se} = \frac{TP}{TP + FN} \tag{16}$$

$$\text{Sp} = \frac{TN}{TN + FP} \tag{17}$$

$$\text{F}_1 = \frac{TP}{TP + \frac{1}{2}(FP + FN)} \tag{18}$$

$$\text{MCC} = \frac{TP \cdot TN - FP \cdot FN}{\sqrt{(TP + FP) \cdot (TP + FN) \cdot (TN + FP) \cdot (TN + FN)}} \tag{19}$$

Along with the metrics mentioned above, we use the ROC (Receiver Operating Characteristics) curve to evaluate the quality of the model classification. This curve is generated by plotting the Sensitivity and False Positive Rate (1− Specificity) for different thresholds of the probability estimated by the model. Based on [90] work, the AUC (Area Under the Curve) can be understood as a summary of the ROC curve, the AUC value and the quality of the model can be seen in Table 5.

Table 5. Interpretation of AUC Values.

Range	Result	Range	Result
0.5 – 0.6	Bad	0.7 – 0.8	Acceptable
0.8 – 0.9	Good	> 0.9	Excellent

Preprints.org (www.preprints.org) | NOT PEER-REVIEWED | Posted: 15 April 2024 doi:10.20944/preprints202404.0956.v1

3.4. Classifier

In the unsupervised learning models, it was necessary to use a classifier to convert the clusters to the respective classes of the problem, "COVID-19" and "non-COVID-19". The probability required to generate the ROC curves was also extracted in this step, in which the number of patterns contained in each cluster and the class to which it belonged were analyzed. For example, suppose 10 patterns are allocated to a certain cluster during training, of which 9 are from patients with COVID-19. In this case, this cluster will be labeled as COVID-19 by majority vote, the probability of being COVID-19 will be 0.9, and the complementary probability, that is, of the patient being non-COVID-19 will be 0.1, any pattern allocated to this cluster in the test stage will receive this probability. It is worth noting that for the ARTMAP models that have supervised learning it was not possible to extract the probability and consequently generate the ROC curve, due to the model having discrete output.

3.5. Validation

To partition the data, the hold-out cross-validation method was used, randomly dividing the data into training and test sets based on a pre-determined rate. In addition, the best model found during hold-out validation on each data set was subjected to the repeated hold-out method, also known as Monte Carlo cross-validation [91,92], was employed as a way to obtain a more consistent estimate of model performance. The data was partitioned using the 70–30 ratio, that is, 70% of the samples for training and 30% for testing. For Monte Carlo cross-validation, the process was repeated 50 times, with the data split randomly in each repetition.

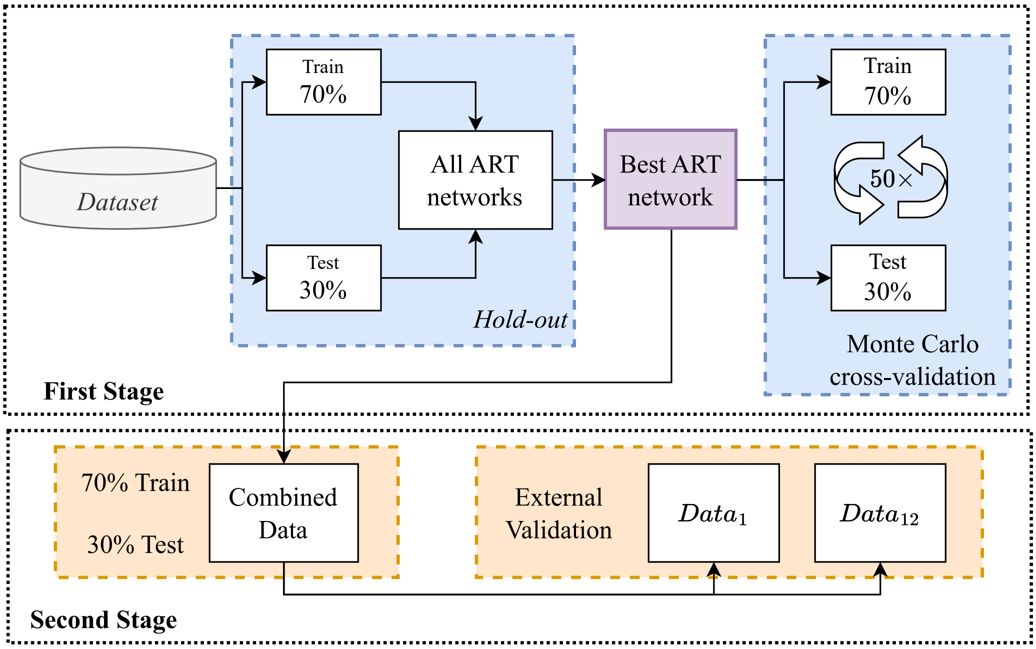

Figure 4. Validation Overview.

4. Computational Results

This section will present the results obtained for COVID-19 diagnostics using the ART networks on each dataset.

4.1. Primeita Etapa

4.1.1. Data$_1$

The performance of various ART networks was evaluated, and the results are presented in Table 6. The SE Fuzzy ART CT network showed the highest accuracy, reaching 0.871, and also demonstrated the greatest ability in correctly detecting patients with COVID-19, as shown by the sensitivity of 0.926.

Notably, fuzzy logic-based networks were found to perform better than Euclidean distance-based networks for this particular dataset.

Table 6. Results obtained by each model for $Data_1$.

Model	ACC	Se	Sp	MCC
SE Fuzzy ART	0.800	0.870	0.670	0.561
SE Euclidean ART	0.706	0.759	0.613	0.370
SE Fuzzy ARTMAP	0.835	0.870	0.774	0.645
SE Fuzzy ART CT	**0.871**	**0.926**	**0.774**	**0.717**
SE Euclidean ART CT	0.741	0.778	0.677	0.450
SE Fuzzy ARTMAP CT	0.800	0.759	0.871	0.608
SE Euclidean ARTMAP CT	0.635	0.778	0.387	0.176

Considering that the network with the best performance in the simple hold-out validation was the SE Fuzzy ART CT, it was used in the Monte Carlo validation to evaluate the network's generalization ability. Table 7 shows the mean metrics as well as the 95% confidence interval (CI) for the Monte Carlo validation.

Table 7. Average result after Monte Carlo cross-validation for $Data_1$.

Metrics	Average result (CI 95%)
ACC	0.8061 (0.7932 – 0.8191)
Se	0.8211 (0.8049 – 0.8373)
Sp	0.7800 (0.7495 – 0.8105)
MCC	0.6555 (0.6264 – 0.6846)
F_1	0.8679 (0.8569 – 0.8788)

To illustrate the results obtained by the best network in each iteration of the Monte Carlo validation, Figure 5 shows the ACC, Se, and Sp for each iteration. It can be seen that the network's performance was not constant in all iterations, reaching a maximum accuracy of 0.9294 and a minimum of 0.7176. On the other hand, Figure 6 presents the average ROC curve and the average AUC obtained by the network in this validation. According to [90], an AUC score above 0.8 can be considered a good performance achieved by the network.

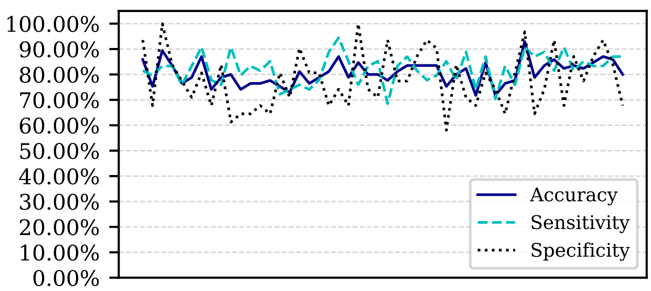

Figure 5. Performance for each of the 50 iterations of the Monte Carlo cross-validation for the $Data_1$.

Preprints.org (www.preprints.org) | NOT PEER-REVIEWED | Posted: 15 April 2024 doi:10.20944/preprints202404.0956.v1

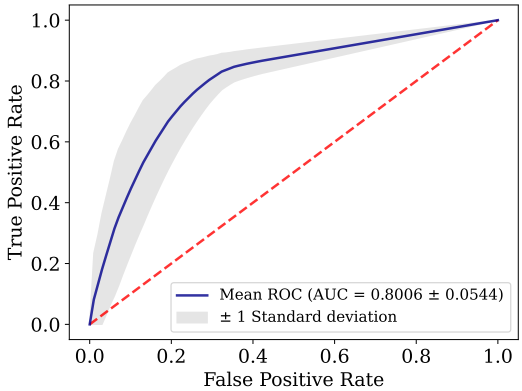

Figure 6. ROC curve for $Data_1$.

4.1.2. $Data_2$

Table 8 presents the results obtained by the networks for $Data_2$. The tested model's achieved approximate performance with MCC ≈ 0.5, and the SE Fuzzy ART CT network achieved the best result, almost perfectly detecting positive and negative patients for COVID-19. Although the SE Euclidean ART CT network achieved the best result in specificity, it was not the best model since it correctly detected only 54.7% of the COVID-19 patients.

Table 8. Results obtained by each model for $Data_2$.

Model	ACC	Se	Sp	MCC
SE Fuzzy ART	0.750	0.746	0.754	0.500
SE Euclidean ART	0.727	0.691	0.762	0.454
SE Fuzzy ARTMAP	0.783	0.792	0.774	0.566
SE Fuzzy ART CT	**0.984**	**0.970**	0.996	**0.967**
SE Euclidean ART CT	0.781	0.547	**1.000**	0.619
SE Fuzzy ARTMAP CT	0.738	0.712	0.762	0.474
SE Euclidean ARTMAP CT	0.697	0.712	0.683	0.394

The SE Fuzzy ART CT Network, which demonstrated the best performance, was subjected to Monte Carlo cross-validation to ensure the reliability of the results, reducing the risk of overfitting. The results are presented in Table 9, where the average results and 95% confidence intervals for the different metrics are presented. The network's performance was remarkable, with an average accuracy of 0.9348, indicating that it successfully classified the data. In addition, the network obtained an MCC of 0.8721, a vital performance measure that considers the balance between sensitivity and specificity.

Table 9. Average result after Monte Carlo cross-validation for $Data_2$.

Metrics	Average result (CI 95%)
ACC	0.9348 (0.9282 – 0.9413)
Se	0.8992 (0.8885 – 0.9098)
Sp	0.9682 (0.9594 – 0.9770)
MCC	0.8721 (0.8592 – 0.8850)
F_1	0.9301 (0.9231 – 0.9371)

Figure 7 illustrates the network's performance in ACC, Se, and Sp for each iteration of the Monte Carlo validation. The results showed that the network was highly stable performing well in almost all iterations. The network achieved a maximum accuracy of 0.9775 and a minimum of 0.875, and of the 50 iterations, only five were below 0.91 in accuracy. These results suggest that the network

Preprints.org (www.preprints.org) | NOT PEER-REVIEWED | Posted: 15 April 2024 doi:10.20944/preprints202404.0956.v1

is highly robust and can be used effectively for the classification task. It should also be noted that the stability in the network's performance over the different iterations of the Monte Carlo validation strongly indicates its generalizability and ability to handle different types of input data.

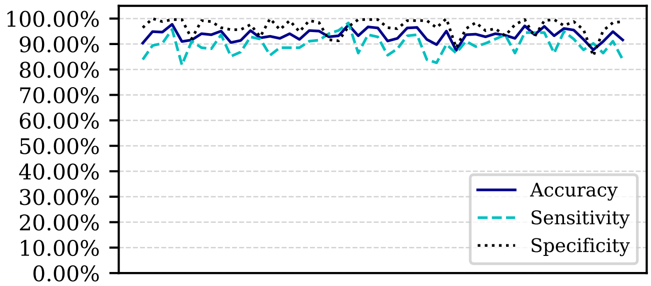

Figure 7. Performance for each of the 50 iterations of the Monte Carlo cross-validation for the $Data_2$.

In Figure 8, the ROC curve and the average AUC obtained after Monte Carlo validation are presented. The AUC value obtained was 0.9395, which suggests that the network has excellent discrimination ability, according to [90].

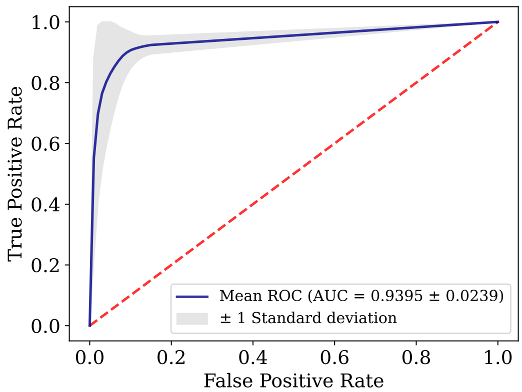

Figure 8. ROC Curve for $Data_2$.

4.1.3. $Data_3$

This dataset needs to more balanced, containing 13.33% data from patients with COVID-19 and 86.67% non-COVID-19 patients. As expected, this unbalance impaired the classification ability of the implemented models, resulting in a low predictive performance as can be seen in Table 10.

Table 10. Results obtained by each model for $Data_3$.

Model	ACC	Se	Sp	MCC
SE Fuzzy ART	0.889	0.208	0.994	0.382
SE Euclidean ART	0.878	0.500	0.936	0.452
SE Fuzzy ARTMAP	0.867	0.375	0.942	0.359
SE Fuzzy ART CT	0.944	0.583	1.000	0.740
SE Euclidean ART CT	**0.972**	**0.792**	**1.000**	**0.876**
SE Fuzzy ARTMAP CT	0.889	0.458	0.955	0.468
SE Euclidean ARTMAP CT	0.872	0.458	0.936	0.417

When working with unbalanced classes, evaluating the performance of a model can be challenging, as traditionally used metrics such as accuracy, sensitivity, and specificity can be misleading and may not provide an accurate representation of model performance [87,88]. Instead, it is recommended to

Preprints.org (www.preprints.org) | NOT PEER-REVIEWED | Posted: 15 April 2024 doi:10.20944/preprints202404.0956.v1

use metrics suitable for unbalanced data, such as the Matthews Correlation Coefficient (MCC) and Area Under the ROC Curve (AUC) [88,89].

In this context, the best performing network for the dataset in question was the SE Euclidean ART CT, achieving an MCC of 0.876. This indicates that the model had a strong correlation between the predicted and actual classes, taking into account both true and false positives and negatives. Table 11 presents the average metrics as well as the 95% confidence interval obtained by the SE Euclidean ART CT network after Monte Carlo validation.

Table 11. Average result after Monte Carlo cross-validation for the $Data_3$.

Metrics	Average result (CI 95%)
ACC	0.9265 (0.9180 – 0.9350)
Se	0.4714 (0.4045 – 0.5382)
Sp	0.9965 (0.9951 – 0.9979)
MCC	0.6195 (0.5656 – 0.6734)
F_1	0.5924 (0.5268 – 0.6580)

By analyzing the results presented in Table 11, it can be seen that the specificity obtained by the network was very high, with a value of 99.65%. This result was expected since most of the dataset samples were from patients who were not infected with COVID-19. However, the average sensitivity obtained by the network was only 0.4714, which indicates that the network did not perform well in detecting COVID-19 positive cases.

Looking at the MCC, a suitable metric for unbalanced data sets, it is noted that the SE Euclidean ART CT network obtained an average MCC of 0.6195 after Monte Carlo validation. While this is not a high value, it is still considered acceptable. Comparing the results obtained in Table 10 and Table 11, it is evident that there was a reduction in the network's performance after Monte Carlo validation. The network could not correctly detect positive COVID-19 cases in some iterations of the validation, with the sensitivity falling below 30% in some iterations, as illustrated in Figure 9.

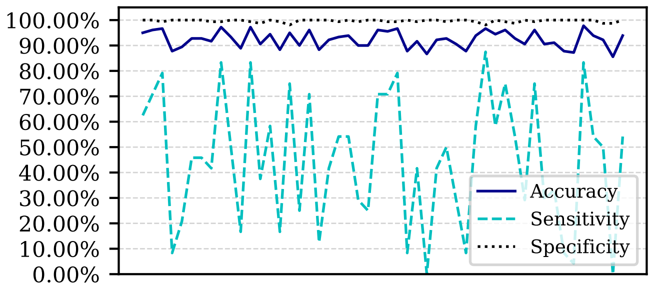

Figure 9. Performance for each of the 50 iterations of the Monte Carlo cross-validation for the $Data_3$.

The ROC curve and the AUC can be seen in Figure 10. By analyzing them, we can see that while specificity remained relatively stable at all cut-off points, there was considerable variation in sensitivity, i.e., the ability to detect positive patients correctly. The mean AUC was 0.7458, with a standard deviation of 0.1265, achieving acceptable performance according to [90].

Table 12 Comparison the results obtained by the neural networks used in this paper and the results found in the literature for the same data sets. The table includes metrics such as ACC, Se, Sp, MCC, F_1, and AUC (ROC).

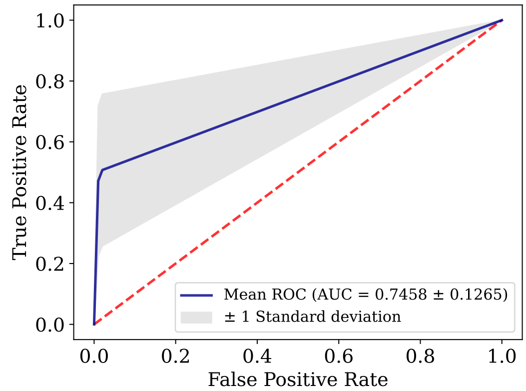

Figure 10. ROC curve for $Data_3$.

Table 12. Comparison of the results for each data set.

Author	Model	Data	Partition	ACC	Se	Sp	MCC	F_1-Score	AUC
This study	SE Fuzzy ART	$Data_1$	70–30	0.8000	0.8704	0.6774	0.5610	0.8468	0.7739
	SE Euclidean ART	$Data_1$	70–30	0.7059	0.7593	0.6129	0.3697	0.7664	0.6861
	SE Fuzzy ARTMAP	$Data_1$	70–30	0.8353	0.8704	0.7742	0.6446	0.8704	-
	SE Fuzzy ART CT	$Data_1$	70–30	0.8706	0.9259	0.7742	0.7170	0.9009	0.8501
	SE Euclidean ART CT	$Data_1$	70–30	0.7412	0.7778	0.6774	0.4496	0.7925	0.7276
	SE Fuzzy ARTMAP CT	$Data_1$	70–30	0.8000	0.7593	0.8710	0.6078	0.8283	-
	SE Euclidean ARTMAP CT	$Data_1$	70–30	0.6353	0.7778	0.3871	0.1763	0.7304	-
	SE Fuzzy ART CT	$Data_1$	Monte Carlo	0.8061	0.8211	0.7800	0.6555	0.8679	0.8006
[93]	ET	$Data_1$	4-Fold	0.8000	0.7500	**0.9444**	0.6133	0.8478	0.7710
	DNN	$Data_1$	4-Fold	**0.9211**	**0.9614**	0.8456	**0.8250**	**0.9388**	**0.9220**
	TWRF	$Data_1$	70-30	0.8600	0.9500	0.7500	-	-	-
[21]	RF	$Data_1$	80-20	0.8200	0.9200	0.6500	-	-	0.8400
This study	SE Fuzzy ART	$Data_2$	70–30	0.7500	0.7459	0.7540	0.4996	0.7426	0.7499
	SE Euclidean ART	$Data_2$	70–30	0.7275	0.6907	0.7619	0.4540	0.7102	0.7263
	SE Fuzzy ARTMAP	$Data_2$	70–30	0.7828	0.7924	0.7738	0.5659	0.7792	-
	SE Fuzzy ART CT	$Data_2$	70–30	**0.9836**	**0.9703**	0.9960	**0.9674**	**0.9828**	**0.9481**
	SE Euclidean ART CT	$Data_2$	70–30	0.7807	0.5466	**1.000**	0.6194	0.7068	0.7733
	SE Fuzzy ARTMAP CT	$Data_2$	70–30	0.7377	0.7119	0.7619	0.4745	0.7241	-
	SE Euclidean ARTMAP CT	$Data_2$	70–30	0.6967	0.7119	0.6828	0.3942	0.6942	-
	SE Fuzzy ART CT	$Data_2$	Monte Carlo	0.9348	0.8992	0.9682	0.8721	0.9301	0.9395
[93]	ET	$Data_2$	4-Fold	0.8498	0.8788	0.8221	0.7012	0.8509	0.8510
	DNN	$Data_2$	4-Fold	0.9316	0.9327	0.9302	0.8633	0.9263	0.9320
[58]	KNN	$Data_2$	*hold-out*	0.8600	0.8000	0.9200	-	-	0.8700
This study	SE Fuzzy ART	$Data_3$	70–30	0.8889	0.2083	0.9936	0.3824	0.3333	0.6010
	SE Euclidean ART	$Data_3$	70–30	0.8778	0.5000	0.9359	0.4524	0.5217	0.7179
	SE Fuzzy ARTMAP	$Data_3$	70–30	0.8667	0.3750	0.9423	0.3595	0.4286	-
	SE Fuzzy ART CT	$Data_3$	70–30	0.9444	0.5833	1.0000	0.7404	0.7368	0.7917
	SE Euclidean ART CT	$Data_3$	70–30	**0.9722**	0.7917	**1.0000**	**0.8758**	0.8837	0.8962
	SE Fuzzy ARTMAP CT	$Data_3$	70–30	0.8889	0.4583	0.9551	0.4685	0.5238	-
	SE Euclidean ARTMAP CT	$Data_3$	70–30	0.8722	0.4583	0.9359	0.4175	0.4889	-
	SE Euclidean ART CT	$Data_3$	Monte Carlo	0.9265	0.4714	0.9965	0.6195	0.5924	0.7458
[93]	ET	$Data_3$	4-Fold	0.9200	0.7143	0.9301	0.4530	0.4545	0.6590
	DNN	$Data_3$	4-Fold	0.9333	0.7705	0.9547	0.6904	0.7249	0.8597
[54]	LSTM	$Data_3$	10-Fold	0.8666	**0.9942**	-	-	0.9189	0.6250
	CNN-LSTM	$Data_3$	80–20	0.9230	0.9368	-	-	**0.9300**	**0.9000**

SE: Self-Expanding; **CT**: Continuous Training; **ET**: Extremely Randomized Trees; **DNN**: Deep Neural Network; **RF**: Random Forest; **TWRF**: Three-way Random Forest; **KNN**: K Nearest neighbors; **LSTM**: Long short-term memory; **CNN**: Convolutional Neural Networks.

The results obtained for $Data_1$ were quite promising, as the SE Fuzzy ART CT network achieved AUC of 0.8501 and 0.8006 in hold-out and Monte Carlo validation, respectively. These results were better than those obtained by commonly used models such as RF and ET, often used for classification tasks. Although the performance of the SE Fuzzy ART CT network was good, the DNN deep learning model used by [93] obtained even better results, achieving an AUC value of 0.9220.

When examining the results for $Data_2$, it can be seen that the SE Fuzzy ART CT network achieved outstanding performance. It obtained an AUC of 0.9481 in the hold-out validation, indicating high accuracy in distinguishing between COVID-19 positive and negative patients. It outperformed machine learning models traditionally used in classification tasks such as ET, KNN, and even the deep learning algorithm DNN, which achieved an AUC of 0.9320. The sensitivity of the ART network was also significantly higher at 97.03%, indicating it is effective in correctly identifying positive patients. It is worth noting that even when the SE Fuzzy ART CT network was subjected to Monte Carlo cross-validation, it maintained its good performance with an AUC of 0.9395, outperforming DNN once again.

For $Data_3$, the SE Euclidean ART CT network achieved AUC of 0.8962, a result similar to that obtained with the CNN-LSTM model used by [54], which achieved AUC of 0.9000. However, after performing Monte Carlo cross-validation, a decrease in the performance of the SE Euclidean ART CT network was observed due to a significant imbalance between classes.

The Comparison of the computational time (in seconds) between the two best models implemented in this paper (SE Fuzzy ART CT and SE Euclidean ART CT), with the best model obtained by [93] the Deep Neural Network (DNN), can be seen in Table 13. It is worth noting that the computational time given in the table considers only the training and testing time. Also, the best algorithms for each dataset are highlighted in bold.

Table 13. Computational time (in seconds) for each dataset.

Model	$Data_1$	$Data_2$	$Data_3$
SE Fuzzy ART CT	1.25	**6.34**	5.14
SE Euclidean ART CT	1.22	0.62	**1.67**
DNN	**20.2**	40.32	21.01

When analyzing the computational time in Table 13, it is clear that the ART networks showed significantly faster convergence than the DNN. This is due to the nature of the network and accentuated by the self-expansion mechanism. In addition, it can be seen that the Euclidean distance-based neural network obtained a slightly shorter time than the fuzzy neural network. This difference can be attributed to the fact that the Euclidean network not requiring normalization and encoding of the input data. Consequently, the size of the input data entered into the Euclidean network is halved, leading to faster processing. Another relevant feature of ART networks is that they do not suffer from catastrophic forgetting, unlike those based on the back-propagation algorithm and deep learning models, as reported by [61].

4.2. Second Stage

In this second stage, we sought to compare the performance of the winning model from the previous stage, SE Fuzzy ART CT, with traditional models frequently used in the literature. To do this, the combination of data described in subsection 3.2 was used. Algorithms such as K-Nearest Neighbors (KNN), Random Forest (RF), Multi-layer Perceptron (MLP), Logistic Regression (LR), Extra Trees (ET), XGBoost (XGB) and Naive Bayes (NB) were implemented in Python with the Scikit-Learn library [94]. The parameters of each model were optimized using the GridSearchCV method, exploring various combinations of hyperparameters in order to identify the one that resulted in the best performance. The results obtained are presented in the Table 14, highlighting the superiority of the ART network over traditional models, achieving an MCC of 0.9628.

In addition, the Figure 11 shows the ROC curve and AUC for each model. The SE Fuzzy ART CT network obtained the best AUC, with a value of 0.9770, indicating that it has a high ability to distinguish between classes. Among the traditional models tested, the RF algorithm obtained the best performance, with AUC and MCC of 0.8504 and 0.5510, respectively. However, these results are

Preprints.org (www.preprints.org) | NOT PEER-REVIEWED | Posted: 15 April 2024 doi:10.20944/preprints202404.0956.v1

significantly lower than those of the ART network. The RF algorithm's ability to distinguish between classes is around 12% lower than that of the ART network.

Table 14. Results obtained by each model for the combined data set.

Model	SE Fuzzy ART CT	KNN	RF	MLP	LR	ET	XGB	NB
ACC	**0.9828**	0.7277	0.7931	0.7825	0.7617	0.7748	0.7333	0.7429
Se	**0.9667**	0.5986	0.7014	0.6806	0.6389	0.5806	0.8722	0.6806
Sp	**0.9920**	0.8019	0.8458	0.8411	0.8323	0.8866	0.6534	0.7788
F_1-Score	**0.9762**	0.6162	0.7123	0.6955	0.6619	0.6531	0.7048	0.6590
MCC	**0.9628**	0.4059	0.5510	0.5267	0.4790	0.4988	0.5076	0.4536

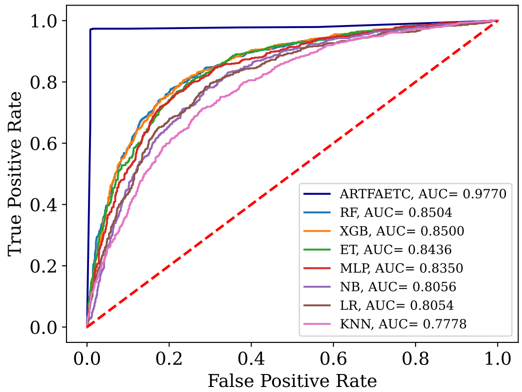

Figure 11. ROC curve and AUC for the combined data set.

The Table 15 and Figure 12 show, respectively, the metrics and the ROC curve along with the AUC of the models trained with the combined data and validated with $Dados_{12}$, i.e. the data collected in Spain.

Table 15. Results obtained by each model trained with the combined data and validated with $Dados_{12}$.

Model	SE Fuzzy ART CT	KNN	RF	MLP	LR	ET	XGB	NB
ACC	**0.9770**	0.7169	0.7834	0.7724	0.7547	0.7633	0.7308	0.7331
Se	**0.9661**	0.5834	0.6813	0.6625	0.6286	0.5609	0.8595	0.6637
Sp	**0.9838**	0.7991	0.8462	0.8400	0.8323	0.8879	0.6515	0.7759
F_1-Score	**0.9698**	0.6110	0.7057	0.6893	0.6614	0.6436	0.7087	0.6547
MCC	**0,9513**	0,3903	0,5355	0,5112	0,4714	0,4838	0,5076	0,4374

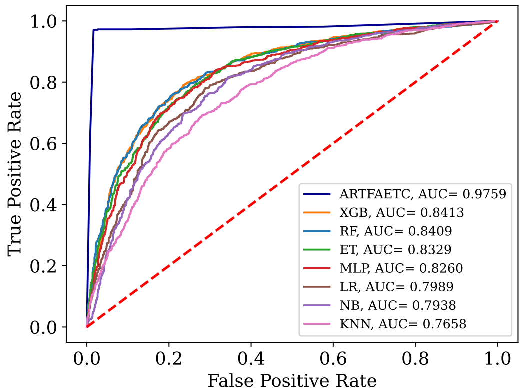

Figure 12. ROC curve and AUC obtained by each model trained with the combined data and validated by $Dados_{12}$.

Preprints.org (www.preprints.org) | NOT PEER-REVIEWED | Posted: 15 April 2024 doi:10.20944/preprints202404.0956.v1

Although it showed a slight decline in performance when compared to the results presented in Table 15 and Figure 11, the SE Fuzzy ART CT network still outperformed the traditional models, which also showed a reduction in performance when tested with the new data. The model obtained an AUC of 0.9759, a significantly better performance than the traditional models, which obtained AUCs of 0.8413 for XGB and 0.8409 for RF.

When the SE Fuzzy ART CT network trained with the combined data was submitted to the Data_1 validation set, there was a reduction in its performance compared to the results obtained with the combined data. This reduction was only 1.71% in terms of AUC, from 0.9770 to 0.9606. The traditional models, on the other hand, showed an increase of less than 0.01% in relation to the AUC obtained with the combined data. However, even with this reduction in performance, the ART network still remained the most effective model in distinguishing between patients with and without COVID-19.

Table 16. Results obtained by each model trained with the combined data and validated by Dados_1.

Modelo	SE Fuzzy ART CT	KNN	RF	MLP	LR	ET	XGB	NB
ACC	**0,9645**	0,7326	0,7863	0,7699	0,7539	0,7654	0,7326	0,7370
Se	**0,9710**	0,6388	0,7168	0,6901	0,6589	0,6042	0,8796	0,7101
Sp	**0,9601**	0,7947	0,8323	0,8227	0,8168	0,8722	0,6352	0,7548
F_1-Score	**0,9561**	0,6556	0,7278	0,7050	0,6809	0,6725	0,7239	0,6827
MCC	**0,9266**	0,4377	0,5522	0,5168	0,4817	0,5011	0,5090	0,4597

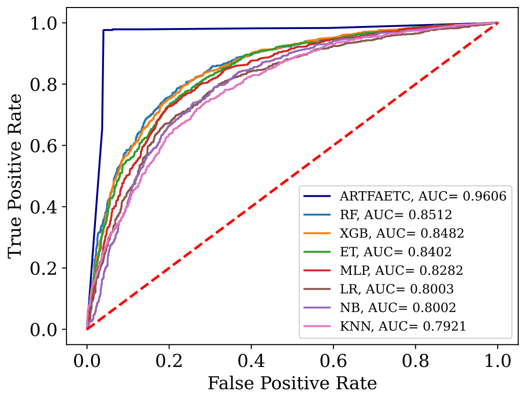

Figure 13. ROC curve and AUC obtained by each model trained with the combined data and validated by Data_1.

4.3. *Discussão*

The combined analysis of the two stages highlights not only the effectiveness of SE Fuzzy ART CT in detecting COVID-19, but also its ability to handle new patient data. In the first part, it did better than other models mentioned in the literature. In the second stage, when we compared conventional models with SE Fuzzy ART CT, we confirmed its superiority. The network's results remained consistent even with data from different countries. The online training capacity, combined with the unsupervised training, were the attributes responsible for the excellent performance and places it as an adaptable and promising tool for accurate, real-time classifications.

In addition to its positive results, the study also addresses some limitations listed by other articles. A study by [95], for example, cites the lack of patients from other geographical locations as a limitation. [95] states that it is necessary to consider patients from different demographic groups in order to establish reliable results. This study addresses this limitation by training and testing the models on data from several hospitals in four countries. This allows the results to be more representative of the population.

 doi:10.20944/preprints202404.0956.v1

In addition, the study tests models with unsupervised learning, a limitation pointed out in the work by [96]. Since unsupervised learning allows models to learn to identify patterns in the data without the need for labels.

5. Conclusion

This article presents the results obtained by neural networks based on Adaptive Resonance Theory (ART) for the classification of COVID-19, using laboratory tests (blood tests) in order to correctly classify infected and healthy patients. A comparison was made between seven different ART architectures, including online training algorithms. The most successful architecture was subjected to a dataset made up of laboratory tests from patients in different countries. When comparing the results of the first stage, it can be seen that the self-expanding fuzzy ART network with continuous training (SE Fuzzy ART CT) and the self-expanding Euclidean ART network with continuous training (SE Euclidean ART CT) outperformed the other ART networks implemented. In addition, in some cases, the networks outperformed the DNN and CNN deep learning models frequently used in the literature. The SE Fuzzy ART CT obtained an AUC of 0.8501 for $Data_1$, 0.9481 for $Data_2$ and 0.8962 for $Data_3$. When considering computational time, the self-expanding ART neural networks with continuous training were more efficient in the three data sets tested.

In the second stage, the self-expanding SE Fuzzy ART CT that won out in the first stage was subjected to a data set from various hospitals in four countries. This network was compared with traditional algorithms in the literature, maintaining an excellent performance that significantly outperformed all traditional models. Even during external validation with data from a different country to that included in the training, validating its generalization capacity.

In addition to the superior results compared to most of the models analyzed, the networks used do not face the main problems associated with traditional algorithms, such as slow learning, catastrophic forgetting and off-line training. Thus, these results highlight the potential of networks based on adaptive resonance theory, such as SE Fuzzy ART CT and SE Euclidean ART CT, as highly effective and reliable tools to aid in the detection of COVID-19, reducing the false negative rate of RT-PCR or even as a viable solution for detection in places with limited resources or underdeveloped countries.

Despite the promising results obtained by the ART networks, in future studies we intend to reduce the size of the data sets, selecting the most significant attributes to detect healthy and COVID-19 patients, and we can also add more information to aid classification, such as the use of imaging tests or symptoms. In addition, it is possible to make some adjustments to the models to improve the quality of the classification, such as modifying the normalization used, extending the research to the β parameter, using the k-Fold cross-validation method as a way of validating and evaluating the model's generalization capacity.

Author Contributions: Conceptualization, R.J.d.S. and M.L.M.L; methodology, R.J.d.S.; software, R.J.d.S.; validation, R.J.d.S., C.R.d.S.J, M.L.M.L, T.A and C.R.M; formal analysis, R.J.d.S., C.R.M and M.L.M.L; investigation, R.J.d.S. and M.L.M.L; resources, R.J.d.S.; data curation, R.J.d.S.; writing—original draft preparation, R.J.d.S.; writing—review and editing, M.L.M.L, C.R.d.S.J, T.A and C.R.M; visualization, R.J.d.S.; supervision, M.L.M.L; project administration, M.L.M.L; funding acquisition, M.L.M.L and C.R.M All authors have read and agreed to the published version of the manuscript.

Funding: This work was supported by National Council for Scientific and Technological Development (CNPq) and Coordenação de Aperfeiçoamento de Pessoal de Nível Superior - Brasil (CAPES) - Finance Code 001.

Institutional Review Board Statement: Not applicable.

Informed Consent Statement: Not applicable.

Data Availability Statement: The data used to support the findings of this study are available from the corresponding author upon request.

Conflicts of Interest: The authors declare no conflict of interest.

References

1. World Health Organization. Coronavirus disease 2019 (covid-19) situation report 92, 2020. https://www.who.int/emergencies/diseases/novel-coronavirus-2019/situation-reports (Accessed on Feb 2, 2024).
2. World Health Organization. Coronavirus disease (covid-19) dashboard, 2020. https://covid19.who.int/ (Accessed on Apr. 6, 2024).
3. World Health Organization. 14.9 million excess deaths associated with the covid-19 pandemic in 2020 and 2021, 2020. www.who.int/news/item/05-05-2022-14.9-million-excess-deaths-were-associated-with-the-covid-19-pandemic-in-2020-and-2021 (Accessed on Dec 5, 2023).
4. World Health Organization. Coronavirus disease (covid-19)., 2020. https://www.who.int/health-topics/coronavirus/#tab=tab_3 (Accessed on Apr. 6, 2024).
5. Wang, Y.; Zheng, K.; Gao, W.; Lv, J.; Yu, C.; Wang, L.; Wang, Z.; Wang, B.; Liao, C.; Li, L. Asymptomatic and pre-symptomatic infection in Coronavirus Disease 2019 pandemic. *Medical Review* **2022**, *2*, 66–88. https://doi.org/10.1515/mr-2021-0034.
6. Weissleder, R.; Lee, H.; Ko, J.; Pittet, M.J. COVID-19 diagnostics in context. *Science translational medicine* **2020**, *12*, eabc1931. https://doi.org/10.1126/scitranslmed.abc1931.
7. Corman, V.; Bleicker, T.; Brünink, S.; Drosten, C.; Landt, O.; Koopmans, M.; Zambon, M.; Peiris, M. Diagnostic detection of Wuhan coronavirus 2019 by real-time RT-PCR. *Geneva: World Health Organization* **2020**, *13*.
8. Zhang, L.; Xiao, M.; Wang, Y.; Peng, S.; Chen, Y.; Zhang, D.; Zhang, D.; Guo, Y.; Wang, X.; Luo, H.; et al. Fast screening and primary diagnosis of COVID-19 by ATR–FT-IR. *Analytical chemistry* **2021**, *93*, 2191–2199. https://doi.org/10.1021/acs.analchem.0c04049.
9. Salathé, M.; Althaus, C.L.; Neher, R.; Stringhini, S.; Hodcroft, E.; Fellay, J.; Zwahlen, M.; Senti, G.; Battegay, M.; Wilder-Smith, A.; et al. COVID-19 epidemic in Switzerland: on the importance of testing, contact tracing and isolation. *Swiss medical weekly* **2020**. https://doi.org/10.4414/smw.2020.20225.
10. Kaye, A.D.; Okeagu, C.N.; Pham, A.D.; Silva, R.A.; Hurley, J.J.; Arron, B.L.; Sarfraz, N.; Lee, H.N.; Ghali, G.; Gamble, J.W.; et al. Economic impact of COVID-19 pandemic on healthcare facilities and systems: International perspectives. *Best Practice & Research Clinical Anaesthesiology* **2021**, *35*, 293–306. https://doi.org/10.1016/j.bpa.2020.11.009.
11. Gholipour, K.; Behpaie, S.; Iezadi, S.; Ghiasi, A.; Tabrizi, J.S. Costs of inpatient care and out-of-pocket payments for COVID-19 patients: A systematic review. *PLOS ONE* **2023**, *18*, 1–18. https://doi.org/10.1371/journal.pone.0283651.
12. An, X.; Xiao, L.; Yang, X.; Tang, X.; Lai, F.; Liang, X.H. Economic burden of public health care and hospitalisation associated with COVID-19 in China. *Public Health* **2022**, *203*, 65–74. https://doi.org/10.1016/j.puhe.2021.12.001.
13. Reis, A.A.d.S.; Santos, R.d.S. The gold standard on the molecular diagnosis for COVID19: What do we know about the sovereignty of this method? *Brazilian Journal of Health Review* **2020**, *3*, 5986–5992. https://doi.org/10.34119/bjhrv3n3-157.
14. Hope, M.D.; Raptis, C.A.; Shah, A.; Hammer, M.M.; Henry, T.S. A role for CT in COVID-19? What data really tell us so far. *The Lancet* **2020**, *395*, 1189–1190. https://doi.org/10.1016/S0140-6736(20)30728-5.
15. Pradhan, A.; Prabhu, S.; Chadaga, K.; Sengupta, S.; Nath, G. Supervised learning models for the preliminary detection of COVID-19 in patients using demographic and epidemiological parameters. *Information* **2022**, *13*, 330. https://doi.org/10.3390/info13070330.
16. Ai, T.; Yang, Z.; Hou, H.; Zhan, C.; Chen, C.; Lv, W.; Tao, Q.; Sun, Z.; Xia, L. Correlation of chest CT and RT-PCR testing in coronavirus disease 2019 (COVID-19) in China: a report of 1014 cases. *Radiology* **2020**. https://doi.org/10.1148/radiol.2020200642.
17. Tahamtan, A.; Ardebili, A. Real-time RT-PCR in COVID-19 detection: issues affecting the results. *Expert review of molecular diagnostics* **2020**, *20*, 453–454. https://doi.org/10.1080/14737159.2020.1757437.
18. Shrestha, L.B.; Foster, C.; Rawlinson, W.; Tedla, N.; Bull, R.A. Evolution of the SARS-CoV-2 omicron variants BA. 1 to BA. 5: Implications for immune escape and transmission. *Reviews in Medical Virology* **2022**, *32*, e2381. https://doi.org/10.1002/rmv.2381.
19. Li, Z.; Yi, Y.; Luo, X.; Xiong, N.; Liu, Y.; Li, S.; Sun, R.; Wang, Y.; Hu, B.; Chen, W.; et al. Development and clinical application of a rapid IgM-IgG combined antibody test for SARS-CoV-2 infection diagnosis. *Journal of Medical Virology* **2020**, *92*, 1518–1524. https://doi.org/10.1002/jmv.25727.

20. Kistenev, Y.V.; Vrazhnov, D.A.; Shnaider, E.E.; Zuhayri, H. Predictive models for COVID-19 detection using routine blood tests and machine learning. *Heliyon* **2022**, p. e11185. https://doi.org/10.1016/j.heliyon.2022.e11185.
21. Brinati, D.; Campagner, A.; Ferrari, D.; Locatelli, M.; Banfi, G.; Cabitza, F. Detection of COVID-19 infection from routine blood exams with machine learning: a feasibility study. *Journal of medical systems* **2020**, *44*, 1–12. https://doi.org/10.1007/s10916-020-01597-4.
22. Riquelme, D.; Akhloufi, M.A. Deep learning for lung cancer nodules detection and classification in CT scans. *Ai* **2020**, *1*, 28–67. https://doi.org/10.3390/ai1010003.
23. Chung, M.; Bernheim, A.; Mei, X.; Zhang, N.; Huang, M.; Zeng, X.; Cui, J.; Xu, W.; Yang, Y.; Fayad, Z.A.; et al. CT Imaging Features of 2019 Novel Coronavirus (2019-nCoV). *Radiology* **2020**, *295*, 202–207. https://doi.org/10.1148/radiol.2020200230.
24. Suganya, D.; Kalpana, R. Prognosticating various acute covid lung disorders from COVID-19 patient using chest CT Images. *Engineering Applications of Artificial Intelligence* **2023**, *119*, 105820. https://doi.org/10.1016/j.engappai.2023.105820.
25. Nafisah, S.I.; Muhammad, G.; Hossain, M.S.; AlQahtani, S.A. A Comparative Evaluation between Convolutional Neural Networks and Vision Transformers for COVID-19 Detection. *Mathematics* **2023**, *11*. https://doi.org/10.3390/math11061489.
26. Khishe, M.; Caraffini, F.; Kuhn, S. Evolving Deep Learning Convolutional Neural Networks for Early COVID-19 Detection in Chest X-ray Images. *Mathematics* **2021**, *9*. https://doi.org/10.3390/math9091002.
27. Hassan, M.M.; AlRakhami, M.S.; Alabrah, A.A.; AlQahtani, S.A. An Intelligent Edge-as-a-Service Framework to Combat COVID-19 Using Deep Learning Techniques. *Mathematics* **2023**, *11*. https://doi.org/10.3390/math11051216.
28. Kovács, A.; Palásti, P.; Veréb, D.; Bozsik, B.; Palkó, A.; Kincses, Z.T. The sensitivity and specificity of chest CT in the diagnosis of COVID-19. *European radiology* **2021**, *31*, 2819–2824. https://doi.org/10.1007/s00330-020-07347-x.
29. Pan, F.; Ye, T.; Sun, P.; Gui, S.; Liang, B.; Li, L.; Zheng, D.; Wang, J.; Hesketh, R.L.; Yang, L.; et al. Time course of lung changes on chest CT during recovery from 2019 novel coronavirus (COVID-19) pneumonia. *Radiology* **2020**. https://doi.org/10.1148/radiol.2020200370.
30. Raptis, C.A.; Hammer, M.M.; Short, R.G.; Shah, A.; Bhalla, S.; Bierhals, A.J.; Filev, P.D.; Hope, M.D.; Jeudy, J.; Kligerman, S.J.; et al. Chest CT and coronavirus disease (COVID-19): a critical review of the literature to date. *AJR Am J Roentgenol* **2020**, *215*, 839–842. https://doi.org/10.2214/AJR.20.23202.
31. Smith-Bindman, R. CT Radiation and the Risk of Cancer. *Current Radiology Reports* **2015**, *3*, 3. https://doi.org/10.1007/s40134-014-0085-5.
32. Wiest, P.W.; Locken, J.A.; Heintz, P.H.; Mettler, F. CT scanning: A major source of radiation exposure. *Seminars in Ultrasound, CT and MRI* **2002**, *23*, 402–410. https://doi.org/10.1016/S0887-2171(02)90011-9.
33. Ahsan, M.M.; Luna, S.A.; Siddique, Z. Machine-Learning-Based Disease Diagnosis: A Comprehensive Review. In Proceedings of the Healthcare. MDPI, 2022, Vol. 10, p. 541. https://doi.org/10.3390/healthcare10030541.
34. Mirzaei, G.; Adeli, H. Machine learning techniques for diagnosis of alzheimer disease, mild cognitive disorder, and other types of dementia. *Biomedical Signal Processing and Control* **2022**, *72*, 103293. https://doi.org/10.1016/j.bspc.2021.103293.
35. Wu, J.; Zhang, P.; Zhang, L.; Meng, W.; Li, J.; Tong, C.; Li, Y.; Cai, J.; Yang, Z.; Zhu, J.; et al. Rapid and accurate identification of COVID-19 infection through machine learning based on clinical available blood test results. *MedRxiv preprint* **2020**. https://doi.org/10.1101/2020.04.02.20051136.
36. Sun, L.; Song, F.; Shi, N.; Liu, F.; Li, S.; Li, P.; Zhang, W.; Jiang, X.; Zhang, Y.; Sun, L.; et al. Combination of four clinical indicators predicts the severe/critical symptom of patients infected COVID-19. *Journal of Clinical Virology* **2020**, *128*, 104431. https://doi.org/10.1016/j.jcv.2020.104431.
37. Lv, C.; Guo, W.; Yin, X.; Liu, L.; Huang, X.; Li, S.; Zhang, L. Innovative applications of artificial intelligence during the COVID-19 pandemic. *Infectious Medicine* **2024**, *3*, 100095. https://doi.org/10.1016/j.imj.2024.100095.
38. Hussain, L.; Nguyen, T.; Li, H.; Abbasi, A.A.; Lone, K.J.; Zhao, Z.; Zaib, M.; Chen, A.; Duong, T.Q. Machine-learning classification of texture features of portable chest X-ray accurately classifies COVID-19 lung infection. *BioMedical Engineering OnLine* **2020**, *19*, 1–18. https://doi.org/10.1186/s12938-020-00831-x.

39. Zargari Khuzani, A.; Heidari, M.; Shariati, S.A. COVID-Classifier: An automated machine learning model to assist in the diagnosis of COVID-19 infection in chest x-ray images. *Scientific Reports* **2021**, *11*, 1–6. https://doi.org/10.1038/s41598-021-88807-2.
40. Marar, R.W.; Marar, H.W. A 15-Gbps BiCMOS XNOR gate for fast recognition of COVID-19 in binarized neural networks. *International Journal of Electrical and Computer Engineering* **2022**, *12*, 997. https://doi.org/10.11591/ijece.v12i1.pp997-1002.
41. Carelli, G.Z.; Carvalho, B.R.d.B.; Molin, B.D.; Duarte, C.R.; Martins, G.K.F.; Wendt, G.W.; Silva, M.C.B.; Guedes, S.J.K.O.; Ferreto, L.E.D. Laboratory markers in patients with COVID-19. *Research, Society and Development* **2020**, *9*, e30191211115–e30191211115. https://doi.org/10.33448/rsd-v9i12.11115.
42. Silva, G.F.R.; Callante, A.A.; Nascimento, D.P.; Araujo, I.P.; Ribeiro, C.H.M.A.; Prete, A.C.L. Comparison of the biochemical and hematological profiles of patients with COVID-19 in their different outcomes: Hospital discharge and death. *Research, Society and Development* **2022**, *11*, e25611225772–e25611225772. https://doi.org/10.33448/rsd-v11i2.25772.
43. Liu, Y.; Yang, Y.; Zhang, C.; Huang, F.; Wang, F.; Yuan, J.; Wang, Z.; Li, J.; Li, J.; Feng, C.; et al. Clinical and biochemical indexes from 2019-nCoV infected patients linked to viral loads and lung injury. *Science China Life Sciences* **2020**, *63*, 364–374. https://doi.org/10.1007/s11427-020-1643-8.
44. Khartabil, T.; Russcher, H.; van der Ven, A.; De Rijke, Y. A summary of the diagnostic and prognostic value of hemocytometry markers in COVID-19 patients. *Critical reviews in clinical laboratory sciences* **2020**, *57*, 415–431. https://doi.org/10.1080/10408363.2020.1774736.
45. Palladino, M. Complete blood count alterations in COVID-19 patients: A narrative review. *Biochemia medica* **2021**, *31*, 0–0. https://doi.org/10.11613/BM.2021.030501.
46. Sun, D.w.; Zhang, D.; Tian, R.h.; Li, Y.; Wang, Y.s.; Cao, J.; Tang, Y.; Zhang, N.; Zan, T.; Gao, L.; et al. The underlying changes and predicting role of peripheral blood inflammatory cells in severe COVID-19 patients: A sentinel? *Clinica chimica acta* **2020**, *508*, 122–129. https://doi.org/10.1016/j.cca.2020.05.027.
47. Elderdery, A.Y.; Elkhalifa, A.M.; Alsrhani, A.; Zawbaee, K.I.; Alsurayea, S.M.; Escandarani, F.K.; Alhamidi, A.H.; Idris, H.M.; Abbas, A.M.; Shalabi, M.G.; et al. Complete Blood Count Alterations of COVID-19 Patients in Riyadh, Kingdom of Saudi Arabia. *Journal of Nanomaterials* **2022**, *2022*. https://doi.org/10.1155/2022/6529641.
48. Batista, A.F.d.M.; Miraglia, J.L.; Donato, T.H.R.; Chiavegatto Filho, A.D.P. COVID-19 diagnosis prediction in emergency care patients: a machine learning approach. *MedRxiv preprint* **2020**. https://doi.org/10.1101/2020.04.04.20052092.
49. Tordjman, M.; Mekki, A.; Mali, R.D.; Saab, I.; Chassagnon, G.; Guillo, E.; Burns, R.; Eshagh, D.; Beaune, S.; Madelin, G.; et al. Pre-test probability for SARS-Cov-2-related infection score: The PARIS score. *PLoS One* **2020**, *15*, e0243342. https://doi.org/10.1371/journal.pone.0243342.
50. Yang, H.S.; Hou, Y.; Vasovic, L.V.; Steel, P.A.; Chadburn, A.; Racine-Brzostek, S.E.; Velu, P.; Cushing, M.M.; Loda, M.; Kaushal, R.; et al. Routine laboratory blood tests predict SARS-CoV-2 infection using machine learning. *Clinical chemistry* **2020**, *66*, 1396–1404. https://doi.org/10.1093/clinchem/hvaa200.
51. Joshi, R.P.; Pejaver, V.; Hammarlund, N.E.; Sung, H.; Lee, S.K.; Furmanchuk, A.; Lee, H.Y.; Scott, G.; Gombar, S.; Shah, N.; et al. A predictive tool for identification of SARS-CoV-2 PCR-negative emergency department patients using routine test results. *Journal of Clinical Virology* **2020**, *129*, 104502. https://doi.org/10.1016/j.jcv.2020.104502.
52. Goodman-Meza, D.; Rudas, A.; Chiang, J.N.; Adamson, P.C.; Ebinger, J.; Sun, N.; Botting, P.; Fulcher, J.A.; Saab, F.G.; Brook, R.; et al. A machine learning algorithm to increase COVID-19 inpatient diagnostic capacity. *Plos one* **2020**, *15*, e0239474. https://doi.org/10.1371/journal.pone.0239474.
53. AlJame, M.; Ahmad, I.; Imtiaz, A.; Mohammed, A. Ensemble learning model for diagnosing COVID-19 from routine blood tests. *Informatics in Medicine Unlocked* **2020**, *21*, 100449. https://doi.org/10.1016/j.imu.2020.100449.
54. Alakus, T.B.; Turkoglu, I. Comparison of deep learning approaches to predict COVID-19 infection. *Chaos, Solitons & Fractals* **2020**, *140*, 110120. https://doi.org/10.1016/j.chaos.2020.110120.
55. Kukar, M.; Gunčar, G.; Vovko, T.; Podnar, S.; Černelč, P.; Brvar, M.; Zalaznik, M.; Notar, M.; Moškon, S.; Notar, M. COVID-19 diagnosis by routine blood tests using machine learning. *Scientific reports* **2021**, *11*, 1–9. https://doi.org/10.1038/s41598-021-90265-9.

56. Tschoellitsch, T.; Dünser, M.; Böck, C.; Schwarzbauer, K.; Meier, J. Machine learning prediction of SARS-CoV-2 polymerase chain reaction results with routine blood tests. *Laboratory medicine* **2021**, *52*, 146–149. https://doi.org/10.1093/labmed/lmaa111.
57. Soltan, A.A.; Kouchaki, S.; Zhu, T.; Kiyasseh, D.; Taylor, T.; Hussain, Z.B.; Peto, T.; Brent, A.J.; Eyre, D.W.; Clifton, D.A. Rapid triage for COVID-19 using routine clinical data for patients attending hospital: development and prospective validation of an artificial intelligence screening test. *The Lancet Digital Health* **2021**, *3*, e78–e87. https://doi.org/10.1016/S2589-7500(20)30274-0.
58. Cabitza, F.; Campagner, A.; Ferrari, D.; Resta, C.D.; Ceriotti, D.; Sabetta, E.; Colombini, A.; Vecchi, E.D.; Banfi, G.; Locatelli, M.; et al. Development, evaluation, and validation of machine learning models for COVID-19 detection based on routine blood tests. *Clinical Chemistry and Laboratory Medicine (CCLM)* **2021**, *59*, 421–431. https://doi.org/10.1515/cclm-2020-1294.
59. Alves, M.A.; Castro, G.Z.; Oliveira, B.A.S.; Ferreira, L.A.; Ramírez, J.A.; Silva, R.; Guimarães, F.G. Explaining machine learning based diagnosis of COVID-19 from routine blood tests with decision trees and criteria graphs. *Computers in Biology and Medicine* **2021**, *132*, 104335. https://doi.org/10.1016/j.compbiomed.2021.104335.
60. Rahman, T.; Khandakar, A.; Abir, F.F.; Faisal, M.A.A.; Hossain, M.S.; Podder, K.K.; Abbas, T.O.; Alam, M.F.; Kashem, S.B.; Islam, M.T.; et al. QCovSML: A reliable COVID-19 detection system using CBC biomarkers by a stacking machine learning model. *Computers in Biology and Medicine* **2022**, *143*, 105284. https://doi.org/10.1016/j.compbiomed.2022.105284.
61. Grossberg, S. A path toward explainable AI and autonomous adaptive intelligence: deep learning, adaptive resonance, and models of perception, emotion, and action. *Front Neurorobot* **2020**, *14*, 36. https://doi.org/10.3389/fnbot.2020.00036.
62. Grossberg, S. Adaptive pattern classification and universal recoding: II. Feedback, expectation, olfaction, illusions. *Biological cybernetics* **1976**, *23*, 187–202. https://doi.org/10.1007/BF00340335.
63. Grossberg, S. How does a brain build a cognitive code? In *Studies of mind and brain*; Springer, 1982; pp. 1–52. https://doi.org/10.1007/978-94-009-7758-7_1.
64. Carpenter, G.A.; Grossberg, S. A massively parallel architecture for a self-organizing neural pattern recognition machine. *Computer vision, graphics, and image processing* **1987**, *37*, 54–115. https://doi.org/10.1016/S0734-189X(87)80014-2.
65. Carpenter, G.A.; Grossberg, S. ART 2: Self-organization of stable category recognition codes for analog input patterns. *Applied optics* **1987**, *26*, 4919–4930. https://doi.org/10.1364/AO.26.004919.
66. Carpenter, G.A.; Grossberg, S.; Rosen, D.B. Fuzzy ART: Fast stable learning and categorization of analog patterns by an adaptive resonance system. *Neural Networks* **1991**, *4*, 759–771. https://doi.org/10.1016/0893-6080(91)90056-B.
67. Carpenter, G.A.; Grossberg, S.; Reynolds, J.H. ARTMAP: Supervised real-time learning and classification of nonstationary data by a self-organizing neural network. *Neural Networks* **1991**, *4*, 565–588. https://doi.org/10.1016/0893-6080(91)90012-T.
68. Carpenter, G.A.; Grossberg, S.; Markuzon, N.; Reynolds, J.H.; Rosen, D.B. Fuzzy ARTMAP: A neural network architecture for incremental supervised learning of analog multidimensional maps. *IEEE Transactions on neural networks* **1992**, *3*, 698–713. https://doi.org/10.1109/72.159059.
69. Zadeh, L.A. Fuzzy sets. *Information and control* **1965**, *8*, 338–353. https://doi.org/10.1016/S0019-9958(65)90241-X.
70. Kenaya, R.; Cheok, K.C. Euclidean ART neural networks. In Proceedings of the World Congress on Engineering and Computer Science, San Francisco, US, 2008; pp. 963–968.
71. Moreno, A.L. *ART and ARTMAP Neural Networks with Continuous Training: A detailed presentation of the main types of ART and ARTMAP neural networks.*; Novas Edicoes Academicas: Brazil, 2016. (In Portuguese).
72. Moreno, A.L. Transient stability analysis using a modified Euclidean fuzzy Art-Artmap neural network with continuous training. PhD thesis, São Paulo State University, Ilha Solteira, BR, 2010. Available at: http://hdl.handle.net/11449/100305. (In Portuguese).
73. Barros, A.C.; Tonelli-Neto, M.S.; Decanini, J.G.M.S.; Minussi, C.R. Detection and classification of voltage disturbances in electrical power systems using a modified Euclidean ARTMAP neural network with continuous training. *Electric Power Components and Systems* **2015**, *43*, 2178–2188. https://doi.org/10.1080/15325008.2015.1073814.

74. Cabitza, F.; Campagner, A.; Soares, F.; de Guadiana-Romualdo, L.G.; Challa, F.; Sulejmani, A.; Seghezzi, M.; Carobene, A. The importance of being external. methodological insights for the external validation of machine learning models in medicine. *Computer Methods and Programs in Biomedicine* **2021**, *208*, 106288. https://doi.org/10.1016/j.cmpb.2021.106288.
75. Odhiambo, C.; Oyaro, B.; Odipo, R.; Otieno, F.; Alemnji, G.; Williamson, J.; Zeh, C. Evaluation of locally established reference intervals for hematology and biochemistry parameters in Western Kenya. *Plos one* **2015**, *10*, e0123140. https://doi.org/10.1371/journal.pone.0123140.
76. Rosenfeld, L.G.; Malta, D.C.; Szwarcwald, C.L.; Bacal, N.S.; Cuder, M.A.M.; Pereira, C.A.; Figueiredo, A.W.; Silva, A.G.d.; Machado, Í.E.; Silva, W.A.d.; et al. Reference values for blood count laboratory tests in the Brazilian adult population, National Health Survey. *Brazilian Journal of Epidemiology* **2019**, *22*. https://doi.org/10.1590/1980-549720190003.supl.2. (In Portuguese).
77. Lugada, E.S.; Mermin, J.; Kaharuza, F.; Ulvestad, E.; Were, W.; Langeland, N.; Asjo, B.; Malamba, S.; Downing, R. Population-based hematologic and immunologic reference values for a healthy Ugandan population. *Clinical and Vaccine Immunology* **2004**, *11*, 29–34. https://doi.org/10.1128/CDLI.11.1.29-34.2004.
78. Mann, H.B.; Whitney, D.R. On a Test of Whether one of Two Random Variables is Stochastically Larger than the Other. *The Annals of Mathematical Statistics* **1947**, *18*, 50 – 60. https://doi.org/10.1214/aoms/1177730491.
79. Norman, G.R.; Streiner, D.L. *Biostatistics: the bare essentials*, 4 ed.; People's Medical Publishing House-USA: Shelton, Connecticut, 2014.
80. Montgomery, D.C.; Peck, E.A.; Vining, G.G. *Introduction to linear regression analysis*; John Wiley & Sons: New York, 2006; p. 612.
81. Hoffman, K.; Kunze, R.A. *Linear Algebra*, 2 ed.; PHI Learning, 2004.
82. Craney, T.A.; Surles, J.G. Model-Dependent Variance Inflation Factor Cutoff Values. *Quality Engineering* **2002**, *14*, 391–403. https://doi.org/10.1081/QEN-120001878.
83. Agnello, L.; Giglio, R.V.; Bivona, G.; Scazzone, C.; Gambino, C.M.; Iacona, A.; Ciaccio, A.M.; Lo Sasso, B.; Ciaccio, M. The Value of a Complete Blood Count (CBC) for Sepsis Diagnosis and Prognosis. *Diagnostics* **2021**, *11*. https://doi.org/10.3390/diagnostics11101881.
84. Kermali, M.; Khalsa, R.K.; Pillai, K.; Ismail, Z.; Harky, A. The role of biomarkers in diagnosis of COVID-19–A systematic review. *Life sciences* **2020**, *254*, 117788. https://doi.org/10.1016/j.lfs.2020.117788.
85. Samprathi, M.; Jayashree, M. Biomarkers in COVID-19: an up-to-date review. *Frontiers in pediatrics* **2021**, *8*, 607647. https://doi.org/10.3389/fped.2020.607647.
86. Keykavousi, K.; Nourbakhsh, F.; Abdollahpour, N.; Fazeli, F.; Sedaghat, A.; Soheili, V.; Sahebkar, A.; et al. A Review of Routine Laboratory Biomarkers for the Detection of Severe COVID-19 Disease. *International journal of analytical chemistry* **2022**, *2022*. https://doi.org/10.1155/2022/9006487.
87. Parikh, R.; Mathai, A.; Parikh, S.; Sekhar, G.C.; Thomas, R. Understanding and using sensitivity, specificity and predictive values. *Indian journal of ophthalmology* **2008**, *56*, 45. https://doi.org/10.4103/0301-4738.37595.
88. Huang, J.; Ling, C. Using AUC and accuracy in evaluating learning algorithms. *IEEE Transactions on Knowledge and Data Engineering* **2005**, *17*, 299–310. https://doi.org/10.1109/TKDE.2005.50.
89. Boughorbel, S.; Jarray, F.; El-Anbari, M. Optimal classifier for imbalanced data using Matthews Correlation Coefficient metric. *PloS one* **2017**, *12*, e0177678. https://doi.org/10.1371/journal.pone.0177678.
90. Mandrekar, J.N. Receiver operating characteristic curve in diagnostic test assessment. *Journal of Thoracic Oncology* **2010**, *5*, 1315–1316. https://doi.org/10.1097/JTO.0b013e3181ec173d.
91. Dudoit, S.; van der Laan, M.J. Asymptotics of cross-validated risk estimation in estimator selection and performance assessment. *Statistical methodology* **2005**, *2*, 131–154. https://doi.org/10.1016/j.stamet.2005.02.003.
92. Borra, S.; Di Ciaccio, A. Measuring the prediction error. A comparison of cross-validation, bootstrap and covariance penalty methods. *Computational statistics & data analysis* **2010**, *54*, 2976–2989. https://doi.org/10.1016/j.csda.2010.03.004.
93. Rikan, S.B.; Azar, A.S.; Ghafari, A.; Mohasefi, J.B.; Pirnejad, H. COVID-19 diagnosis from routine blood tests using artificial intelligence techniques. *Biomedical Signal Processing and Control* **2022**, *72*, 103263. https://doi.org/10.1016/j.bspc.2021.103263.
94. Pedregosa, F.; Varoquaux, G.; Gramfort, A.; Michel, V.; Thirion, B.; Grisel, O.; Blondel, M.; Prettenhofer, P.; Weiss, R.; Dubourg, V.; et al. Scikit-learn: Machine Learning in Python. *Journal of Machine Learning Research* **2011**, *12*, 2825–2830.

95. Krishnaraj Chadaga, Srikanth Prabhu, V.B.N.S.S.U.; Chadaga, R. Artificial intelligence for diagnosis of mild–moderate COVID-19 using haematological markers. *Annals of Medicine* **2023**, *55*, 2233541. https://doi.org/10.1080/07853890.2023.2233541.
96. Chadaga, K.; Prabhu, S.; Bhat, V.; Sampathila, N.; Umakanth, S.; Chadaga, R. A Decision Support System for Diagnosis of COVID-19 from Non-COVID-19 Influenza-like Illness Using Explainable Artificial Intelligence. *Bioengineering* **2023**, *10*. https://doi.org/10.3390/bioengineering10040439.

ARTIGOS COMPLETOS EM EVENTOS

O trabalho intitulado **OTIMIZAÇÃO DE ESTRATÉGIAS DE NEGÓCIO DE MICRO E PEQUENO EMPREENDIMENTO ATRAVÉS DE TÉCNICAS DE DATA SCIENCE**, de autoria de **Ademir José Fazzio Junior** , **Mara Lúcia Martins Lopes** e **Carlos Roberto dos Santos Junior** foi aprovado na modalidade Apresentação Oral, para apresentação no evento VIII ERMAC Regional 9 – Ilha Solteira a ser realizado 27/05/2024.

ILHA SOLTEIRA-SÃO PAULO-BRASIL

{assinatura.comissao}

Douglas Domingues Bueno - douglas.bueno@unesp.br

Data do Aceite:27/05/2024

OTIMIZAÇÃO DE ESTRATÉGIAS DE NEGÓCIO DE MICRO E PEQUENO EMPREENDIMENTO ATRAVÉS DE TÉCNICAS DE DATA SCIENCE

Ademir J. Fazzio Junior[1], Carlos R. Santos Júnior[2], Mara L. M. Lopes[1]

[1] Universidade Estadual Paulista "Júlio de Mesquita Filho", ademir.fazzio@unesp.br; mara.lopes@unesp.br;
[2] Instituto Federal de São Paulo, "Campus de Presidente Prudente, carlos.rsantos@ifsp.edu.br;

RESUMO: As recentes evoluções tecnológicas possibilitaram a coleta e armazenamento de grandes conjuntos de dados, transformando-os em ativos valiosos para empresas. Este trabalho visa aplicar técnicas de *Data Science* e *Data Mining* em colaboração com um microempreendedor de uma hamburgueria. A análise dos dados de vendas e faturamento, junto com o desenvolvimento de métricas de negócio e estratégias baseadas em dados, busca melhorar o desempenho do empreendimento. Utilizando a metodologia CRISP-DM, o processo inclui compreensão do negócio, dos dados, preparação, modelagem, avaliação e implementação. O objetivo é entender o impacto multifatorial sobre diferentes metas e maximizar o potencial de lucro.

Palavras-chave: *Data Science*; CRISP-DM; *Machine Learning*; Inteligência Artificial;

1 INTRODUÇÃO

A evolução tecnológica dos últimos anos, principalmente nos ramos de *software*, *hardware* e *web* tornou possível a coleta e armazenamento de grandes conjuntos de dados. Isso impulsionou as empresas começaram a enxergar seus dados não como informações operacionais, mas sim como ativos importantes no desenvolvimento de estratégias de negócios.

Muitas técnicas para explorar os dados são empregadas em grandes empresas, as quais utilizam bons profissionais e investimentos para infraestrutura necessária. Porém, nos micro e pequenos empreendimentos, há uma falta de conhecimento para o uso dessas ferramentas e técnicas. Um estudo realizado pelo SEBRAE em 2020 chamado de Pesquisa de Sobrevivência de Empresas indicou que 30% microempreendedores individuais (MEIs) fecham as portas antes mesmo de completarem 5 anos. No caso de microempresas o cenário é um pouco melhor apresentando taxa de mortalidade de 21,6%, depois de completarem 5 anos e para empresas de pequeno porte, 17%. Isso indica uma correlação negativa entre o tamanho da empresa e a taxa de mortalidade, o que está relacionado a diversos fatores. Segundo os pesquisadores, essas taxas comprovam a tese proposta de que quanto maior a empresa, mais bem preparado o empreendedor, que também tem uma ação de empreender por oportunidades de mercado, e não somente por necessidade financeira (ASN Nacional, 2021).

Outro estudo realizado em 2021 mundialmente encomendado pela Dell Technologies à Consultoria Forrester indicou que apenas 28% dos tomadores de decisões em empresas usaram os insights dos dados para desenvolver novos produtos e serviços. Além disso, mais da metade dos tomadores de decisão, que participaram do estudo, pontuaram sua cultura de dados como baixa, indicando que essas empresas são novatas ou com pouquíssima experiência. Ou seja, mesmo empresas maiores tendo acesso a tecnologias, conhecimentos e colaboradores capacitados, ainda estão explorando e experimentando como os dados podem ajudá-las (Forrester Consulting, 2021).

O seguinte trabalho busca propor uma aplicação de técnicas de Ciência de Dados e Inteligência de Mercado em um micro e pequeno empreendimento do ramo alimentício utilizando linguagem *Python* no intuito de impulsionar os resultados do empreendedor, oferecer conhecimento sobre a informação a disposição, desenvolver compreensão sobre seu empreendimento e utilizar técnicas de aprendizado de máquina para inferir hipóteses.

2 DATA SCIENCE APLICADO NA ANÁLISE DE EMPREENDIMENTO

Inicialmente foram feitas indagações ao empreendedor para melhor entendimento do empreendimento, dentre elas tem-se: quais eram os tipos de dados gerados e qual era o sistema de armazenamento desses dados. Os dados foram fornecidos pela empresa mediante um acordo de confidencialidade dos dados.

A coleta de dados ocorreu através de uma visita ao estabelecimento e foi feito um acesso ao sistema CRM (*Customer* Relationship *Manager*), que é um sistema de gerenciamento de interações com os clientes, ou seja, realiza o gerenciamento de pedidos, histórico de itens vendidos, fechamento e abertura de caixas e entre outros procedimentos de administração de negócios. Com o acesso, coletou-se, de início, 5 conjuntos de dados para análise e compreensão da informação. A Tabela 1 apresenta os 5 conjuntos de dados, seus respectivos nomes e as extensões de arquivos usadas.

Tabela 1: Conjuntos de Dados.

Nome	Conteúdo	Extensão do Arquivo
Caixa	Dados do Caixa Diário	XLSX
Combos	Dados dos Combos de Lanches	XLSX
Histórico de Itens Vendidos	Dados Sobre os Itens Vendidos	XLSX
Pedidos	Dados dos Pedidos Feitos Diariamente	XLSX
Produtos	Dados Sobre os Produtos	XLSX

Com a compreensão de negócio e a obtenção dos dados, foi possível iniciar a exploração e entendimento dessa informação, realizando uma análise exploratória mais profunda. Utilizou-se o *Google Colab* com Python, que é um ambiente de desenvolvimento e prototipação disponibilizado pelo *Google*; e diversas bibliotecas da linguagem como *Pandas*, *Numpy* e *Matplotlib*.

A análise exploratória realizada começou a partir da análise dos dados de vendas de lanches por ser do interesse do empreendedor o aumento das vendas e do faturamento. Foi feita uma análise exploratória das vendas ao longo do tempo, top lanches vendidos e outras análises que levaram a compreensão da base como um todo. Então construiu-se um plano de ação a partir das análises, para ser implementado e avaliado dentro do tempo de 4 meses.

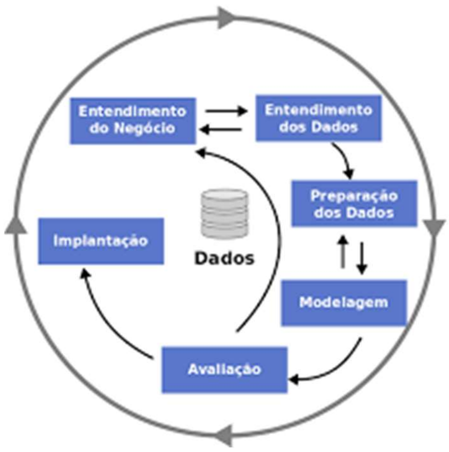

Figura 1: Procedimento padrão CRISP-DM.

Essas etapas suprem um primeiro ciclo da metodologia CRISP-DM, pois o método prevê que vários ciclos possam ocorrer como apresentado na Figura 1. A cada ciclo, uma avaliação é feita e um novo ciclo pode ser organizado e executado. Neste caso, a partir das análises, um plano de ação foi implementado e seu impacto seria medido dentro de 4 meses, possibilitando a maturação do plano e dos efeitos.

3 RESULTADOS E DISCUSSÕES

Após realizada a compreensão dos dados disponíveis, realizou-se a análise exploratória, que revelou *insights* sobre vendas de produtos e padrões temporais nos dados de faturamento. Descobriu-se, analisando os lanches mais vendidos por mês, os *cases* de sucesso da hamburgueria e as preferências dos clientes, o que permitiu o empreendedor a bolar novos “combos” e promoções para atrair novos clientes, além de recuperar antigos clientes.

Tratando os dados temporais e realizando uma padronização na informação, permitiu que análises temporais fossem feitas, relevando correlações lineares fortes entre as informações entre faturamento semanal, quantidade de lanches vendidos e o valor médio dos produtos. As Figuras 2 e 3 mostram a correlação temporal, em uma série temporal dessas informações.

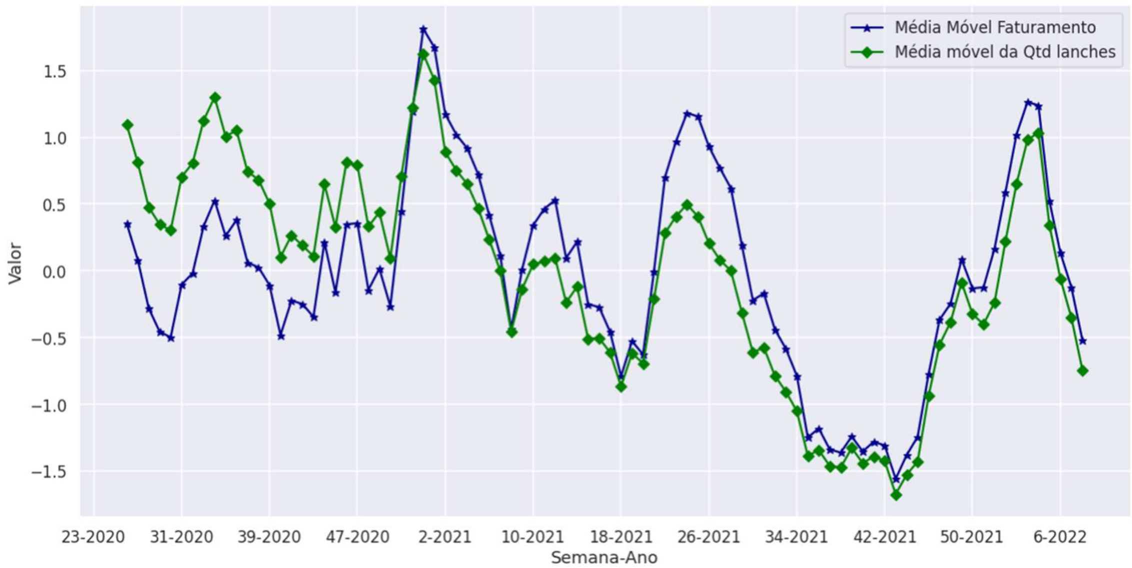

Figura 2: Faturamento Semanal vs Qtd Lanches Vendidos.

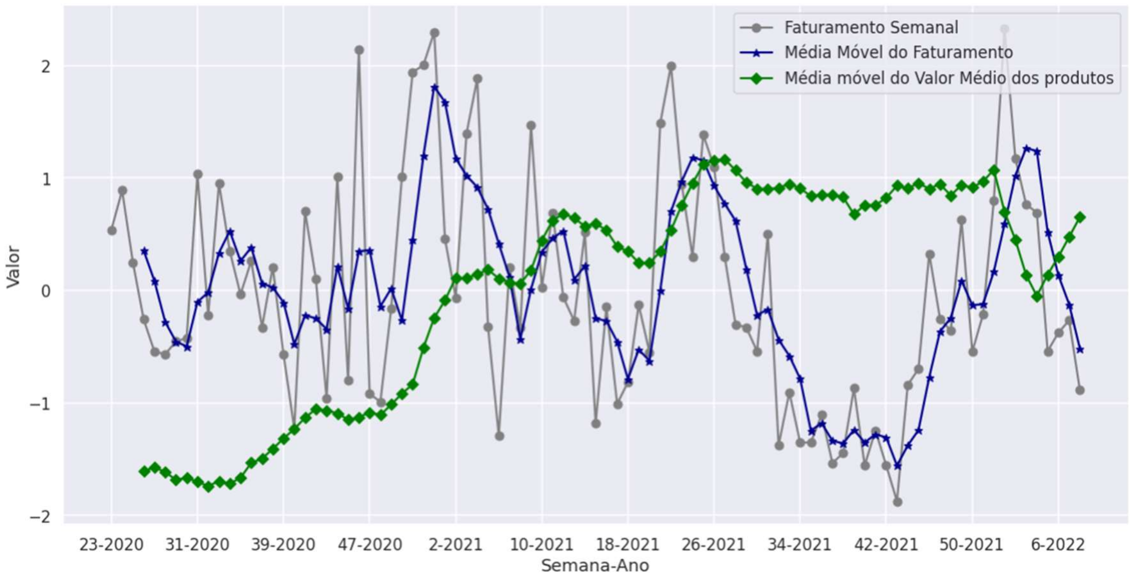

Figura 3: Média Móvel Faturamento x Média Móvel Valor Médio Produtos.

Confrontou-se a quantidade de lanches vendidos com o valor médio dos produtos o que pode ser verificado na Figura 4 e observe que a média móvel da quantidade de lanches vendidos tem uma tendência de queda mais clara do que o faturamento criando contraste a medida que a média móvel do valor médios dos produtos crescia. Esse tipo de comportamento pode indicar que há uma correlação negativa, o que foi atestado e resultando em um valor do coeficiente de correlação de -0,53, confirmando que há uma correlação moderada negativa entre as variáveis, isto é, à medida que uma cresce a outra diminui.

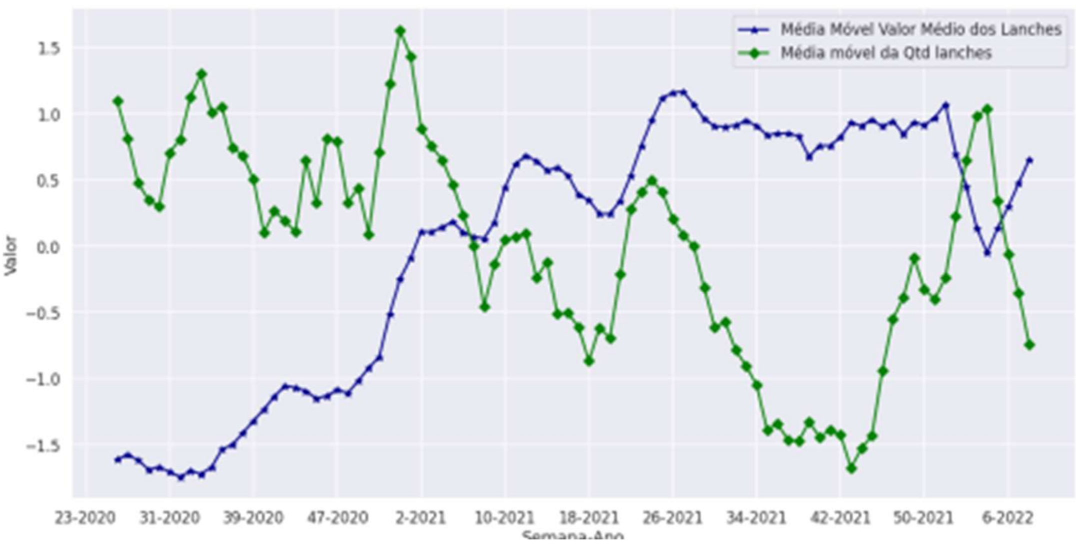

Figura 4: Média Móvel da Qtd Lanches x Média Móvel Valor Médio Produtos.

Na Figura 4 verifica-se que a única variável de controle do empreendedor é o valor dos lanches vendidos e uma vez que os valores são reajustados ao longo do tempo a quantidade de lanches compradas decai. Esse tipo de comportamento é extremamente valioso de conhecimento para o empreendedor pois é possível achar um ponto de equilíbrio onde há lucro no valor dos produtos e também há uma quantidade satisfatória de vendas de lanches.

A partir dessas análise hipóteses foram testadas com regressão linear, atestando o impacto do valor médio dos produtos e a quantidade de produtos vendidos sobre o faturamento semanal. Obteve-se um modelo com um valor de R2 igual a 0,984 e MSE (Mean Squared Error) igual a 0,014. Isso indica que o modelo é bem explicativo com os dados e tem baixa variabilidade, o que já era esperado uma vez que as variáveis inseridas estão correlacionadas.

Realizando-se a conversão (pois os dados estavam padronizados), os coeficientes para o modelo são 21,76 e 233,25 para as variáveis Quantidade de produtos vendidos e Valor médio dos produtos, ou seja, o aumento de qualquer uma dessas variáveis resulta em um impacto positivo no faturamento, no entanto, é mais impactante aumentar 1 ponto no valor médio dos produtos, o que representa R$ 1,00, resultando em um impacto de 233,25 pontos no faturamento, ou seja, R$ 233,25 semanais.

Em seguida, também foi considerando o impacto do IPCA, uma vez que a hipótese é de que o índices de preço está correlacionado com todas essas variáveis, no entanto, agora com valores mensais. Os preditores são o valor médio dos produtos, quantidade de produtos vendidos e IPCA geral. O R2 obtido foi de 0,87 com MSE igual a 875 038,28 o que provavelmente é resultado de uma predição exagerada que influência no valor final da métrica. Os valores dos coeficientes da última regressão feita foram 26,5, 1093,017 e 1975,6 para quantidade de lanches, valor médio dos produtos e IPCA geral, respectivamente. Veja que relacionado com outros preditores o IPCA geral impacta positivamente o faturamento o que é contraintuitivo, pois, realizando um cálculo de correlação linear entre o faturamento e o IPCA geral e de forma exclusiva eles apresentam correlação negativa. Esse comportamento pode ser explicado pelo fato de estar correlacionado com os outros preditores, ou seja, o IPCA geral impacta no valor médio dos produtos e quantidade de lanches vendidos, o que impacta positivamente no faturamento.

Com base nos resultados, o empreendedor implementou novas estratégias visando aumentar as vendas e receita. Através de algumas estratégias já previamente elaboradas, foi acordado que iriam ser implementada estratégias nos próximos meses de combos com promoções especiais, eventos presenciais de *shows* e uma estratégia de *cashback,* no qual a cada compra o cliente acumulava pontos para trocar por produtos do estabelecimento. Essas escolhas se deram ao fato de o objetivo de aumentar a receita provavelmente seria alcançado realizando ações para atrair mais clientes, uma vez que aumentar o valor médio dos produtos pode ter um impacto negativo na quantidade vendida e não há controle sobre a inflação.

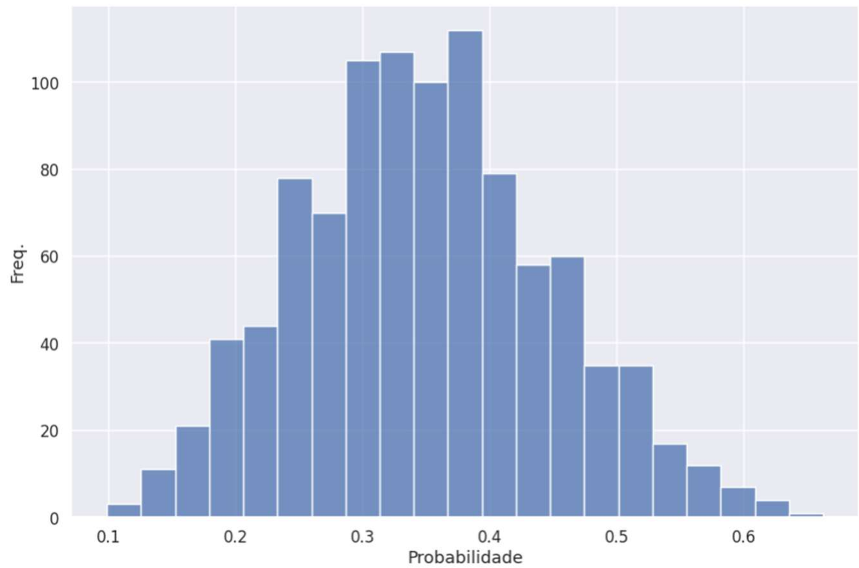

Figura 5: Histograma Beta α = 7 e β = 13.

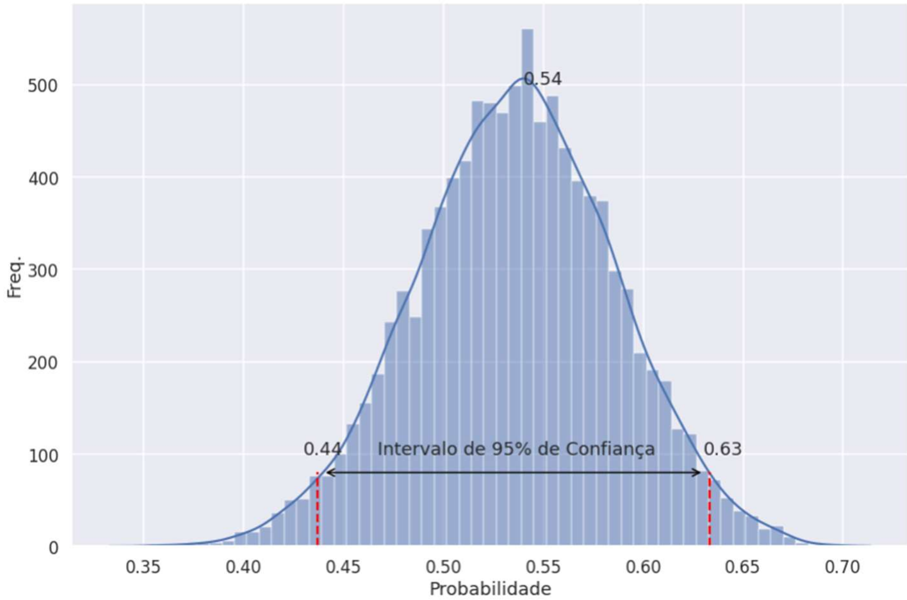

Figura 6: Distribuição a Posteriori atualizando α e β.

Após 4 meses de monitoramento e nova coleta de dados, foi utilizado inferência bayesiana e análise descritiva para avaliar mudanças. Foi escolhido essa abordagem porque o empreendedor aplicou as mudanças de forma súbita e não ideal para a condução de um experimento, sendo difícil avaliar os resultados com um teste A/B, por exemplo. Por conta disso, a saída seria realizar uma análise descritiva e uma inferência bayesiana no qual os parâmetros das distribuições a *priori* eram o estado anterior e com a atualização dos dados, será gerado uma distribuição a *posteriori*, refletindo o impacto da mudança.

Formulou-se uma pergunta para ser respondida, "Qual a probabilidade da estratégia atual ser melhor do que a estratégia anterior?", considerando um alvo de R$ 2000,00 de faturamento diário. Estabeleceu-se uma distribuição beta a priori com os dados da estratégia anterior, que pode ser vista na Figura 5, e atualizou-se essa informação com os novos dados, criando a distribuição a posteriori, que pode ser vista na Figura 6.

De forma geral, houve um aumento expressivo na probabilidade de se atingir o faturamento alvo, passando de uma chance de aproximadamente 39%, em média, para 54%, representando um aumento de 38% na probabilidade. Além disso, em um intervalo de 95% de confiança, as chances de se atingirem esse resultado são de 44% a 63%. Infelizmente não é possível indicar qual das estratégias implementadas foi a que gerou mais resultado devido ao fato das complicações de se realizar um teste controlado, uma vez que, em ambientes dinâmicos como empreendimentos que estão fora do ramo de tecnologia, organizar um experimento controlado e realizar um Teste A/B possa atrapalhar até mesmo o funcionamento do estabelecimento.

Além das implicações da implementação de um experimento controlado, essa melhoria no faturamento apenas reflete o aumento dos ganhos, mas não do lucro. Uma forma mais adequada de analisar a eficiência das estratégias implementadas seria a análise percentual do lucro sobre os ganhos atuais em relação ao passado. Essa análise revelaria se a estratégia está retornando uma maior margem de lucro e trazendo maiores benefícios ao empreendedor, uma vez que os ganhos podem ser altos mas se a margem de lucro for baixa, ainda é uma estratégia que agregou pouco. Infelizmente, no caso desse estudo, só houve acesso aos dados de faturamento e não dos lucros do empreendedor e, para futuros projetos, seria interessante validar essa métrica.

4 CONCLUSÕES

Este estudo aplicou técnicas baseadas em Ciência de Dados a um micro e pequeno empreendimento, oferecendo *insights* valiosos para a tomada de decisão. A análise inicial revelou uma queda nas vendas, impulsionando o foco na recuperação do faturamento. Ao explorar as relações entre variáveis como quantidade vendida, valor médio dos produtos e o IPCA, foi possível identificar que havia correlação entre as variáveis, assim como poderiam criar impactos desejáveis e indesejáveis. Com base nisso, estratégias eficazes, como promoções de combos e implementação de *cashback*, foram desenvolvidas e implementadas. Infelizmente o tipo de ambiente que um empreender está inserido impede que um teste controlado seja realizando.

Para contornar o problema de testes controlados, a implementação de uma inferência bayesiana foi feita, apresentando um resultado significativo na probabilidade, aumentando as chances de atingir as metas diárias de receita. Embora o crescimento do faturamento tenha sido notável, é importante reconhecer que esse aumento não garante necessariamente uma melhoria direta no lucro líquido, dada a presença de custos associados às melhorias implementadas, ou seja, é importante que na implementação de estudos futuros, uma avaliação dessa variável seja feita, no intuito de mensurar por completo o impacto das estratégias.

O estudo demonstra claramente o potencial das técnicas de Ciência de Dados para impulsionar o desempenho e a tomada de decisões em empreendimentos de menor porte, colaborando com a hipótese que microempreendedores individuais empreender por necessidade, muitas vezes despreparados. Porém, com a implementação de técnicas inteligentes e baseadas em dados, é possível reverter essa situação e até oferecer possibilidades antes não vistas.

5 REFERÊNCIAS

P. Bruce, A. Bruce, P. Gedeck. Pratical Statistics for Data Science. Sebastopol, CA: O'Reilly, 2020.

Forrester Consulting, "Unveiling Data Challenges Afflicting Businesses Around The World", 2021, https://www.delltechnologies.com/asset/en-us/solutions/industry-solutions/industry-market/data-paradox-forrester-thought-leadership-paper.pdf

G. Joel. Data Science from Scratch. Sebastopol, CA: O'Reilly Media, 2019.

P.-S. Laplace. Essai philosophique sur les probabilités. Paris: Courcier, 1814.

W. Mckinney Python for Data Analysis. Sebastopol, CA: O'Reilly, 2018.

F. Provost, T. Fawcett. Data Science para negócios. Rio de Janeiro, RJ: Alta Books, 2016.

ASN Nacional, Três em cada 10 MEI fecham as portas em até cinco anos de atividade no Brasil, 2021. Disponível em: https://agenciasebrae.com.br/brasil-empreendedor/tres-em-cada-10-mei-fecham-as-portas-em-ate-cinco-anos-de-atividade-no-brasil/

C. Stucchio. Bayesian A/B Testing at VWO. Wingify, 2015. Disponível em: https://vwo.com/downloads/VWO_SmartStats_technical_whitepaper.pdf

R. Van de Schoot, S. Depaoli, R. King, Kramer, B.; K. Märtens, M. G. Tadesse, M. VanNucci, A. Gelman, D. Veen, J. Willemsen, C. Yau. Bayesian statistics and modelling. Nature Reviews Methods Primers, 2021.

Coordenação geral: Daniela Buske, Eudes Naziazeno e Luiz-Rafael Santos

19/Setembro - Quinta-feira - 17h00 às 19h20

Atualizado em 21/08/24 17:33.

Sala Baboá 01 & 02

Área Temática:

ST02 - Biomatemática (ST02-D)

Coordenação: Sandro Mazorche

---

1 — 17h00 — #657 | The role of import and increasing mosquito abundance in vector-borne disease invasion scenarios

- **Nico Stollenwerk (Basque Center for Applied Mathematics (BCAM), Bilbao, Spain)**
- Maira Aguiar

2 — 17h20 — #692 | Estudo do Tamanho Final de uma Epidemia no Modelo SIQR CTMC

- **Michelle Lau (Universidade do Estado do Rio de Janeiro)**
- Zochil González Arenas

3 — 17h40 — #726 | Modelos Populacionais: Da Teoria de Lotka com o uso das Funções de Mittag-Leffler

- **Sandro Mazorche (Universidade Federal de Juiz de Fora)**
- Thaís Souza Oliveira

4 — 18h00 — #729 | Classificação de Arritmias no Tempo e Tempo-Frequência: Uma Abordagem Baseada em Subproblemas

- **Reginaldo José Da Silva (UNESP/FEIS)**
- Andréia Da Silva Santos De Faria
- André Luiz Caliari Costa
- Thays Aparecida De Abreu Santos
- Carlos Roberto Dos Santos Junior
- Angela Leite Moreno
- Mara Lúcia Martins Lopes

Proceeding Series of the Brazilian Society of Computational and Applied Mathematics, v. 11, n. 1, 2025.

Trabalho apresentado no XLIII CNMAC, Centro de Convenções do Armação Resort - Porto de Galinhas - PE, 2024

Proceeding Series of the Brazilian Society of Computational and Applied Mathematics

Classificação de Arritmias no Tempo e Tempo-Frequência: Uma Abordagem Baseada em Subproblemas

Reginaldo J. Silva[1] Andréia S. Santos [2] Thays A. Abreu[3] Mara L. M. Lopes[4]
UNESP, Ilha Solteira, SP
André L. C. Costa[5]
USP, Ribeirão Preto, SP
Carlos R. S. Júnior[6]
IFSP, Hortolândia, SP
Angela L. Moreno[7]
UNIFAL, Alfenas, MG

Resumo. As arritmias cardíacas são um problema comum que requer detecção precoce para um tratamento eficaz. No entanto, a identificação precisa dessas arritmias pode ser desafiadora devido às sutis diferenças na morfologia dos sinais cardíacos. O uso de algoritmos de aprendizado de máquina tem sido explorado para aprimorar essa detecção, mas enfrenta um desafio devido ao desequilíbrio na distribuição dos dados entre as diferentes classes. Desta forma, neste estudo a proposta é dividir o problema principal em dois subproblemas, com o objetivo de reduzir o impacto do desequilíbrio das classes. Além disso, foi utilizado um ponto de corte adaptativo extraído do treinamento. Simulações foram realizadas nos domínios do tempo e do tempo-frequência, revelando melhorias na sensibilidade com essa abordagem.

Palavras-chave. Reconhecimento de Padrões, Aprendizado de Máquina, Transformada de Fourier Janelada.

1 Introdução

A arritmia cardíaca é uma condição cardíaca que afeta um número significativo de pessoas em todo o mundo, estima-se que cerca de 40 milhões de indivíduos no Brasil sejam afetados por algum tipo de arritmia cardíaca [16]. Essa condição torna-se mais prevalente com o avanço da idade, tornando-se um desafio significativo de saúde pública devido ao envelhecimento populacional observado em muitos países [17]. O termo arritmia é usado para descrever um padrão de batimento cardíaco anormal que se desvia do ritmo cardíaco sinusal regular [8].

A detecção precoce e precisa das arritmias cardíacas é crucial para um tratamento eficaz, e o eletrocardiograma (ECG) é uma ferramenta comumente utilizada para esse fim [5]. Ele registra a atividade elétrica do coração, fornecendo informações essenciais para identificar problemas cardíacos, incluindo arritmias. A identificação de arritmias depende do reconhecimento de padrões específicos de ECG associados a cada tipo [12]. Esses padrões são frequentemente comparados com critérios e diretrizes padronizados, para determinar o tipo específico de arritmia [7]. No entanto, mesmo para médicos experientes, a identificação precisa com base apenas na análise do ECG pode ser um desafio [2].

[1]reginaldo.silva@unesp.br
[2]andreia.faria@unesp.br
[3]thays.abreu@unesp.br
[4]mara.lopes@unesp.br
[5]alcc.biologygen@usp.br
[6]carlos9.rsj@gmail.com
[7]angela.moreno@unifal-mg.edu.br

Com o avanço das técnicas de aprendizado de máquina, tais algoritmos tem ganhado destaque para aprimorar a detecção [1]. Embora os algoritmos apresentem resultados promissores, ainda enfrentam desafios significativos. Um desses desafios é o desequilíbrio na distribuição dos dados entre as diferentes classes, o que pode prejudicar a capacidade dos algoritmos de classificação [6]. Uma abordagem frequente envolve a aplicação de técnicas de balanceamento de dados, como *oversampling* ou *undersampling* [6]. Apesar da sua ampla adoção, é essencial considerar que o emprego de tais técnicas podem influenciar a classificação de forma que se afaste de uma aplicação real.

Desta forma, este estudo explora uma abordagem alternativa para a classificação de arritmias, fragmentando o problema principal em subproblemas nos quais o desequilíbrio dos dados não exerça um impacto significativo sobre a classificação. Além disso, a proposta inclui a adaptação do ponto de corte na probabilidade, definido a partir do conjunto de treinamento e aplicando validação cruzada *k-fold*. Para avaliar a eficácia dessa estratégia, foram utilizados dados no domínio do tempo e no domínio tempo-frequência, empregando a Transformada de Fourier Janelada, também conhecida como *Short-time Fourier Transform* (STFT) [13]. Redes neurais convolucionais foram utilizadas para a classificação e os resultados comparados com a literatura.

2 Materiais e Métodos

2.1 Processamento do Sinal e Estrutura do Modelo

O conjunto de dados MIT-BIH [11] utilizado nas simulações consiste em 48 registros de ECG de 47 indivíduos distintos, cada registro com duração de trinta minutos e amostrados a uma taxa de 360Hz. Cada registro contém dois canais, que podem incluir a derivação modificada II (MLII), V1, V2, V4 ou V5, dependendo do registro. A derivação MLII foi utilizada por estar presente na maioria dos registros. Além disso, cada batimento cardíaco foi anotado independentemente por dois ou mais cardiologistas especialistas.

O conjunto de dados de arritmias do MIT-BIH foi processado usando uma série de etapas. Primeiramente, o sinal de ECG foi extraído da derivação MLII. Em seguida, o sinal foi filtrado usando um filtro *notch* para remover interferências de linha de energia elétrica. Após o filtro, os sinais foram padronizados usando z-score conforme a equação (1):

$$z = \frac{x - \mu}{\sigma}, \tag{1}$$

em que μ e σ são, respectivamente, o valor médio e o desvio padrão do sinal. Essa padronização foi realizada para garantir que os dados estejam na mesma escala, média zero e desvio um [14]. Em seguida, os picos R foram detectados usando o algoritmo XQRS da biblioteca WFDB [19]. Os batimentos cardíacos foram então segmentados em janelas de 300 pontos, sendo 100 pontos antes do pico R detectado e 200 pontos após. A Figura 1 mostra uma janela de 10s do sinal original, bem como uma amostra do sinal processado (domínio do tempo) que foi utilizado no processo de classificação das arritmias.

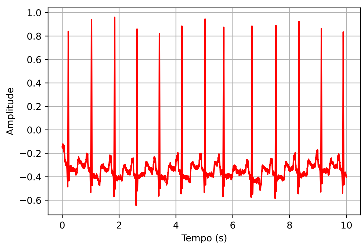

(a) Janela de 10s do sinal.

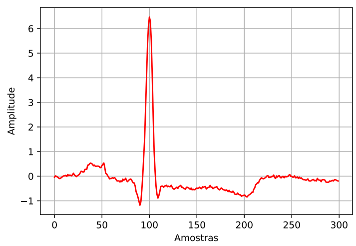

(b) Sinal segmentado.

Figura 1: Exemplo de sinal de ECG. Fonte: dos autores.

Além disso, foi aplicada a STFT aos segmentos de sinal para obter representações no domínio tempo-frequência. Define-se a STFT de um sinal discreto $x[n]$ como [13]:

$$X[n, \omega] = \sum_{m=-\infty}^{\infty} x[n+m] \cdot w[m] \cdot e^{-j\omega m}, \tag{2}$$

em que $x[n]$ representa o sinal, enquanto $w[n]$ é uma janela deslizante. Essa abordagem possibilita uma análise da variação da frequência ao longo do tempo, o resultado obtido, representado por $X[n, \omega)$, é uma matriz bidimensional conhecida como espectrograma. Os cálculos foram realizados com uma janela de 118 pontos e sobreposição de 50% resultando em uma dimensão de 60 × 7. A Figura 2 apresenta os espectros de um sinal, na Figura 2 (a), mostra o sinal com a interferência de 60Hz na linha de energia e a Figura 2 (b) apresenta o sinal após a aplicação do filtro *notch* para remoção dessa frequência.

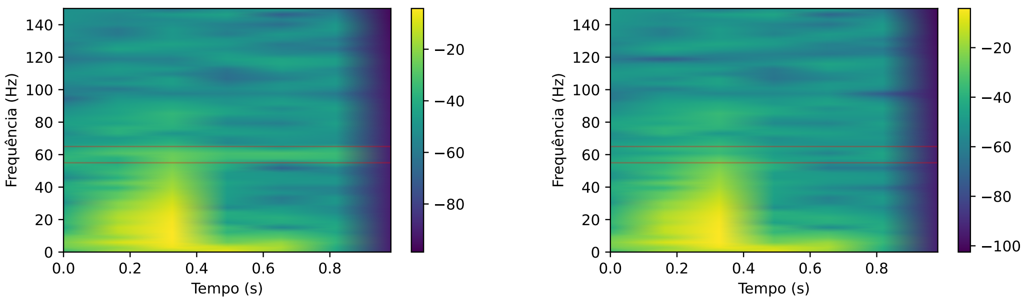

(a) Sinal segmentado sem filtrar. (b) Sinal segmentado filtrado.

Figura 2: Espectro de sinal de ECG segmentado. Fonte: dos autores.

Após a obtenção dos espectros com dimensão de 60×7, foi realizada a aplicação da interpolação de Lanczos 2D para um redimensionamento de 60×60. Essa interpolação é uma técnica comumente utilizada para redimensionamento de imagens que preserva melhor os detalhes e reduz artefatos em comparação com outros métodos de interpolação [9].

A interpolação de Lanczos 2D é realizada por meio da operação de convolução linear entre os valores originais $s_{i,j}$ e uma função de janela de Lanczos $L(x)$ [9]. A fórmula da interpolação de Lanczos 2D é dada pela equação (3):

$$S(x, y) = \sum_{i=\lfloor x \rfloor - a+1}^{\lfloor x \rfloor + a} \sum_{j=\lfloor y \rfloor - a+1}^{\lfloor y \rfloor + a} s_{i,j} \cdot L(x-i) \cdot L(y-j), \tag{3}$$

em que $S(x, y)$ representa o valor interpolado na posição (x, y), $s_{i,j}$ são os valores originais, $L(x)$ é a função de janela de Lanczos definida pela equação (4), o parâmetro a determina o comprimento da janela.

$$L(x) = \begin{cases} 1, & x = 0, \\ \dfrac{a\,\text{seno}(\pi x)\,\text{seno}\left(\frac{\pi x}{a}\right)}{\pi^2 x^2} & \text{se } 0 < |x| < a, \\ 0 & \text{caso contrário.} \end{cases} \tag{4}$$

Por fim, as 16 classes do conjunto original foram agrupadas em cinco categorias, seguindo as diretrizes estabelecidas pela *Association for the Advancement of Medical Instrumentation* (AAMI) EC57 [3]. A quantidade de amostras em cada classe pode ser visto na Tabela 1.

DOI: 10.5540/03.2025.011.01.0360

Tabela 1: Quantidade de amostras em cada classe.

Classe	Normal (0)	SVEB (1)	VEB (2)	F (3)	Q (4)
Quantidade	87404	2683	3564	593	1286

SVEB: Batimento ectópico supraventricular, VEB: Batimento ectópico ventricular, F: Batimento de fusão, Q: Batimento desconhecido

Para mitigar o efeito do desbalanceamento dos dados durante a classificação, o problema foi dividido em dois subproblemas, nos quais o desbalanceamento foi reduzido. O primeiro subproblema envolveu a classificação de pacientes em duas categorias: normais e anormais, agrupando todas as classes de arritmias (SVEB, VEB, F e Q da Tabela 1). Por sua vez, o segundo subproblema focou na classificação das quatro classes de arritmias, eliminando a influência que a alta quantidade de dados normais poderia ter sobre a classificação.

A arquitetura do modelo utilizado para as simulações pode ser visto na Figura 3. O modelo foi treinado utilizando o otimizador Adam com taxa de aprendizado de 0,001, lote de 128 amostras e 100 épocas.

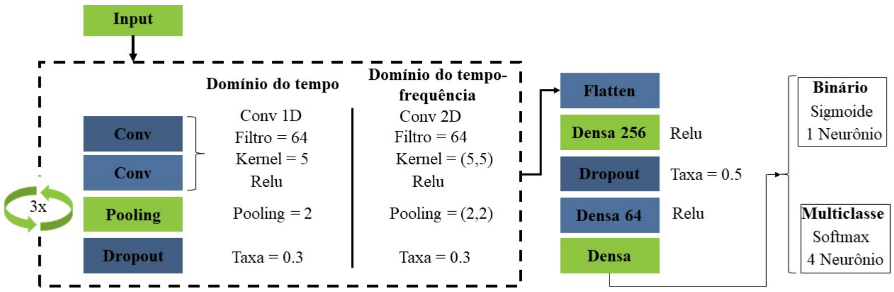

Figura 3: Arquitetura do modelo. Fonte: dos autores.

O método *Hold-out* foi utilizado para dividir o conjunto de dados em treino e teste com uma proporção de 70–30. Em seguida, o conjunto de treinamento foi dividido novamente utilizando *k-fold* com $k = 2$, dentro deste conjunto de treinamento e validação foi extraído o ponto de corte a partir do índice Youden aplicado a curva ROC que foi posteriormente utilizado no teste. Essa abordagem também colabora para classificação mesmo diante de classes desbalanceadas, visto que o índice Youden na curva ROC busca o ponto de corte que maximiza tanto a sensibilidade quanto a especificidade.

3 Resultados Computacionais

A Figura 4 apresenta as curvas ROC para cada subproblema tanto no domínio do tempo quanto no tempo-frequência. Analisando os resultados é possível observar que o modelo obteve desempenho satisfatório em ambos os domínios, com AUC-ROC variando entre 0,9949 e 0,9972. Além disso, observa-se que no domínio tempo-frequência, os resultados foram superiores aos obtidos no domínio do tempo, indicando que a inclusão de informações sobre a frequência do sinal contribuiu para melhorar o desempenho do modelo.

Na classificação das arritmias no subproblema 2, nota-se que o modelo teve certa dificuldade em classificar a classe 3 que corresponde a batimentos de fusão tanto no domínio do tempo quanto tempo-frequência. Essa dificuldade pode ser comparada com resultados anteriores encontrados em outros estudos [2, 18], evidenciando um desafio recorrente na classificação desses tipos específicos de batimentos.

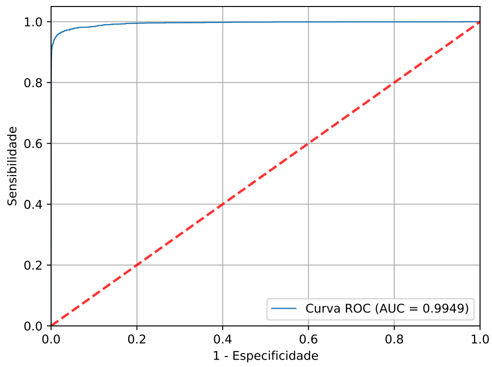

(a) Subproblema 1 (Domínio do tempo).

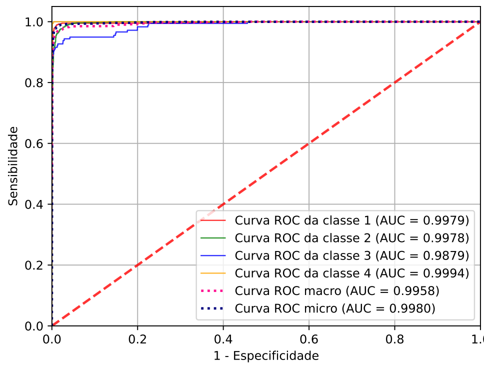

(b) Subproblema 2 (Domínio do tempo).

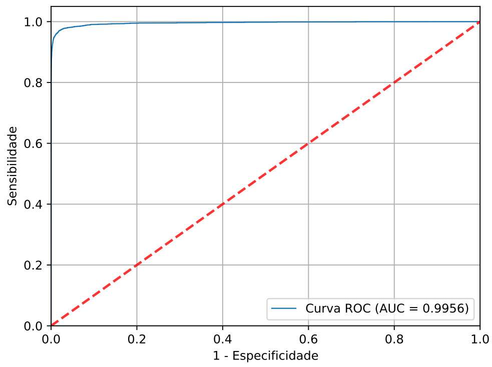

(c) Subproblema 1 (Domínio tempo-frequência).

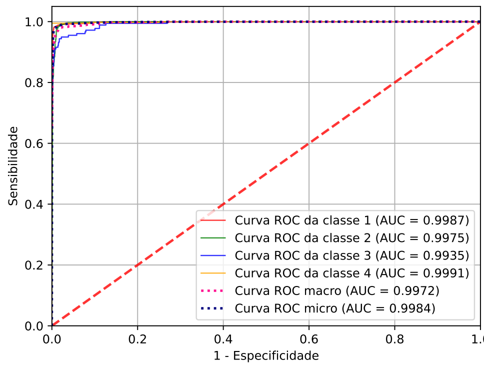

(d) Subproblema 2 (Domínio tempo-frequência).

Figura 4: Curva ROC dos resultados obtidos. Fonte: dos autores.

A Tabela 2 apresenta uma comparação entre os resultados obtidos neste estudo e alguns dos trabalhos disponíveis na literatura.

Tabela 2: Comparativo do resultados com a literatura.

Autor	Domínio	Tipo	ACC	*Se*	*Sp*	AUC-ROC
Este	Tempo	Binário	0,9901	0,9709	0,9990	0,9949
Estudo	Tempo	Multiclasse	0,9836	0,9610	0,9933	0,9958
	Tempo-Frequência	Binário	0,9906	0,9651	0,9973	0,9956
	Tempo-Frequência	Multiclasse	0,9778	0,9577	0,9916	0,9972
[10]	Tempo-Frequência	Multiclasse	0,9450	0,7030	–	–
[18]	Tempo	Multiclasse	0,9766	0,5099	0,9320	–
[15]	Tempo	Binário	0,9600	0,8300	0,9800	–
[2]	Tempo	Multiclasse	0,9900	0,9400	0.9900	$\approx$ 1,0000
[4]	Tempo-Frequência	Multiclasse	0,9960	0,9580	–	–

ACC: Acurácia, *Se*: Sensibilidade, *Sp*: Especificidade

Comparando esses resultados observa-se que para a classificação binária, este estudo superou em termos de acurácia, sensibilidade e especificidade os resultados obtidos em [15]. Por outro lado, comparando a classificação multiclasse, nota-se que os resultados deste estudo ainda se destacam, alcançando resultados superiores aos obtidos por [2, 10, 18]. Vale ressaltar que o valor de AUC

DOI: 10.5540/03.2025.011.01.0360

apresentado em [2] foi aproximado, não representando a verdadeira precisão do resultado obtido. No entanto, ao se considerar a sensibilidade e especificidade, os resultados obtidos neste trabalho prevalecem superiores.

4 Considerações Finais

Este estudo apresenta o uso de redes neurais convolucionais para a classificação de arritmias no domínio do tempo e tempo-frequência, uma abordagem simples foi utilizada para reduzir o impacto do desbalanceamento das classes que consistiu na subdivisão do problema em uma tarefa binária (Normal vs. Anormal) e outra de classificação multiclasse, abrangendo quatro tipos distintos de arritmias. Os resultados demonstraram a eficácia dessa abordagem, alcançando elevadas taxas de acurácia, sensibilidade e especificidade para ambos os subproblemas e domínios. Além disso, as curvas ROC exibiram valores notáveis de AUC-ROC, confirmando a capacidade da metodologia utilizada. Essa técnica de subdivisão pode ser especialmente útil ao utilizar algoritmos de treinamento on-line, minimizando o impacto que os dados normais podem ter sobre classes menos representadas.

Esses resultados mostram que é possível obter um desempenho sólido, ao dividir o problema, sem comprometer a qualidade. Em pesquisas futuras, pretende-se abordar o desequilíbrio diretamente no modelo, introduzindo um viés que equilibre a tendência do modelo de se concentrar na classe majoritária. Isso tem o potencial de tornar algoritmos de detecção mais robustos e confiáveis. Além de testar essa abordagem em algoritmos de treinamento contínuo (on-line).

Agradecimentos

Os autores agradecem ao Conselho Nacional de Desenvolvimento Científico e Tecnológico (CNPq) e à Coordenação de Aperfeiçoamento de Pessoal de Nível Superior - Brasil (CAPES) - Código de Financiamento 001 pelo auxílio financeiro.

Referências

[1] U. R. Acharya et al. “Automated detection of arrhythmias using different intervals of tachycardia ECG segments with convolutional neural network”. Em: **Information Sciences** 405 (2017), pp. 81–90. DOI: 10.1016/j.ins.2017.04.012.

[2] A. A. Ahmed et al. “Classifying Cardiac Arrhythmia from ECG Signal Using 1D CNN Deep Learning Model”. Em: **Mathematics** 11.3 (2023). DOI: 10.3390/math11030562.

[3] ANSI/AAMI EC57. **Testing and Reporting Performance Resultsof Cardiac Rhythm and ST Segment Measurement Algorithms**. Ed. por American National Standards Institute (ANSI). Association for the Advancement of Medical Instrumentation (AAMI), 1998.

[4] Y. Han et al. “Novel Transformation Deep Learning Model for Electrocardiogram Classification and Arrhythmia Detection using Edge Computing”. Em: **Journal of Grid Computing** 22.1 (2023), p. 7. DOI: 10.1007/s10723-023-09717-3.

[5] S. P. Karunathilake e G. U. Ganegoda. “Secondary Prevention of Cardiovascular Diseases and Application of Technology for Early Diagnosis”. Em: **BioMed Research International** 2018 (2018), p. 5767864. DOI: 10.1155/2018/5767864.

[6] V. López et al. "An insight into classification with imbalanced data: Empirical results and current trends on using data intrinsic characteristics". Em: **Information Sciences** 250 (2013), pp. 113–141. DOI: 10.1016/j.ins.2013.07.007.

[7] A. Lorga et al. "Diretrizes para Avaliação e Tratamento de Pacientes com Arritmias Cardíacas". Em: **Arquivos Brasileiros de Cardiologia** 79 (2002), pp. 1–50. DOI: 10.1590/S0066-782X2002001900001.

[8] S. Ma et al. "An effective data enhancement method for classification of ECG arrhythmia". Em: **Measurement** 203 (2022), p. 111978. DOI: 10.1016/j.measurement.2022.111978.

[9] B. N. Madhukar e R. Narendra. "Lanczos Resampling for the Digital Processing of Remotely Sensed Images". Em: **Proceedings of International Conference on VLSI, Communication, Advanced Devices, Signals & Systems and Networking**. 2013, pp. 403–411.

[10] V. Mondéjar-Guerra et al. "Heartbeat classification fusing temporal and morphological information of ECGs via ensemble of classifiers". Em: **Biomedical Signal Processing and Control** 47 (2019), pp. 41–48. DOI: 10.1016/j.bspc.2018.08.007.

[11] G. B. Moody e R. G. Mark. "The impact of the MIT-BIH Arrhythmia Database". Em: **IEEE Engineering in Medicine and Biology Magazine** 20.3 (2001), pp. 45–50. DOI: 10.1109/51.932724.

[12] K. A. K. Niazi et al. "Identifying best feature subset for cardiac arrhythmia classification". Em: **Science and Information Conference**. 2015, pp. 494–499. DOI: 10.1109/SAI.2015.7237188.

[13] A. V. Oppenheim e R. W. Schafer. **Discrete-Time Signal Processing**. Pearson Education, 2011.

[14] G. K. Panicker et al. "Z-Score for Benchmarking Reader Competence in a Central ECG Laboratory". Em: **Annals of Noninvasive Electrocardiology** 14.1 (2009), pp. 19–25. DOI: 10.1111/j.1542-474X.2008.00269.x.

[15] G. Sivapalan et al. "ANNet: A Lightweight Neural Network for ECG Anomaly Detection in IoT Edge Sensors". Em: **IEEE Transactions on Biomedical Circuits and Systems** 16.1 (2022), pp. 24–35. DOI: 10.1109/TBCAS.2021.3137646.

[16] SOBRAC. **Arritmias cardíacas: 10 informações úteis para seu coração bater no ritmo certo**. Online. Acessado em 07/02/2024, https://sobrac.org/publico-geral/?p=4463.

[17] United Nations - UN. **World Population Aging 2017**. Online. Acessado em 08/02/2024, https://www.un.org/en/development/desa/population/publications/pdf/ageing/WPA2017_Highlights.pdf. 2017.

[18] Y. Xia, Y. Xiong e K. Wang. "A transformer model blended with CNN and denoising autoencoder for inter-patient ECG arrhythmia classification". Em: **Biomedical Signal Processing and Control** 86 (2023), p. 105271.

[19] C. Xie et al. **Waveform Database Software Package (WFDB) for Python**. Online. Acessado em 22/02/2024, https://doi.org/10.13026/9njx-6322. 2022.

RESUMO EXPANDIDO

O trabalho intitulado **DISPOSITIVO INTELIGENTE DE MAPEAMENTO DE DOENÇAS VIRAIS**, de autoria de **Bruna Moreira da Silva** , **Mara Lúcia Martins Lopes** , **Thays Ap. de Abreu Santos** e **Carlos Roberto dos Santos Junior** foi aprovado na modalidade Pôster, para apresentação no evento VIII ERMAC Regional 9 – Ilha Solteira a ser realizado 21/05/2024.

ILHA SOLTEIRA-SÃO PAULO-BRASIL

{assinatura.comissao}

Douglas Domingues Bueno - douglas.bueno@unesp.br

Data do Aceite:21/05/2024

DISPOSITIVO INTELIGENTE DE MAPEAMENTO DE DOENÇAS VIRAIS

Bruna M. da Silva[1], Thays A. A. Santos[1], Carlos R. Santos Júnior[2], Mara L. M. Lopes[1]

[1] Universidade Estadual Paulista "Júlio de Mesquita Filho", bm.silva@unesp.br; thays.abreu@unesp.br; mara.lopes@unesp.br;
[2] Instituto Federal de São Paulo, "Campus de Presidente Prudente, carlos.rsantos@ifsp.edu.br;

RESUMO: O estudo apresenta uma ferramenta desenvolvida para a detecção de doenças no fígado causadas por vírus utilizando os conceitos de aprendizado de máquina, mais precisamente, rede neural artificial. A estrutura neural utilizada foi a Rede Neural ARTMAP *Fuzzy* a qual foi treinada a partir de um banco de dados informativo de portadores e não-portadores do vírus HCV disponibilizados pelo repositório UCI *Machine Learning Repository*. Os resultados obtidos trouxeram uma porcentagem positiva em relação a taxa de acertos, mostrando a eficiência do sistema projetado que evidenciam a grandeza do uso da inteligência artificial como tecnologia e ferramenta para definição de diagnóstico médico, podendo não só auxiliar os profissionais de saúde como também impulsionar as técnicas de diagnóstico e pesquisa. A metodologia se mostrou promissora e espera-se que a ferramenta possa ser utilizada como base para demais avanços na área de patologia clínica.

Palavras-chave: *Machine Learning*; Inteligência Artificial; Rede ARTMAP *Fuzzy*; Hepatites Virais.

1 INTRODUÇÃO

As hepatites virais representam um grave problema de saúde pública, tanto no Brasil quando no mundo, possuindo uma alta taxa de mortalidade e morbidade. A doença causa a inflamação do tecido hepático (Manual Técnico, 2016), que quando não tratada pode evoluir para cirrose ou câncer. As hepatites virais são classificadas em hepatite A (HAV), hepatite B (HBV), hepatite C (HCV), hepatite D (HDV) e hepatite E (HEV) (Ministério da Saúde, 2022). Apesar das semelhanças diversas entre as hepatites em seu estudo clínico, existem formas de análise para identificar a doença, tais como o diagnóstico sorológico, por genotipagem etc. O uso de uma rede neural artificial (RNA) pode ser desenvolvido como uma alternativa de ferramenta de diagnóstico de doenças no fígado causada pelos vírus da hepatite. O uso de RNA envolve um sistema treinado com um banco de dados para identificar padrões e comportamentos no processo de diagnóstico de rede, sendo aplicável na detecção de doenças virais com base em dados clínicos. Dos modelos de redes neurais artificiais utilizou-se uma rede baseada na Teoria da Ressonância Adaptativa (*Adaptive Ressonance Theory* - ART). Essa arquitetura possui uma característica importante que resolve o problema de estabilidade e plasticidade o qual proporciona um aprendizado contínuo com a inserção de novos padrões de entrada, mantendo a memória de padrões anteriores. Neste estudo será utilizada a rede ARTMAP *Fuzzy* (Carpenter et al., 1999) que é composta por duas redes ART.

2 REDE NEURAL ARTMAP FUZZY UTILIZADA NA IDENTIFICAÇÃO DO VÍRUS HCV

O banco utilizado contém dados de 418 pacientes (346 são pessoas saudáveis e 72 pacientes são pessoas doentes) e 12 indicadores referentes a exames patológicos: doença (hepatite, fibrose e cirrose), sexo, albumina, fosfatase, alamina, aspartato, bilirrubina, CSR, CHOL, creatinina, gama e proteína (Hoffmann et al., 2018). Através de um estudo criterioso através da média, valores máximo e mínimo para cada pessoa separados por sexo (masculino e feminino) foram definidos os dados de entrada da rede neural que são: Aspartato aminotransferase, Bilirrubina, Gama glutamil transferase e Sexo (masculino – 10 e feminino – 11) e a saída da rede neural representa a saúde do paciente (saudável -1 e doente – 0). A tabela 1 mostra os parâmetros utilizados pela rede ARTMAP *Fuzzy*.

Tabela 1: Parâmetros de Rede.

Parâmetro de Escolha ($\propto > \mathbf{0}$)	Taxa de Treinamento ($\boldsymbol{\beta}$)	Parâmetro de Vigilância ($\rho a, \rho b, \rho ab$)
0,1	1	0,9; 0,9; 1

Foram utilizados na fase de treinamento 70% dos dados de pessoas saudáveis e doentes (levando em consideração a mesma proporção em cada sexo) e 30% foram selecionados para fase de classificação (diagnóstico). É importante lembrar que os dados que são utilizados na fase de classificação não participaram da fase de treinamento. Com relação a seleção dos dados de pessoas doentes foram sorteados na mesma proporção (70% dos dados) para cada patologia (hepatite, fibrose e cirrose).

3 RESULTADOS E DISCUSSÕES

Foram realizados 100 testes sendo que o banco de dados de entrada e saída da rede neural são todos distintos e foram selecionados de maneira aleatória. A Tabela 2 apresenta as métricas (Parikh *et al.*, 2008) encontradas para o melhor e pior resultado obtido em 100 classificações da rede neural ARTMAP *Fuzzy*.

Tabela 2: Métricas de Análise para Classificação de Doenças Hepáticas.

Métricas	**Resultados**	
	Melhor	**Pior**
Acurácia	0,9680	0,5760
Precisão	0,9048	0,2714
Sensibilidade	0,9048	0,9048
Especificidade	0,9808	0,5096
F1-Score	0,9048	0,4176

Observa-se na Tabela 2 que para o melhor resultado todas as métricas mostram uma boa classificação utilizando a metodologia proposta e, mesmo para o pior resultado obtido a probabilidade de classificar corretamente uma pessoa doente é alta e, isto torna-se importante para controle da doença (sensibilidade).

4 CONCLUSÕES

Neste trabalho desenvolveu-se um sistema inteligente utilizando RNA como ferramenta, que pode agir como um equipamento médico para auxiliar na identificação de doenças virais do fígado. O conjunto de dados utilizados apresenta um desbalanceamento em relação ao sexo, a doenças etc. além de possuir um conjunto de dados muito pequeno. Esses fatores interferem no resultado o que pode ser observado na acurácia obtida entre o melhor e pior resultados. Porém observa-se uma acurácia média de 86% e uma sensibilidade de aproximadamente 91% o que indica a eficácia da metodologia. A ferramenta proposta tem como principal finalidade servir como um incentivo científico na determinação de métodos de diagnósticos clínicos partindo de inteligência artificial como um novo recurso menos invasivo e de baixo custo.

REFERÊNCIAS

Manual Técnico para o Diagnóstico das Hepatites Virais. Ministério da Saúde, Secretaria de Vigilância em Saúde, Departamento de Vigilância, Prevenção e Controle das IST, do HIV/Aids e das Hepatites Virais, Brasília: Ministério da Saúde, 2016., p. 123.

Ministério da Saúde: Secretaria de Atenção Primária a Saúde (SAPS). Luta contra Hepatites Virais: Ministério da Saúde lança campanha de conscientização e novo boletim epidemiológico, 2022. Disponivel em: https://aps.saude.gov.br/noticia/18216.

G. A. Carpenter, et al. Fuzzy ARTMAP: A Neural Network Architecture For Incremental. IEEE Transactions on Neural Networks, Setembro 1999., p. 698-713

G. F. Hoffmann, et al. HCV data. UC Irvine Machine Learning Repository, 2018. Disponivel em: https://archive.ics.uci.edu/ml/datasets/HCV%2Bdata.

R. Parikh et al. Understanding and using sensitivity, specificity and predictive values. Indian journal of ophthalmology 2008, 56, 45.

O trabalho intitulado **APLICAÇÃO DO ORANGE DATA MINING PARA PREVISÃO DA RESISTÊNCIA MECÂNICA AS TENSÕES NORMAIS DE COMPRESSÃO**, de autoria de **Murilo Henrique Lima De Souza** , **Thays Ap. de Abreu Santos** , **Carlos Roberto dos Santos Junior** , **Reginaldo José da Silva** e **Mara Lúcia Martins Lopes** foi aprovado na modalidade Pôster, para apresentação no evento VIII ERMAC Regional 9 – Ilha Solteira a ser realizado 21/05/2024.

ILHA SOLTEIRA-SÃO PAULO-BRASIL

{assinatura.comissao}

Douglas Domingues Bueno - douglas.bueno@unesp.br

Data do Aceite:21/05/2024

VIII ERMAC
Regional 9 • Ilha Solteira • 2024
Encontro Regional de Matemática Aplicada e Computacional

FACULDADE DE ENGENHARIA UNESP CÂMPUS DE ILHA SOLTEIRA

APLICAÇÃO DO ORANGE DATA MINING PARA PREVISÃO DA RESISTÊNCIA MÊCANICA ÀS TENSÕES NORMAIS DE COMPRESSÃO

Murilo H. L. de Souza[1], Thays A. A. Santos[1], Carlos R. Santos Júnior[2], Reginaldo, J. da Silva[1], Mara L. M. Lopes[1]

[1] Universidade Estadual Paulista "Júlio de Mesquita Filho", murilo.l.souza@unesp.br; thays.abreu@unesp.br; reginaldo.silva@unesp.br; mara.lopes@unesp.br;
[2] Instituto Federal de São Paulo, "Campus de Presidente Prudente, carlos.rsantos@ifsp.edu.br;

RESUMO: Este estudo emprega o *software Orange Data Mining* para explorar as seguintes técnicas de Predição: Regressão Linear e Rede Neural Artificial *Perceptron* na análise das tensões normais de compressão. Foi utilizado um conjunto de dados provenientes de blocos de Alvenaria Estrutural com substituição parcial de cimento pela Cinza do Bagaço da Cana de Açúcar, visando investigar a viabilidade dessas técnicas na predição dessas tensões. Os resultados demonstram que ambas as técnicas utilizadas pelo *Orange* possibilitaram predições com análise de erros bem pequenos. Essas descobertas ressaltam não apenas a eficácia das técnicas de predição utilizadas, mas também o potencial da inteligência artificial na análise e previsão de propriedades mecânicas de materiais de construção, bem como a utilização do *software Orange* que é uma ferramenta de grande potencial que possui inúmeras acessórios que são aplicadas de forma simples sem a necessidade de código.

Palavras-chave: *Orange Data Mining*; Regressão Linear; Inteligência Artificial; Tensões de Compressão.

1 INTRODUÇÃO

No contexto atual, a preservação do meio ambiente e a busca pela sustentabilidade são prioridades globais. A indústria da construção civil é uma das principais fontes de emissão de CO^2 na atmosfera, motivando a busca por alternativas mais sustentáveis (Freire, 2016). Áreas como Engenharia de Construção Civil e Ciência dos Materiais estão colaborando para desenvolver materiais alternativos que reduzam essas emissões. No caso do concreto, materiais alternativos estão sendo estudados, mas é crucial que mantenham as propriedades mecânicas necessárias para sua utilização estrutural. Essas iniciativas visam promover uma construção mais sustentável e amigável ao meio ambiente. Com o propósito de auxiliar na avaliação da resistência mecânica de misturas de concreto que empregam cinza proveniente do bagaço da Cana de Açúcar como substituto do cimento em blocos de Alvenaria Estrutural em escala reduzida (1:4), usou-se o *software* de mineração de dados *Orange Data Mining*.

2 PREVISÃO DA RESISTÊNCIA MECÂNICA ATRAVÉS DO *ORANGE DATA MINING*

O *software Orange Data Mining* possibilitou, por meio de suas funcionalidades, o mapeamento da rede neural e a extração do gráfico de regressão linear com a incorporação de um conjunto de dados de blocos de Alvenaria Estrutural em escala reduzida (1:4) com 5 substituições das cinzas de bagaço de cana de açúcar além de um grupo controle, a fim de realizar comparações. Os dados foram obtidos de forma experimental no qual foram utilizados a carga de ruptura e a variação de porcentagem das cinzas do bagaço de cana de açúcar (1-controle, 2-5%, 3-10%, 4-15%, 5-25% e 6-50%) (Berti, 2023). Em ambas as técnicas foram aplicados 70% dos dados para o ajuste de cada modelo e os 30% restantes para a etapa de previsão, selecionados de forma aleatória. A Figura 1 destaca a estrutura utilizada para a aprendizagem dos métodos (ajustes), predição e os comandos utilizados nas análises das técnicas utilizados e a Tabela 1 apresenta os dados utilizados no estudo.

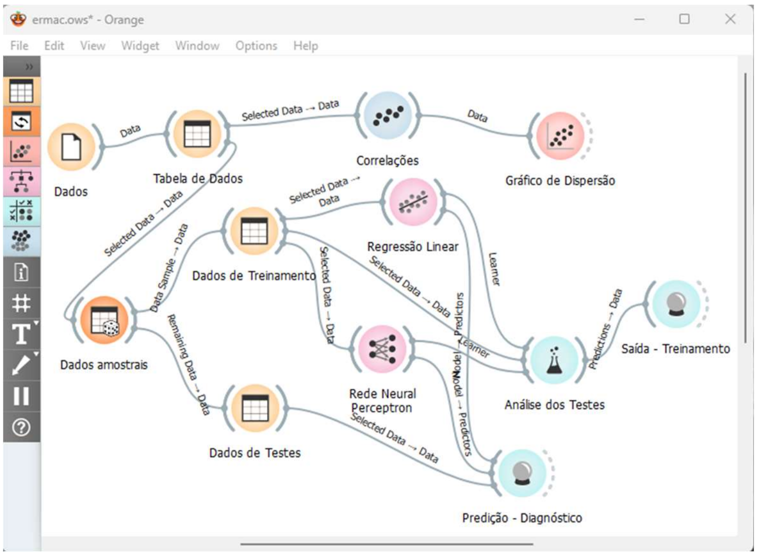

Figura 1: Estrutura do Orange Data Mining.

Tabela 1: Banco de Dados.

CP	Carga Máxima de Ruptura(kgf)	Resistência a Compressão(Mpa)
1	517.1	2.07
1	522.08	2.09
1	547.17	2.19
1	477.41	1.91
1	472.43	1.89
2	322.5	1.29
2	283.62	1.14
2	342.43	1.37
2	192.67	0.77
2	306.92	1.23
3	347.25	1.39
3	396.42	1.59
3	290.05	1.16
3	295.51	1.18
3	397.55	1.59
4	352.71	1.41
4	184.47	0.74
4	277.51	1.11
4	238.78	0.96
4	121.8	0.49
4	234.77	0.94
5	1414.03	5.66
5	1153.19	4.62
5	1345.39	5.39
6	947.26	3.79
6	686.42	2.75
6	604.05	2.42
6	851.16	3.41

3 RESULTADOS E DISCUSSÕES

O *Orange* apresenta uma tela que fornece os resultados de predição obtidos a partir dos modelos ajustados. Na Figura 2 observa-se do lado esquerdo, os valores de resistência previstos por cada técnica e os valores de erros absolutos relativos calculados. Também são apresentadas as características utilizadas para prever a resistência a compressão dos blocos: carga máxima de ruptura e porcentagem de cinzas provenientes do bagaço de cana de açúcar. Observa-se a eficácia de ambos os métodos através do coeficiente de determinação (R^2) e o erro percentual médio absoluto (MAPE) que indicam um ajuste perfeito.

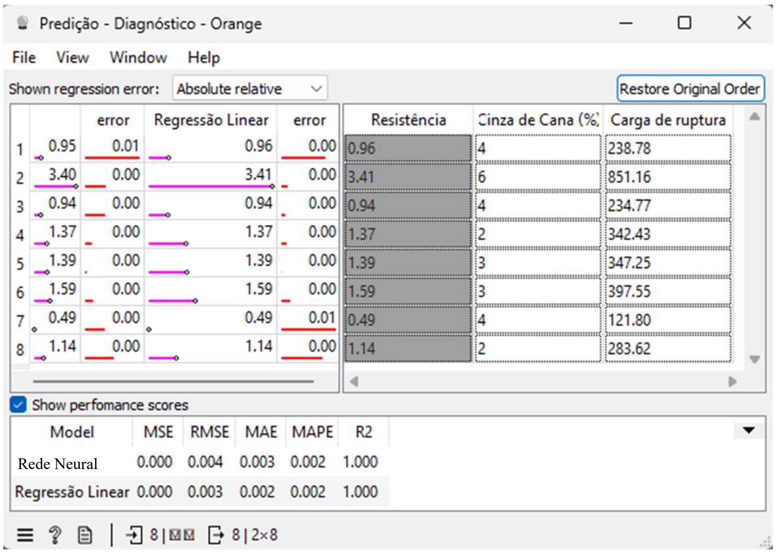

Figura 2: Tela de Resposta da Predição do Orange Data Mining.

4. CONCLUSÃO

A utilização do *software Orange Data Mining* emerge como uma estratégia promissora para a análise de dados. Ao explorar as propriedades mecânicas, comportamentais e ao realizar as previsões observa-se a versatilidade e eficácia dessa ferramenta na investigação de fenômenos complexos. Assim, esta pesquisa destaca a importância e o potencial do *Orange Data Mining* na exploração e compreensão das propriedades de materiais sujeitos a tensões mecânicas.

REFERÊNCIAS

J. V. M. Berti. Efeitos da substituição parcial de cinza do bagaço de cana-de-açúcar na produção de blocos de alvenaria estrutural em escala reduzida (1:4). Dissertação de Mestrado em Engenharia Civil - Faculdade de Engenharia de Ilha Solteira, Universidade Estadual Paulista (Unesp), 2023.

D. Freire. Especialistas discutem papel da indústria do cimento nas emissões de CO^2. Agência FAPESP, [s.l], 27 jun. 2016.